Jaqueline
Marques

Ignition, Combustion and Detection of Polyurethane Foams
With Ammonium Nitrate and Sodium Bicarbonate

September
2013

· U C ·

Jaqueline Edite Marques

Ignition, Combustion and Detection of Polyurethane Foams with Ammonium Nitrate and Sodium Bicarbonate Additives

Forensic Chemistry Master Degree

Chemistry Department

FCTUC

September, 2013

· U C ·

Universidade de Coimbra

Jaqueline Edite Marques

IGNITION, COMBUSTION AND DETECTION OF POLYURETHANE FOAMS WITH AMMONIUM NITRATE AND SODIUM BICARBONATE ADDITIVES

Dissertação apresentada para provas de Mestrado em Química Forense

Professor Doutor José Leandro Simões de Andrade Campos

Professor Doutor Hugh Douglas Burrows

Setembro de 2013

Universidade de Coimbra

Jaqueline Edite Marques

IGNITION, COMBUSTION AND DETECTION OF POLYURETHANE FOAMS WITH AMMONIUM NITRATE AND SODIUM BICARBONATE ADDITIVES

Dissertação apresentada para provas de Mestrado em Química Forense

Professor Doutor José Leandro Simões de Andrade Campos

Professor Doutor Hugh Douglas Burrows

Setembro de 2013

Universidade de Coimbra

“Foi o tempo que tu passaste com a tua rosa que tornou a tua rosa tão importante.”

Antoine de Saint-Exupéry, *O Principezinho*

ACKNOWLEDGMENTS

Uma tese é um trabalho individual, mas está longe de ser um trabalho solitário. Pois estou rodeada de pessoas que nunca deixaram tal acontecer.

Em primeiro lugar quero agradecer aos meus pais e ao meu irmão, eles são o meu verdadeiro pilar, sem eles nada disto seria possivel.

Ao Professor José Campos pela sua verdadeira orientação durante este ano. Por ter partilhado imensos conhecimentos sobre as mais diversas áreas.

Ao Professor Hugh Burrows por toda a disponibilidade e apoio durante a realização desta tese.

A todos os meus amigos, que estando longe ou perto, sempre me fizeram chegar as melhores palavras de motivação.

Aos colegas de laboratório por terem proporcionado um excelente de trabalho.

A todos, os meus sinceros agradecimentos,

Jaqueline Marques

ABSTRACT

The flame propagation of expanded and syntactic polyurethane foams, obtained by free expansion or by adding hollow plastic microspheres, is presented. It was added to the original polyurethane small concentrations of ammonium nitrate in order to allow an existing local flame. To decrease the flame temperature it was added sodium bicarbonate, also in small concentrations. To understand the effect of other types of additives in polyurethane foams surface fires, cellulosic aluminium paint was used.

The prediction of the combustion characteristics of these energetic systems was performed using a thermochemical computer code, THOR. It was also studied the prediction of temperature and ignition delay by Semenov model of ignition and Frank-Kamenetskii phenomenological approach.

Were performed DSC and TGA records of polyol and hollow plastic microspheres.

Cylindrical test samples, rounded by PVC tube, were prepared and burned. Expanded polyurethane foams always present extinction. Various configurations were tested: plain cylindrical test samples, samples where seven tunnels were open and samples where a tunnel was open (flame propagation, driven by PMMA slab). Some of these samples were painted with cellulosic aluminium. Flame propagation allows a more complete pyrolysis and burning of material. Painted samples presented an easier ignition.

Syntactic polyurethane foams with ammonium nitrate increased concentrations burn quite well. The sodium bicarbonate has a very small influence in these reactive materials, because for concentrations less than 5 mass percent samples still burn quite well. It is very interesting the influence of hollow polyethylene microspheres in PU foam combustion phenomena, allowing flame propagation for syntactic PU foams for conditions where there is extinction for PU expanded foams. Microspheres ensure a more homogeneous distribution and increase thermal insulation of foam, reducing the thickness between existing flame and internal ignition layer. Syntactic polyurethane foams without paint have higher mass loss.

In some tests it was allowed the direct measurement of sample mass while being tested. Thermocouples records show burning temperatures up to $\approx 1400\ ^{o}C$ and flame propagation on the level of $mm.s^{-1}$.

Detection was performed by infrared spectroscopy comparing the spectrums of fresh and burned samples with the additives.

Keywords: Ignition; Combustion; Detection; Polyurethane foam; Expanded; Syntactic; Hollow plastic microspheres; Ammonium Nitrate; Sodium Bicarbonate; Aluminium; DSC-TGA; Infrared

RESUMO

Neste trabalho é apresentada a propagação de chama de espumas de poliuretano expandido e sintático, obtidas por auto-expansão ou pela adição de esferas ocas de plástico. Ao poliuretano original foram adicionadas pequenas concentrações de nitrato de amónio, com o objectivo aumentar a chama local existente. Para diminuir a temperatura da chama foi adicionado, também em pequenas quantidades, bicarbonato de sódio. Com o intuito de se compreender o efeito de outros aditivos na superfície das espumas de poliuretano, foi adicionada tinta de alumínio celluloso.

A previsão das características de combustão destes sistemas energéticos foi realizada pelo código THOR.

Também foi estudada a previsão de temperatura e o atraso da ignição pelo modelo de inflamação de Semenov e pela aproximação fenomenológica de Frank-Kamenetskii abordagem fenomenológico.

Foram realizadas análises térmicas (DSC-TGA) de um dos polióis usado e das esferas ocas de plástico.

Amostras cilíndricas, dentro de um tubo de PVC, foram preparadas e queimadas. Espumas de poliuretano expandido apresentaram sempre extinção. Foram testadas diversas configurações: configuração original, amostras onde foram abertos 7 túneis e amostras onde foi aberto apenas um túnel, onde era colocada uma placa de PMMA para funcionar como impulsionador de propagação de chama. Algumas destas amostras foram pintadas com tinta de alumínio celuloso. Propagação da chama, pela placa de PMMA, permite uma pirólise e combustão mais completa do material. Amostras pintadas apresentaram uma ignição mais fácil.

Espumas de poliureatno sintático com concentrações de nitrato de amónio acrescidas queimam bem. O bicarbonato de sódio tem um influência muito pequena na nestes materiais reactivos, porque com concentrações mais baixas que 5 percento de massa, os materiais queimam muito bem.

As microsferas ocas de polietileno contribuem para o fenómeno de combustão nas espumas de poliuretano, permitindo a propagação da chama nas espumas sintáticas em condições nas quais ocorre a extinção para a espumas expandidas. As microsferas asseguram uma distribuição mais homogénea e um aumento de isolação térmicas da

espuma, pela redução da espessura entre a chama existente e a camada interna da ignição. As espumas de poliuretano sintáticas pintada perdem menos massa que as outras.

Nalguns testes foi permitido a medição directa da massa da amostra, enquanto está a ser testada Os registos dos termopares mostram temperaturas de queima até ≈ 1400 ºC e propagação das chamas sobre o nível de $mm.s^{-1}$.

A detecção foi realizada por espectroscopia de infravermelho comparando os espectros de amostras frescas e queimada com os aditivos.

Palavras-chave: Ignição; Combustão; Detecção; Espuma de poliuretano; Expandida; Sintática; Microsferas ocas de Plástico; Nitrato de Amónio; Bicarbonato de Sódio; Alumínio; DSC-TGA; Infravermelho

TABLE OF CONTENTS

LIST OF FIGURES

LIST OF TABLES

ABBREVIATIONS & NOMENCLATURE

$[O_2]$ - O_2 concentration in air (%)

A - Pre-exponential factor (min^{-1})

ACPO - Acrylic Polyol

AN - Ammonium Nitrate

ANFO - Ammonium Nitrate and Fuel Oil

AP - Ammonium Perchlorate

BDO - 1,4-butanediol

B_i – Covolume of component i

BR - Burning Rate

C_p - Heat capacity of PU ($J.Kg^{-1}.K^{-1}$)

CE - Chain extender

CFC - Chlorofluorocarbons

D_0 - Diffusion coefficient of O_2 ($m^2.s^{-1}$)

DSC - Differential Scanning Calorimetry

DTA - Differential thermal analysis

E_a - Activation energy ($J.mol^{-1}$)

EPA - Environment Protection Agency

FTIR - Fourier transform infrared spectroscopy

G – Global Gibbs free energy

h - Convective heat transfer coefficient ($W.m^{-2}.K^{-1}$)

H – Enthalpy

H_f – Formation enthalpy

HCFC - Hydrochlorofluorocarbons

HPM - Hollow Plastic Microspheres

HS - Hard segment

I_p - Calorific power of PU ($J.Kg^{-1}$)

IR - Infrared

k - Boltzmann constant

k_f - Thermal conductivity ($W.m^{-1}.K^{-1}$)

L – Length (m)

m – Number of atomic species

MDI - 4,4-diphenylmethane diisocyanate

m_f – Final mass (g)

m_i – Initial mass (g)

n – Number of chemical components

N_{AV} - Avogadro number

Nu - Nusselt number

ODP - Ozone Depletion Potential

PE – Polyethylene

PEPO - Polyester Polyol

PMMA - Polymethylmethacrylate

PP – Polypropylene

PS – Polystyrene

PU – Polyurethane

PVC – Polyvinylchloride

q_1 – Heat production term

q_2 – Heat loss term

r – Equivalence ratio

R - Molar gas constant ($J.K^{-1}.mol^{-1}$)

r_{0i} - Intermolecular distance at minimum value of the intermolecular potential

SB - Sodium Bicarbonate

SN - Sodium Nitrate

SS - Soft segment

T – Temperature (K) or (ºC)

t – Time (s)

Tb – Combustion temperature

TDI - Toluene Diisocyanate

Tg – Gas environmental temperature

Th – Thermocouple

Tp – Particle temperature

TGA - Thermo-Gravimetric Analysis

V – Volume

X_i – Mole number of i compound

β - Stoichiometric mass ratio between PU and air

Γ – Gamma

γ – gamma

ε_i – Buckingham parameter

θ - Adimensional temperature

λ – Diameter (m)

ρ - Apparent density of PU ($Kg.m^{-3}$)

ρ_0 - Density of O_2 ($Kg.m^{-3}$)

σ_r – Stefan-Boltzman constant ($W.m^{-2}.K^{-4}$)

Ω - polynomial obtained by the compositions of the factors interpotential of the particles

ω_i – Potential of *i* compound

CHAPTER 1 - INTRODUCTION

The technical-scientific area to which this work relates is the field of forensic chemistry, in particular in the investigation of evaluation of fire and explosion protection of porous materials of construction.

Since the 20's, materials in the form of porous plates and coatings have been used in construction. The principle of insulation lies in the fixation of gases inside microcavities, which implies that the material has a low bulk density. In the past, many materials have been tried as base materials. Nowadays, as a result of an increasing qualification and standardization they are reduced to three: glass fibers, polyurethane foams and cellulosic fibers foams. However, these materials have the inconvenient of not ensuring effective protection to fire or accidental explosions. Many flame-retardant additives have been tried. Their success has been very limited mainly because these materials have to have a long lifetime. Furthermore, their possible combustion during an accidental fire also generates recognized toxic gases (Marques et al., 2013).

A forensic chemist may have the task of investigating a fire location. The process of fire investigation is very difficult due to the deterioration of the place. A burned down place usually suffers major changes, from the devastation, the charred remains, collapsed structures, water-soaked ashes, along with smoke. It has to undergo a process of expert analysis, which is similar to the examination of crime scenes in that the scene must be preserved and evidence collected and analysed, but with numerous additional difficulties and dangers. The basic function of a researcher at the fire scene is first, determine the origin of the fire, and second to examine closely the source location to try to determine what it was that caused the fire. From this, it is possible to perform an analysis of the present material, the fuel load and the state of detritus in various places to make the detection and identification of relevant chemical materials collected at the crime scene, to reconstruct and identify the mechanisms of ignition (Nicholas, 2008).

Figure 1 presents a diagram with all the factors of the starter causes, the characteristics of confinement and space, the properties of the fuel mixture and the properties of the incendiary materials. These are all the constraints that leads to a major fire.

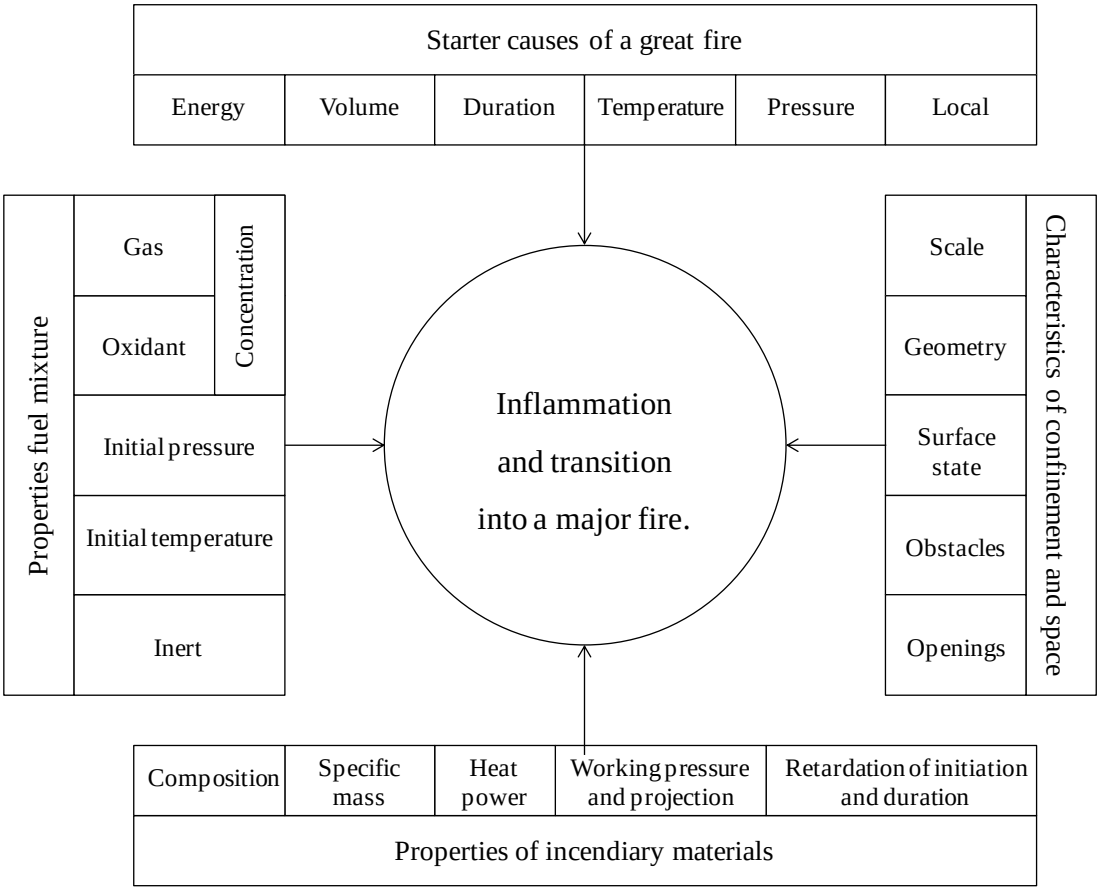

Figure 1 - Main factors and characteristics conditioning the existence of a major fire (adapted from Campos, 1982).

The phenomenon of fire has engaged mankind from the beginning. Chemically, fire is a type of oxidation, which is the combination of oxygen with other substances to produce new substances (Prager et al., 2006).

A simple representation of fire is given by the fire triangle according to Figure 2. The fire triangle demonstrates that the interaction of the three components heat, fuel and oxygen is needed. If one of these components is withdrawn, the fire will not start or it will be extinguished. While heat and oxygen have to be stated as quantitative variables of the fire, the fuel might be available in gaseous, liquid or solid form (Prager et al., 2006).

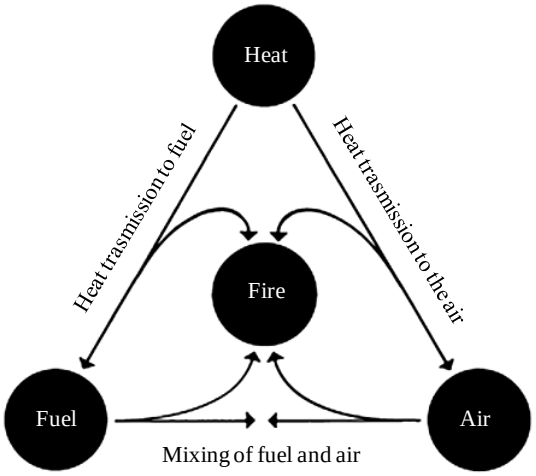

Figure 2 - Fire triangle (adapted from Prager et al., 2006).

In the case studied in this work, the fuel is solid, polyurethane foam. A solid must be hot enough to decompose into gaseous products (pyrolysis); there is a range of temperatures where different materials give off enough decomposition products to form an ignitable mixture with atmospheric oxygen. The fuel had to be vaporized or decomposed by heat supply because under such conditions only oxidation will occur (Prager et al., 2006).

To start fire, the minimum temperature needed to spontaneously ignite fuel, known as ignition temperature, must be reached. The heat evolved when a substance burns is known as heat of combustion (Saferstein, 2011).

An additional factor, besides the liberation of energy, needed to explain fire is the rate or speed at which the oxidation reaction takes place. A fuel will achieve a reaction rate with oxygen sufficient to produce a flame only when it is in the gaseous state (Saferstein, 2011).

The development of the fire is characterized by different phases, which are contained within by the two end positions: ignition and extinguishing. Figure 3 demonstrates the typical course of a fire. After the ignition, flame spread occurs, according to a chain of ignition as result of the flame formation and a significant increase of the temperature level. The surface spread of flame will be dominated by the speed of temperature increase of the burning material. The size of the flames is crucial for the feedback effect. In large flames the radiant portion is dominant. The convection part decreases with an increase in size of the flames unless the convection part becomes dominant due to ventilation effects. After a specific temperature has been reached, flashover occurs if

enough oxygen is available. Any combustibles within the compartment will be set on fire. The fully developed fire passes over to the decay phase (Prager et al., 2006).

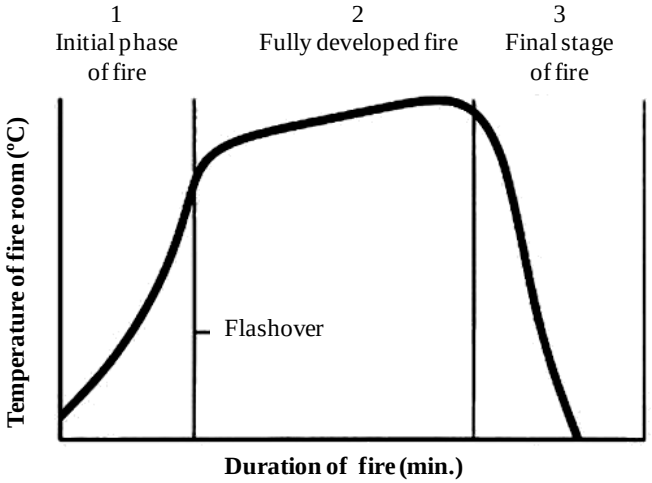

Figure 3 - Stages of a fire (adapted from Prager et al., 2006).

Figure 4 represents an organizational chart that shows the necessary factors that leads to a major fire, such as fuel and oxidant, and which properties have a big impact for the fire to happen. The processes are demonstrated by which the fuel and oxidizer pass after suffering an incentive to give up combustion to achieve a large-scale fire.

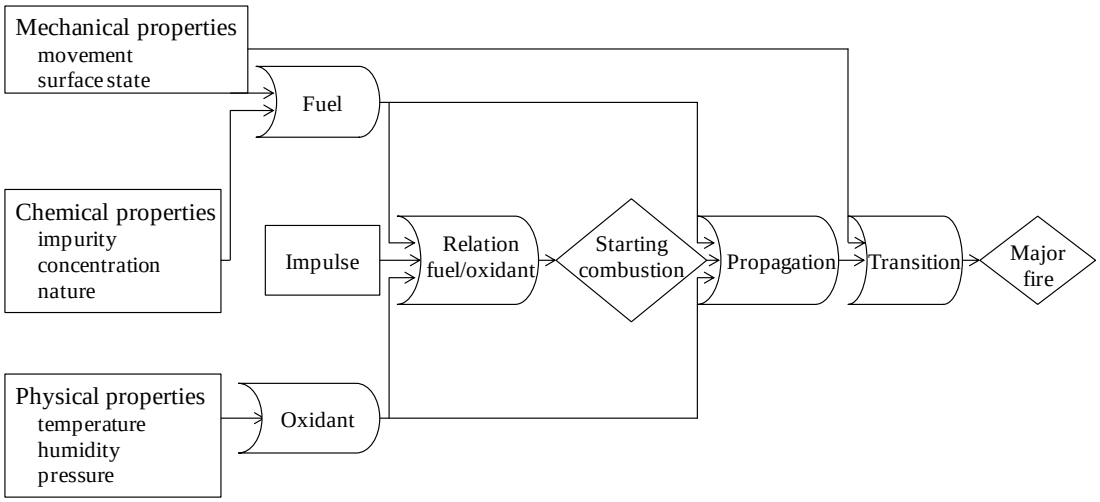

Figure 4 - Organizational chart of formation of a large-scale fire (adapted from Campos, 1982).

As it was mention before, some kinds of materials of construction, have the inconvenience of not ensuring effective protection towards fire. An updated assessment

of these problems will be developed in this study for the particular case of polyurethane foams (Marques et al., 2013).

This kind of foam is widely used in the insulation of houses and other large size confinements, such as warehouses and disco clubs. However, there are a lot of accidental fires in these foams, generally generated by a heterogeneous, small ignition point (projected burning particle) that generates, inside polyurethane, a self-propagated flame kernel. The conditions of ignition and flame propagation generally are not clearly discussed, because there are a lot of additives (coatings and paints) on the surface of these materials (Marques et al., 2013).

The accidental fires of polyurethane foams, generally generated by a heterogeneous ignition small point, will lead us to develop an experimental study based in polyurethane foams, having as increasing flame additive small concentrations of ammonium nitrate particles. In a similar way, the influence is also studied of a retardant flame additive, based in sodium bicarbonates mixed particles, because it is the material that contributes to reduce the flame temperature. In addition, the influence is studied of cellulosic aluminium paint when a sample of polyurethane is ignited (Marques et al., 2013).

A recent accident that is related to the subject of this work was the fire that occurred in the nightclub *Kiss*, in Brazil, at January 27 of 2013, which killed more than 230 people. This was the third deadliest club fire in history. According to information gathered by research conducted when the news became known, the fire occurred unintentionally, when a pyrotechnic material (*Sputnik*) was put to use, whose sparks reached the roof of the club, which led to combustion of sound insulation foam (polyurethane foam). The combustion of polyurethane gave rise to the formation of highly toxic compounds. Inhalation of such compounds results in an extremely dangerous toxic mixture (Marques, 2013).

Sputnik is a pyrotechnic material for outdoor use, a kind volcano or fountain. Many of these propellant mixtures are formed by metals (aluminium or titanium) in small amounts, the most common metal which is used in volcanoes or fountains is aluminium. Aluminium particles present in pyrotechnics are fully capable of carrying out the inflammation of both adjacent and relatively distant material from the original particles, regardless of their size. In the case of the disco *Kiss*, the distance and the radius of

safety to the proper use of pyrotechnic materials were not respected, and the disco had more people than the maximum allowed for that establishment (Marques, 2013).
The soundproofing material used in the roof of the club *Kiss* consisted of a polyurethane foam without fire retardant additive. When the polyurethane was subjected to heat from the pyrotechnics, combustion started because polyurethane is extremely flammable. During combustion, the polyurethane foam produced large quantities of smoke. Polyurethane combustion products are highly toxic, especially carbon monoxide and hydrogen cyanide, whose inhalation causes severe health problems, leading to death, hundreds of people in this case (Marques, 2013).

Other polyurethane fire accidents are not enough reported to be included in this text.
For example the fire that has destroyed most of the Portimão's Retail Park in Algarve. The fire in this large size confinement has begun in a store that sold electric materials (*DeBorla*) and has destroyed all of the stores at the retail centre main block. Examination of the crime scene defends the hypothesis that the fire has been motivated by the overheating of plastic due to the fact that some lights were on. The plastic is PU made, and it was present in the sealing. The sealing was a sandwich panel that is a kind of composite material, made by a structure of three layers: two thin sheets, a rigid and resistant dense material; and a layer of low density material and which can be too rigid and less resilient than the between the other blades (polyurethane foam). Also, during the fire, explosions were heard throughout the night, because the volatile material such as paint added increased the intensity of the blaze (Rees, 2012).

An accident that refers to the use of cellulosic aluminium paint was the *Hindenburg* disaster. *LZ 129 Hindenburg* was a large German commercial passenger-carrying rigid airship. The airship was destroyed by fire on May 6 of 1937. A variety of hypotheses were put forward for the cause of ignition and the initial fuel. The biggest controversy was over whether the fabric skin of the airship, or the hydrogen used for buoyancy, was the initial fuel for the resulting fire. The incendiary paint hypothesis was limited, this theory pointed out that the paint contained iron oxide and aluminium impregnated cellulose acetate butyrate which is highly reactive, In fact, iron oxide and aluminium can be used as components of solid rocket fuel or thermite. More recently, this theory was studied and it was concluded that the incendiary-paint hypothesis is fatally flawed and hence is not applicable to the *Hindenburg* fire (Dessler et al., 2005).

In order to understand the phenomenological problem of ignition and flame propagation of polyurethane foams, our experimental study starts comparing combustion properties (flame propagation velocity and mean flame temperature) of the classic PU expanded foam with the similar syntactic one, using the same PU double formulated reactants. The syntactic polyurethane foam was not free expanded but mixed with hollow plastic microspheres (polyethylene), in order to have the same global apparent density of original expanded PU foam (Marques et al., 2013).

1.1. Thesis outline

The thesis is presented in six chapters. Chapter One provides the motivation for this work, indicating its important role in the area of forensic chemistry.

Chapter Two provides an overview of polyurethane foams and the economic and societal concerns relating to their flammability, specifying its combustion and the possibility of adding other materials to its composition.

Thermal models and various predictive techniques for flame spread and temperature in polyurethane foams are detailed in Chapter Three.

Chapter Four will provide the analytical methodology used and the experimental methodologies and instrumentation for the burning tests of the polyurethane foams, and present some trial tests.

Chapter Five will discuss the results from the sample tests and results obtained by the analytical methodology.

Conclusions and recommendations for future work will be presented in Chapter Six.

CHAPTER 2 - LITERATURE REVIEW

2.1. Polyurethane

2.1.1 History

Polyurethane was discovered by Otto Bayer and coworkers at I.G. Ferbenindustrie at Leverkusen, Germany in 1937 in response to Carother's work on polyamides, or nylons, at E.I. (Éleuthère Irénée) DuPont. Bayer felt stimulated to investigate similar material not covered by DuPont's patent. The first reaction was between an aliphatic isocyanate and a diamine to form polyurea which was infusible and hydrophilic. Further research demonstrated that the reaction of an aliphatic isocyanate with a glycol produces new materials with interesting properties. DuPont and ICI (Imperial Chemical Industries) soon recognized the desirable elastic properties of polyurethanes. The industrial scale production of polyurethane started in 1940, coinciding with World War II. In 1952, when polyisocyanate, especially toluene diisocyanate (TDI), become commercially available an improvement was noticed in the elastomeric properties of polyurethane. In 1952–1954, Bayer developed a different polyester–polyisocyanate system, other formulations and processing techniques were continuously developed such as one and two pack systems (Singh et al., 2009).

2.1.2. General principles

Polyurethanes are extremely large and complex polymers produced by the reaction of isocyanate (R-N=C=O) with compounds containing at least two active hydrogen atoms, such as polyols (R-OH-), producing the urethane linkage. In addition to the repeating urethane linkages, a typical polyurethane structure may contain other moieties such as urea, ester, ether, and aromatic groups may also be present in the structure (Singh et al., 2009).

Polyurethanes are available as both thermoplastics and thermosets. Thermoplastic polyurethanes are linear, segmented copolymers consisting of alternating hard segments

(HSs) and soft segments (SSs). HSs, composed of diisocyanate and short chain extender (CE) molecules such as diols or diamines, are rigid and highly polar. HSs have strong inter-chain interaction due to hydrogen bonding between the urethane/urea groups. The hydrogen bonding association within the HSs in thermoplastic polyurethanes can act as a reinforcing filler for the soft matrix. In contrast, SSs, formed from linear long-chain diols or polyols, are flexible and weakly polar. Thermoset polyurethanes are formed by using either one or a combination of the following parameters, using polyols or isocyanates with functionalities greater than two, or substitution of a trifunctional hydroxyl compound in place of the normal glycol chain extender, or using NCO:OH ratios greater than one, and introducing of a crosslinker into the HS, SS or CE (Chattopadhyay et al., 2009).

Polyurethane foams are the most important thermoset polymers and are manufactured in large quantities in the form of flexible and rigid foams. In Figure 5 the world consumption of polyurethanes is illustrated. Flexible polyurethane foam is produced in large volumes and finds great usage in mattresses and furniture cushioning. However, rigid polyurethane foam is produced in lower volumes, but finds applications in transportation, carpet underlay, refrigeration technology and appliances, building and construction industries, the automotive industry, packaging, and sport goods (Singh et al., 2009). In addition to foams, polyurethanes can also be produced as elastomers, adhesives, binders, coatings, and paints (Wang, 1998).

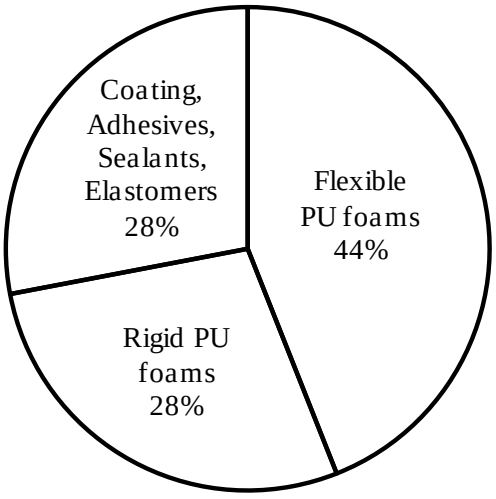

Figure 5 - World consumption of polyurethanes, by products, 2000-2002, (adapted from Ionescu, 2005).

Because of their unique properties, polyurethanes have found a wide variety of applications (Figure 6) in the automotive, furniture, construction, and foot wear industries, as seating, exterior panels, structural foam, furniture, housing for electric equipment, shoe and boot soles, and refrigerator insulation (Wang, 1998).

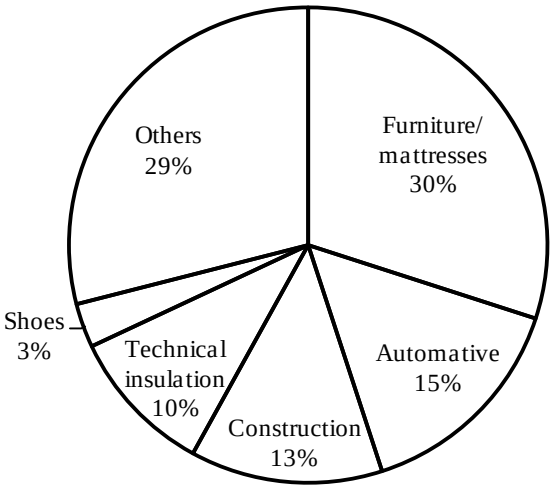

Figure 6 - The main applications of polyurethane, (adapted from Ionescu, 2005).

The worldwide demand for polyurethane foams has been estimated to be about 5 % of the total world consumption of plastics. As it can be seen in Figure 7, polyurethanes follow behind polyethylene (PE), polyvinylchloride (PVC), polypropylene (PP), and polystyrene (PS) as the thermoplastics that are produced in highest volume, (Wang, 1998).

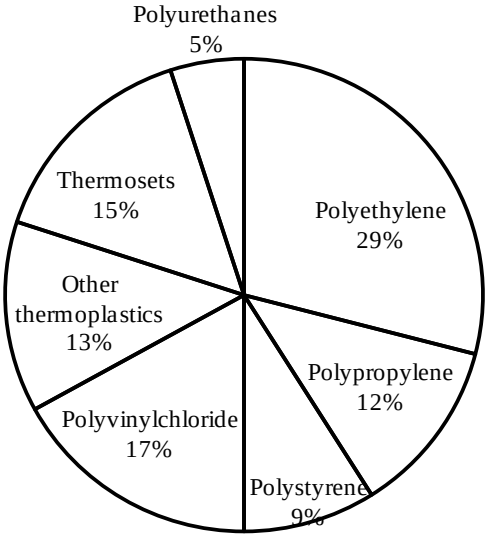

Figure 7 - Polyurethanes and world production of plastics, (adapted from Ionescu, 2005).

2.1.3. Reagents

The wide applicability of polyurethanes is due to versatility in selection of monomeric materials from a huge list the three most important components: macrodiols, diisocyanates and chain extenders. As will be illustrated below, the synthesis of polyurethane involves a simple reaction between a di- or polyisocyanate with a di- and/or polyol (Chattopadhyay et al., 2007).

2.1.3.1. Polyol

The polyol component of polyurethanes can be a polyfunctional polyether, for example polyethylene glycol, polypropylene glycol, PTMG and polycaprolactone diol, or can be a polyester polyol (PEPO), acrylic polyol (ACPO), polycarbonate polyol, castor oil or a mixture of these. The simplest polyols are glycols, such as ethylene glycol, 1,4-butanediol (BDO) and 1,6-hexanediol (Chattopadhyay et al., 2007).

The polyether and polyester polyols are low molecular weight polymers with terminal hydroxyl groups and are the most used in the synthesis of polyurethanes (Neves, 2010).
The low molecular weight and short-chain polyols of high functionality give more rigid, crosslinked polymers because of a high concentration of urethane groups. In contrast, the use of high molecular weight and long-chain polyols with low functionality as the main reactants produces polymer chains with fewer urethane groups and more flexible alkyl chains (Chattopadhyay et al., 2007).
The polyether polyols most used in the formation of polyurethane foams are copolymers of propylene oxide and ethylene oxide. These polymers are diols or triols with different proportions of propylene oxide and ethylene oxide, with this proportion being determined by the final application required for the foam. They are produced by addition of cyclic ethers, such as propylene oxide and ethylene oxide to polyfunctional molecules like ethylene glycol (starter) (Figure 8). The polyether polyols have a lower cost compared to polyester polyols and have a high resistance to hydrolysis. However the polyurethanes based on polyether have a high susceptibility to oxygen and light (Neves, 2010).

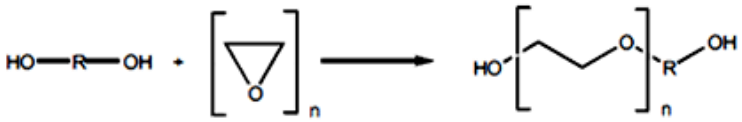

stater ethylene oxide polyether polyol

Figure 8 - Polyether polyol formation, (adapted from Chattopadhyay et al., 2007).

Polyester polyols are generally used in commercial applications, and are prepared from a mixture of two or more diacids reacted with two or more glycols (Figure 9). Their structure will influence the mechanical properties of polyurethane such as flexibility/stiffness. The polyester polyols used in the formation of polyurethanes have a higher molecular weight than polyether polyols and are based on adipic acid and linear glycols such as diethylene glycol or triols such as glycerol. The polyester polyols most widely used in the formation of PU foams are derived from adipic acid and pthalic acid. Polyesters have greater structural resistance to oils, solvents and the oxygen than polyethers, but are more sensitive to hydrolysis and microbial activity. The polyester-based foams have higher tear strength and elongation than the polyether based systems (Neves, 2010).

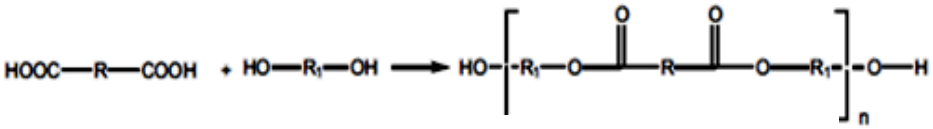

diacid diol (excess) polyester polyol

Figure 9 - Polyester polyol formation, (adapted from Chattopadhyay et al., 2007).

2.1.3.2. Isocyanate

The polyfunctional isocyanate used to prepare PU can be aliphatic, aromatic, alicyclic or polycyclic in structure, with each contributing to the polyurethane properties in different ways. For example, aromatic diisocyanates give more rigid PUs than aliphatic ones, because they have higher reactivity and structural rigidity than aliphatic or cycloaliphatic diisocyanates. However their oxidative and ultraviolet stabilities are lower (Chattopadhyay et al., 2007).

The chemistry involved in the synthesis of polyurethane is centred on the isocyanate reactions. The electronic structure of the isocyanate group can be represented by several resonance structures (Figure 10) - its reactivity toward nucleophilic reagents is mainly

due to the pronounced positive character of the carbon atom in the cumulative double bond sequence consisting of nitrogen, carbon and oxygen, especially in aromatic systems. The electronegativity of the oxygen and nitrogen gives a strong electrophilic character to the carbon in the isocyanate group (Wang, 1998).

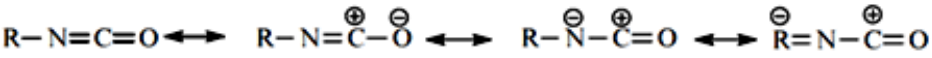

Figure 10 - Resonance structures of the isocyanate group, (adapted from Wang, 1998).

The positive charge at the C atom becomes obvious from the resonance structures. Further, the negative charge can be delocalized onto the oxygen atom, nitrogen atom, and the R group, if R is aromatic. This explains why an aromatic isocyanate has a distinctly higher reactivity than an aliphatic one. The substituents on the aromatic ring can also influence the positive character of the NCO group - an electron withdrawing group in the para or ortho position increases reactivity, while an electron donating group reduces it (Wang, 1998).

Isocyanates are highly reactive chemicals and create several chemically different products when combined with –OH and –NH functional substances. Desired products and side products are formed in different amounts. The common reactions of isocyanates can be divided into two main classes, the reaction of isocyanates with compounds containing reactive hydrogen to give addition products, and the polymerization of isocyanates, a self-addition reaction (Chattopadhyay et al., 2007).
Isocyanates react with hydroxyl (OH containing) compounds to give urethanes (Figure 11). The reactivity of the hydroxy group decreases in the order of primary hydroxy, secondary hydroxy, and phenol, which is very unstable. The addition reaction is an equilibrium reaction and the isocyanate group can be regenerated at elevated temperatures (Chattopadhyay et al., 2007).

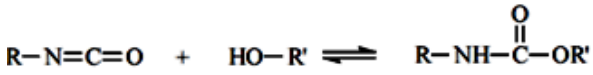

isocyanate hydroxyl urethane

Figure 11 - Urethane linkage formation, (adapted from Wang, 1998).

If the nucleophilic reactant is an NH containing compound, (primary and secondary aliphatic amines and primary aromatic amines), the reaction with isocyanate is rapid, (Figure 12) and it forms urea functional substances (Chattopadhyay et al., 2007).

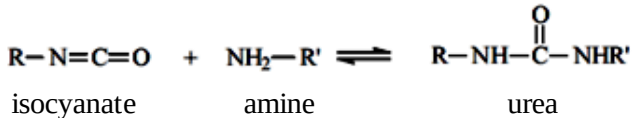

Figure 12 - Urea linkage formation, (adapted from Wang, 1998).

The reaction between isocyanate and water (Figure 13) is a special case of an alcohol/isocyanate reaction. When water reacts with isocyanate it initially forms an unstable carbamic acid, which decomposes and produces an amine and carbon dioxide. The amine formed reacts immediately with the isocyanate group in the system and forms a urea. This reaction is very important for the formation of polyurethane foam, since the carbon dioxide acts as a blowing agent (Chattopadhyay et al., 2007).

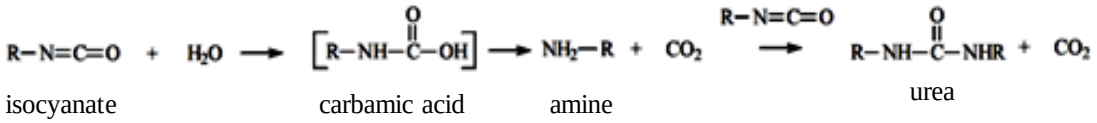

Figure 13 - Reaction between water and isocyanate, (adapted from Wang, 1998).

The urethane and urea formed from the previous reactions still contain active hydrogen. Even though the reactivity of these compounds is lower than the starting alcohol and amine reactants - they are still capable of a nucleophilic attack at the isocyanate group under more rigorous reaction conditions, such as high temperature, humidity level and the more reactive isocyanate. The availability of a lone pair of electrons on the nitrogen atom of urethane and urea groups, makes them nucleophilic centers, and the reaction (Figure 14) results in formation of an allophanate and a biuret (Chattopadhyay et al., 2007).

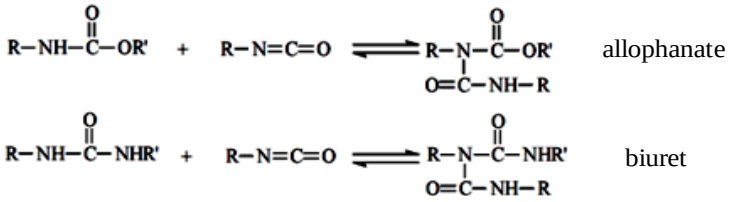

Figure 14 - Formation of allophanate and biuret, (adapted from Wang, 1998).

The self-condensation of isocyanate (Figure 15) results in uretidione rings (dimer), isocyanurate (trimer) or carbodiimide. The trimer isocyanurate rings, unlike uretidione rings, are exceptionally stable (Chattopadhyay et al., 2007).

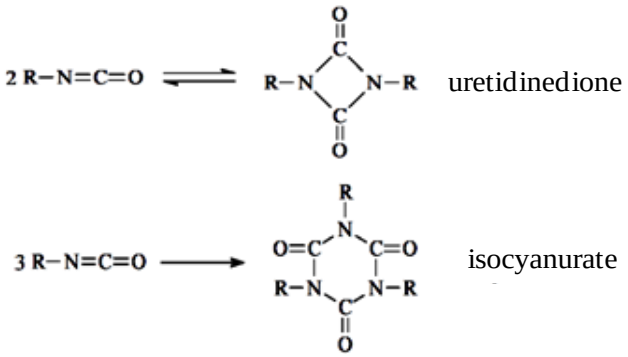

Figure 15 - Self-condensation of isocyanate, (adapted from Wang, 1998).

The formation of carbodiimides is not usually considered a polymerization reaction, although it could be classified as a condensation polymerization between isocyanate molecules with elimination of CO_2. This is due to degradation of isocyanates taking place at high temperatures. The carbodiimides formed in this condensation reaction can further react (Figure 16) reversibly with an isocyanate group to form a uretoneimine (Chattopadhyay et al., 2007).

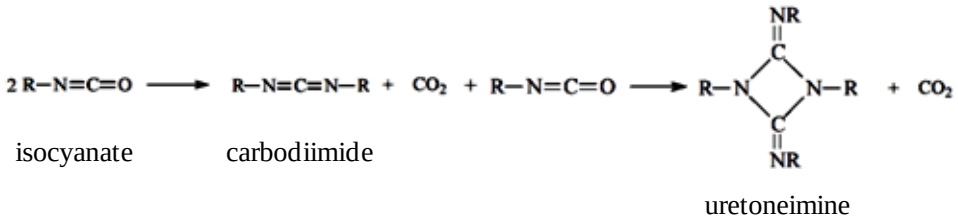

Figure 16 - Formation of uretoneimine, (adapted from Wang, 1998).

The isocyanates most commonly used in the formation of polyurethanes (Figure 17) are those based on aromatic toluene diisocyanate (TDI) and diphenylmethane diisocyanate (MDI). The TDI is marketed in a mixture of 2,4 and 2,6 isomers in the proportions 80/20 (TDI-80/20) and 65/35 (TDI-65/35) or pure (TDI-100). MDI is the most commercialized 4,4-diphenylmethane diisocyanate (Neves, 2010).

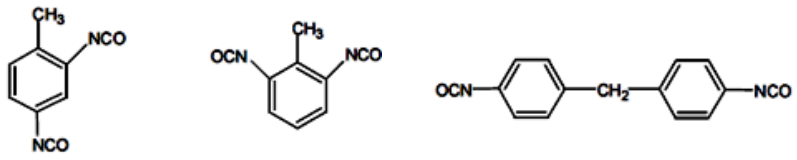

isomer 2,4 isomer 2,6 toluene diisocyanate

4,4-diphenylmethane diisocyanate

Figure 17 - Isocyanates most commonly used. (adapted from Neves, 2010).

2.1.4. Formation of polyurethane

The polyurethanes are a special group of heterochain polymers, characterised by the structure present in Figure 18.

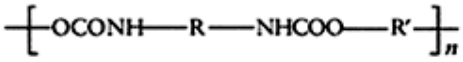

Figure 18 - Structure of polyurethane, (Ionescu, 2005).

The urethane groups –NH-COO- are esters of carbamic acid, a hypothetically unstable (and impossible to obtain under normal conditions) acid [R-NH-COOH]. It is possible to synthesise the urethane groups by various methods, but the most important one involves the reaction between an isocyanate and an alcohol (Ionescu, 2005).

As noted earlier, the reactivity of the hydroxy group decreases in the order of primary hydroxy, secondary hydroxy, and phenol, which is very unstable. The addition reaction is an equilibrium reaction and the isocyanate group can be regenerated at elevated temperatures (Wang, 1998).

The polymerization reaction for producing polyurethanes is represented at Figure 19, it involves the condensation of a polyisocyanate and a polyol (Pinto, 2010).

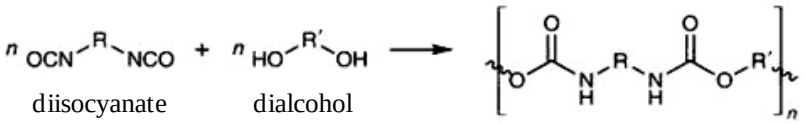

diisocyanate dialcohol polyurethane

Figure 19 - Formation of polyurethane, (adapted from Pinto, 2010).

To ensure complete polymerization of the monomers (polyol and polyisocyanate molecules), the amount of isocyanate (NCO) and alcohol (OH) groups must be equal. In practice, a small excess of isocyanate is used to compensate for the moisture (water) usually present in polyols, which also reacts with isocyanates. The so-called NCO index is a measure of the ratio between the amount of NCO and OH groups in a given formulation, that is, (amount of NCO)/(amount of OH) (Pinto, 2010).

2.1.4.1. Formation of polyurethane foam

To produce foams, a gas must be injected or formed at the same time that the polymerization occurs. Different methods can be used for this purpose. The use of low boiling point solvents that vaporize during polymerization, carbon dioxide injection in the molds, or addition of water to the formulation (Figure 20) are the most common methods of foaming formation. When water is used, the formation of carbon dioxide occurs by reaction with isocyanate (Pinto, 2010).

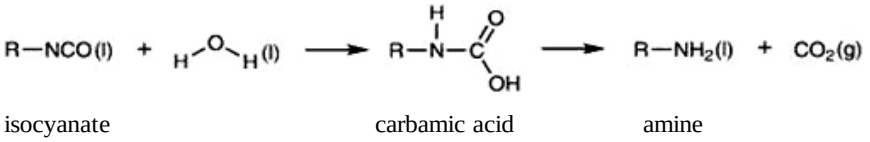

Figure 20 - Formation of carbon monoxide by reaction between water and isocyanate, (adapted from Pinto, 2010).

The intermediate carbamic acid decomposes to carbon dioxide and an amine. In Figure 21 is illustrated that the amine then reacts with another isocyanate to produce a urea (Pinto, 2010).

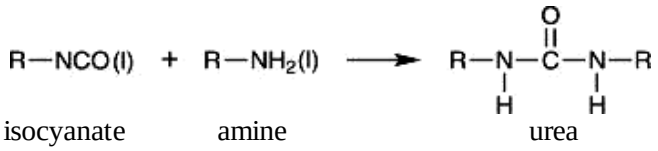

Figure 21 - Formation of urea by reaction between amine and isocyanate, (adapted from Pinto, 2010).

A surfactant is usually used in the formulation to help the stabilization of the gas-liquid emulsion during the initial moments of foam formation, polyether-polysiloxane copolymers are commonly used (Pinto, 2010).

2.1.5. Polyurethane foams general studies

2.1.5.1. Expanded rigid polyurethane foam

Rigid polyurethane foams are usually obtained by reacting a polyol component with an isocyanate component in the presence of a blowing agent, a reaction catalyst and a foam stabilizer. Since rigid polyurethane foams generally have excellent heat insulation properties, they are widely used as various kinds of heat insulating materials, although they have many problems in moldability, uniformity in foaming (Naka et al., 1990).

Expanded polyurethane foams consist of the use of a two components formulation, in which the first component is a material having an hydroxylic content augmented with suitable additives, such as catalysts, surfactants, fillers, pigments and porogenic agents, while the second component is a compound containing two or more isocyanate groups. The production of polyurethane foams is made without the use of porogenic agents, which present objective dangerous characters in respect to the environment (Turchini et al., 1995).

In this work the expanded rigid polyurethane foam used was a commercial formulated product of two liquid solutions, one containing the prepolymer and the other the diisocyanate solution.

2.1.5.2. Syntactic PU foam

A syntactic polyurethane foam formulation prepared from a polyol, a diisocyanate and hollow microspheres provides the aforementioned performance benefits. Thus, the foam can be readily used as modeling stock at ambient and elevated temperatures. It is available for use with computer aided design methods for the production of tools for composite part manufacture. In addition, the instant polyurethane materials have high glass transition temperatures to facilitate their use at elevated temperatures. They exhibit reduced coefficients of thermal expansion, and values which are closer to that of

materials utilized to make composite parts. Further, the materials show improved mechanical strength to permit their use under autoclave pressures and temperatures (Otloski, 1988).

Hollow plastic microspheres are used as a filler material in plastics, in plastic foam compositions and in concrete and asphalt compositions. These can be made from low heat conductivity plastic compositions and blown with a low heat conductivity gas and used to make improved insulation materials and composites and insulating systems. Hollow plastic microspheres are also used as filler in the manufacture of syntactic foam systems. HPM improve insulating materials and insulating systems for use in the construction of formed wall panels. The microspheres are resistant to relatively high temperatures and stable to many chemical reagents and weathering conditions; these characteristics make them suitable for a wide variety of uses (Torobin, 1981).
The microspheres, because they can be made from very stable plastic compositions, are not subject to degradation by outgassing, aging, moisture, weathering or biological attack. The hollow plastic microspheres when used in manufacture of improved insulating materials can be used advantageously alone or in combination with other materials, such as polyurethane foams. The thermal properties of the microspheres can be improved by filling the interstices between them with low conductivity foam, such as polyurethane (Torobin, 1981).

Syntactic PU foam has been taken from a commercial dense (without voids) PU formulated product, and was also formed from combination of two liquid solutions (prepolymer and diisocyanate solutions). A syntactic foam has been formed adding polyethylene hollow microspheres (*Q-cell*) to the original dense polyurethane.
The hollow plastic microspheres used are mainly spherical in shape (≈ 60 μm), uniform in size, wall thickness and strength characteristics (AkzoNobel, 2011).

2.1.6. Thermal decomposition and flammability

The study of the thermal decomposition of the polymers is important to understand the reactions which occur during pyrolysis, as well as the parameters that influence it, thus

helping to improve the performance of the polymers by improving their thermal stability (Neves, 2010).

The thermal degradation and stability of PUs is related to the HS, SS and CE structures. Hence, it is understandable that variations in the type and amount of these three basic building blocks of PUs, namely, diisocyanate, longchain diol or short-chain diol, can lead to alterations in the thermal stability of the resultant product. The degree to which the HS and SS phases separate into microdomains also plays a vital role in determining the thermal stability of segmented PUs. Also, using the same starting materials, the thermal stability of PUs can be varied simply by changing the ratio of the HS to SS (for example the NCO:OH ratio), catalyst concentration, temperature of the reaction and method of synthesis. Therefore, a number of parameters including structural features and reaction conditions, can have a dramatic influence on the thermal stability of the final polymer obtained. Pure PUs generally have low thermal stability at high temperatures. However, some chemical modification of the PU backbone through the introduction of thermally stable heterocyclic structures such as isocyanurate, oxazolidone, imide, triazine or phosphazene are viable methods for improving thermal stability (Chattopadhyay et al., 2009).

The thermal stability of polyurethanes depends on their structure, and is a process that occurs at different stages, resulting from multiple physical and chemical reactions (Figure 22). The decomposition process of polyurethane foam occurs essentially in two stages: there is a first decomposition step at about 300 ºC, which is the thermal decomposition of the hard segments of the foam; and a second phase decomposition at 400 ºC, which is the decomposition of soft segments (Neves, 2010).

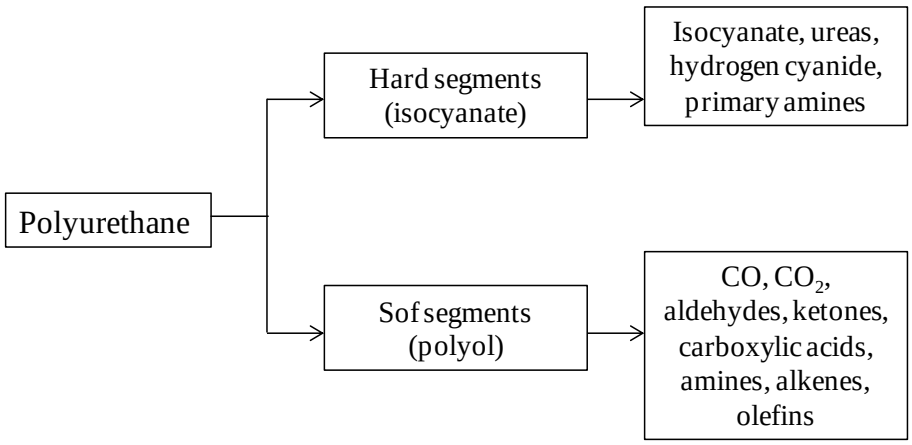

Figure 22 - Scheme of thermal decomposition of polyurethane foam (adapted from Neves, 2010).

Polyurethane decomposition, in the first stage leads to the release of gaseous products, ending with the lost of all volatile material and formation of a residue, whose composition depends on the PU structure. Diisocyanate monomers represent most of the volatile products released, leaving as residue the regenerated polyol (Neves, 2010).

Thermal decomposition of urethane group may occur according to two reactions: a depolymerisation reaction, which is the dissociation of urethane linkage into a isocyanate group and a hydroxyl group, and the dissociation reaction of the urethane linkage involving the possible formation of a 6 membered ring, producing a primary amine, an olefin and carbon dioxide. There are other possibilities of decomposition mechanisms of hard segments of polyurethane, apart from that shown in Figure 23 (Neves, 2010).

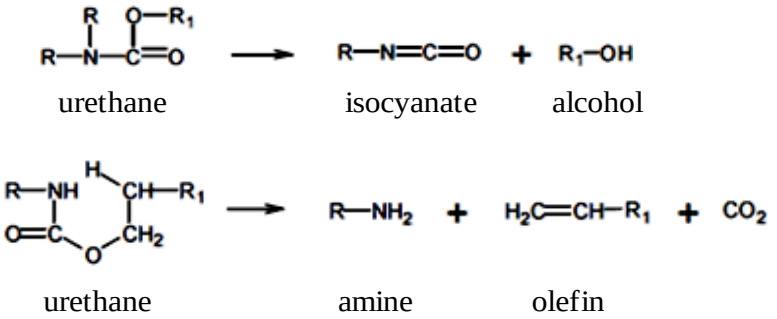

Figure 23 - Urethane group dissociation, (adapted from Neves, 2010).

The soft segments will affect the thermal stability of the polyurethane due to their tendency to form hydrogen bonds between the oxygen of the carbonyl group or the hydroxyl group and the hydrogen of the urethane group from the hard segments. Since the interaction between the two types of segments is stronger in polyester-based polyurethanes, it may be one reason that they are more thermally stable compared with polyether polyurethanes. Unfortunately, the information on the mechanisms of decomposition of soft segments is much less detailed than that on thermal decomposition of hard segments (Neves, 2010).

Increasing the temperature of a PU system results in a thermal activation of the covalent bonds in PU chains. Once a critical temperature is reached, the PU starts decomposing and produces small molecules in the gaseous phase. The decomposed small molecules evaporate, diffuse into the flame zone above the polymer/air interface and mix with air to form a flammable mixture. When the concentration of this mixture and the system

temperature cross the flammability limit, it starts to burn. A part of the exothermic heat that results from the burning process is fed back to the condensed phase and accelerates the degradation of the PU, producing more volatile fragments and sustaining the combustion cycle. Finally, the combustion process ends with a material of different morphology (Chattopadhyay et al., 2007).

The flammability of PU materials presents a threat to both, the integrity of the product and to human health. In the search for an appropriate fire retardant or the synthesis of an inherently non-flammable PU, it is essential to know the structural and energetic features that influence the thermal stability and flammability of PUs. Flammability is associated with the formation of flammable, gaseous decomposition products during the initial decomposition. However, the decomposition rate and extent of decomposition is connected and controlled by the amount of flame propagation. Therefore, it is likely that fire resistant PUs might be prepared by incorporating thermally stable structural units that do not decompose easily but, once they decompose, produce non-combustible products. Additionally, the flow of fuel gases during decomposition is also important for the predication of flame retardancy. In order to stop, delay or retard the burning process, a flame retardant may be added to the PU system, which may or may not be a part of the PU macromolecular chain. The objective of using flame retardants is to lower the PU's inherent fire risk by lowering the combustion rate and flame spreading in the presence of fire (Chattopadhyay et al., 2009).

2.1.6.1. Ignition

The ignition of polyurethane foams includes all gasphase processes that occur between the fuel production step and the occurrence of a visible hot flame. The ignition of polyurethane foams occurs by the interdiffusion of the flammable gases with air. The ignition of polyurethane foams has been extensively studied with various heating sources, thermogravimetric analysis (TGA), small pilot flames, and heat apparatus. By using a series of selected oven temperatures and measuring times to ignition, it is possible to establish the minimum heating rate required for ignition and the initial decomposition temperature at that rate. The thermal stability and ignition of conventional polyurethane foam depend mainly on the composition. When polyurethane foam is subjected to heat, various polyurethane linkages are broken at different temperatures (Singh et al., 2009).

Previous studies have shown that polyurethane foams ignite at a 20 % weight loss and are extinguished at an 80 % weight loss. It was found by the ignition in a glow wire test and then characterization with thermography that polyurethane foams ignite faster than cotton and cellulose acetate but more slowly than polyoxymethylene. It was also found, by smouldering with a siliconite heater as a heat source, that smouldering spreads faster in the upward direction than the downward direction under natural draft conditions. A study on a polyurethane foam ignited in a special apparatus consisting of a nichrome wire sandwiched between porous ceramic honeycomb plates shows that downward smouldering is controlled primarily by the supply of the oxidizer to the reaction zone. The oxygen supply and heat loss are the main factors that influence the foam ignition and smouldering. The forward forced smouldering propagation velocity increases with air flow and then decreases with the air flow rate in a foam material placed horizontally. A polyurethane foam covered with cellulose-based fabric poses a serious smouldering hazard if exposed to a burning cigarette because of the low temperature (400 ºC), which produces a substantial amount of carbon monoxide. In other experiments, the ignitability, heat release rate, effective heat of combustion, and mass loss were obtained by the exposure of polyurethane foams under cone calorimetry test conditions. It has been found by different workers that the uniform heat flux and peak rate of heat release depend to a large extent on the melting behaviour and thickness of the foam, which should be limited to 25 mm. Density was found to be the key variable in controlling ignition resistance (Singh et al., 2009).

2.1.6.1.1. Polymethylmethacrylate

PMMA is a polymer produced through a polymerization process of methyl methacrylate. In this particular case no cross-linking exists between the long chain molecules, and can therefore be considered a thermoplastic. It is composed of vinyl monomers (Figure 24) that is, molecules containing carbon-carbon double bonds, and is thus the product of the radical polymerization of free methyl methacrylate (Steinhaus, 1999).

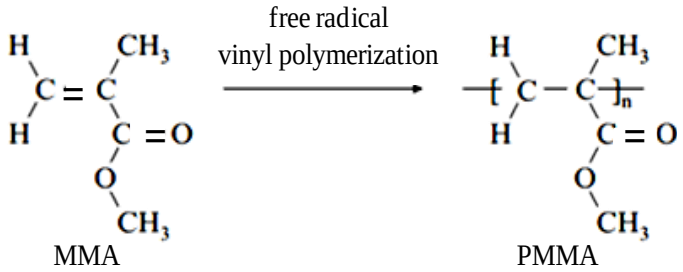

Figure 24 - Polymerisation of PMMA (adapted from Steinhaus, 1999).

PMMA is a member of a family of polymers which chemists call acrylates, or better known under the name acrylics. In general PMMA is a clear plastic, but is also available in an opaque form. When it is used as a clear plastic, it often replaces glass due to its shatterproof characteristics. When it comes to making windows, PMMA has further advantages over glass, because is more transparent. When glass is made too thick, it becomes difficult to see through, but when PMMA is used even at a thickness of 330 mm it is still perfectly transparent. Other areas of application of PMMA are paints, additives in lubricating oils and hydraulic fluids (increases their viscosity at low temperatures) (Steinhaus, 1999).

PMMA application has been restricted by its relatively low mechanical properties and its poor heat resistance (Liu et al., 2010).

The wide variation in the thermal degradation of PMMA can be explained in terms of its structure of the PMMA, molecular weight, morphology and by the experimental conditions employed for preparing the polymer. A two-step degradation process results if the polymer has been prepared in the presence of air due to copolymerisation with oxygen, but not to weak links formed by chain termination, since these would be present in all free-radical polymerisations. PMMA polymerised thermally in absence of oxygen and peroxide impurities is as stable as all polymers initiated by free radicals under air-free conditions. It has a higher molecular weight and, consequently, a lower concentration of labile endgroups, than that prepared in the presence of oxygen, which may account for slight differences observed (Pielichowski et al., 2005).

There is dependence of the rate of thermal degradation of PMMA on molecular weight at low degradation temperatures and thermal degradation starts by a mixture of chain-end and random chain scission initiation, followed by depropagation and first-order termination. Random scission is attributed to pre-oxidation of the polymer on storage at

room temperature. At higher temperatures, a change in molecular-weight dependence is observed, which can be related to depropagation at the end of the polymer chain. The thermal degradation of PMMA also leads to the formation of char, which is produced by the elimination of methoxycarbonyl side chains. The amount of char produced increases with increasing concentration of endgroups and temperature (Pielichowski et al., 2005).

The PMMA material with known physical and chemical properties, has been widely used in studies of flame spread over solid fuels. The plate introduced in the current system is thick enough to be considered thermally thick. The characteristics of flame spread over PMMA plates in the channel are then studied by extensive experimentation, by varying the flow rate and oxygen concentration of the incoming gas stream (Wanga et al., 2004).

2.1.6.2. Combustion

The combustion of polyurethane foams occurs only in the presence of a sufficient amount of oxygen. On combustion, polyurethane foams produce four types of products: combustible gases, noncombustible gases, entrained solid particles, and carbonaceous char. These combustion products vary with the foam composition, temperature level, rate of temperature rise, endotherms, exotherms, and rate of volatile evolution. The heat of combustion raises the temperature of combustible and noncombustible gases, resulting in increasing heat transfer by radiation. The heat transferred from the combustion zone to the adjacent material produces further decomposition and ignition resulting in flame propagation. Polyurethane foams exhibit a highly viscous melt on combustion (Singh et al., 2009).

Combustion of polyurethane foams involves the thermal decomposition of the substrate to yield low molecular mass products that can volatilise from the surface and form a flame. This decomposition process requires a critical heat flux to break the chemical bonds of the foam. The heat flux is the combination of convective and radiative heat fluxes produced by a flame. It may also involve an external heat flux from a radiant source (Ezinwa, 2009).

The heat irradiance must be high enough to overcome the thermal inertia of the foam, which is an important material property that determines the rate of change of surface temperature, the ease of ignition and fire spread. Since the densities of polyurethane

foams are low, which results in a low thermal inertia, the surface temperature of foams rises quickly when ignited. The quick rise in the surface temperature increases their ignition propensity, which results to rapid flame growth. For this ignition to occur, however, the critical temperature of the surface must be reached, which then leads to sustained flaming, depending on the size of the flame. As the flaming combustion continues, the depth of the heated layer increases and heat is conducted into the foam. The subsequent fire growth will depend on how fast the flame spreads and involve more surfaces which are affected by the fuels thermal inertia (Ezinwa, 2009).

Polyurethane foam can behave as a thermally thin or thick material depending on the thermal conduction length. For polyurethane foams that can be treated as thermally thin materials, the velocity of flame propagation has been found to be inversely proportional to the product of the fuels density, specific heat and thickness (Ezinwa, 2009).

In most cases, however, polyurethane foams do not meet the criteria for thermally thin media. Thermally thick foams have a temperature distribution that is affected by its physical depth due to the prolonged time it takes heat energy to penetrate to the opposite side of the material. For such foam specimens, the thermal penetration depth must be less than the physical depth so that increasing the physical thickness of the specimen will not influence the time to ignition (Ezinwa, 2009).

For flame spread over thermally thick materials, the rate of spread is inversely proportional to thermal inertia. This relationship shows that the rate of flame spread is strongly affected by the density of the specimen. For polyurethane foams of low thermal inertia, flame spread can be initiated even if a very small portion of the specimens surface is heated. Due to the air spaces in polyurethane foams, the combustion of these items involves both flaming and smouldering combustion (Ezinwa, 2009).

The mechanism of flame spread involves the movement of flame wave and front (also called the flame base), which occurs at the interface between the burned and unburned fuel substrate where radiant heating produces sufficient combustible gases which act as fuel. In fire safety applications, one important consideration is to determine whether a flame initiated at one point will be limited to a localised, temporary burn or develop to become a large fire. Another consideration is to determine how fast the flame spreads to involve more burning surfaces. The spread rate can also be estimated by measuring the time taken for flame front to move from one point to another on the surface of a burning fuel which results in an increase in area involved in the fire and the heat release rate (Ezinwa, 2009).

2.1.6.3. Smoke and toxicity

A substance in the air that can be adverse to humans and the environment is known as an air pollutant. Some of the major air pollutants are: sulphur oxides (SO_x), nitrogen oxides (NO_x), carbon monoxide (CO), and volatile organic compounds (VOCs) (Singh et al., 2009).

Carbon monoxide is one of the most common toxic agents in forensics studies. It is a product of an incomplete combustion of hydrocarbons, such as polyurethane. It is often referred to as a silent killer, some people refer to it as a "smart" poison, because it enters in the organism easily and voluntarily through breathing. In the case of certain fires, another toxic product that is formed is cyanide (CN), is formed when the temperature reaches 315 ºC and is released in gaseous form, as hydrocyanic acid (hydrogen cyanide, HCN) which may be inhaled by victim. HCN is generated from pyrolysis of organic materials containing nitrogen (N), as is the case of polyurethane foams (Marques, 2013).

Requirements regarding smoke density and toxicity are becoming increasingly stringent because of the increasing interest in fire and consumer safety (Singh et al., 2009).

In cases of fire casualties, it is rarely known which combustion products contribute to the overall toxicity. Usually, carbon monoxide (CO) is the most important factor. However, especially in the case of burning plastics, the contribution of other pyrolysis products can be considerable. These include well-known compounds such as hydrogen cyanide (HCN), nitrogen oxides (NO_2, NO) and aldehydes. Also small amounts of unknown highly toxic substances may contribute to the overall toxicity. Formation of such compounds, even in small-scale fires with moderate total emission, may result in a considerable toxic burden (Busker et al., 1999).

High-density foams produce more smoke than low-density foams. Fire-retardant foams release roughly 5 times more smoke than an untreated foam. The presence of bromine and phosphorous compounds in burning foam increases the evolution of smoke and toxic gases, particularly carbon monoxide and hydrogen cyanide. In particular, phosphorous fire-retardant compounds reduce the thermal decomposition temperature of foams, resulting in an increase in the smoke density. Polyurethane foams produce more smoke than rigid polystyrene, wood, wood wool, and phenolic foam but less than polyvinylchloride, acrylics, and nitrocellulose crystals. Polyurethane foams produce smoke that is double the volume with respect to wood components. In the flaming

mode, a flexible polyurethane foam produces less smoke than a rigid foam, whereas in the nonflaming mode, the smoke difference is quite low (Singh et al., 2009).

2.2. Oxidizers

An oxidizer is a substance that generally releases oxygen to combine with another material for the purpose of combustion. The release can be accompanied by the production of heat. An oxidizer, in terms of chemistry, also known as oxidizing agent is the element or compound in an oxidation-reduction (redox) reaction that accepts an electron from another species the oxidizing agent itself is reduced (Oommen et al., 1999).

Polyurethane is used in pyrotechnic compositions as a fuel and binder. Pyrotechnic compositions are usually homogenized mixtures of small particles of fuels and oxidizers. The polyurethane industry is facing environmental challenges due to the type of auxiliary blowing agents used during the polymerization process. Chlorofluorocarbons (CFCs) have traditionally been the predominant blowing agents for rigid polyurethane foams. Unfortunately, CFCs are one of the major causes for the destruction of the ozone layer due to their high ozone depletion potential (ODP), and therefore, are being phased out as blowing agents in the polyurethane foam industry. The polyurethane industry is searching for alternative blowing agents with low to zero ODPs, and has identified hydrochlorofluorocarbons (HCFCs) (Tang et al., 2002).

In a complementary way, the environmental aspects of combustion products are, nowadays, one of the more important characteristics of new pyrotechnic mixtures. Clean oxidizers always consider ammonium nitrate as the base component of a recent family of gas generators and pyrotechnic composite mixtures, as a candidate to substitute ammonium perchlorate (Marques et al., 2013).

2.2.1. Ammonium Nitrate

Ammonium nitrate (AN) is one of the most commercially important ammonium compounds in terms of usage. It finds extensive applications in the areas of nitrogen fertilizers and explosives. While it acts as a source of ammonia and nitrate ion vital to

the plants in the form of nitrogen fertilizer, in explosives and propellants the nitrate ion is a source of oxygen and finds its application as an oxidizer. AN is the principal component of most industrial explosives. Several compositions of AN such as ANFO ammonium nitrate and fuel oil, amatol, are well known explosives. However, its use in the field of propellants and pyrotechnics is rather limited. This is unlike potassium nitrate which is the principal constituent of the black powder or gun powder, and is even known to have been used in the earliest solid rockets, or ammonium perchlorate which is the main oxidizer of modern solid propellants. The principal use of AN in propellants is restricted to low burning rate (BR), low performance applications, such as gas generators for turbopumps of liquid propellant rocket engines or emergency starters for jet aircraft (Oommen et al., 1999).

AN is hygroscopic, undergoes a room temperature phase transformation involving a significant volume change, and burns very slowly. These adverse properties make it even less attractive as an alternative oxidizer. Nevertheless, it is evident from the extensive literature that many of these problems of AN, which restrict its use as an efficient oxidizer have proven to be surmountable. However, much of the information concerning the various properties of the salt, especially those relevant to its use as an oxidizer, remain either classified or scattered due to its application in strategic areas. AN is a colorless, crystalline salt, and is highly soluble in water. Although it is hygroscopic, it does not form hydrates. It is also soluble in alcohol, acetic acid and nitric acid. AN dissolves in liquid ammonia to form what is known as Divers solution and can be used to strip ammonia from gases. AN has a negative heat of solution in water, and can therefore be used to prepare freezing mixtures (Oommen et al., 1999).

Major applications of AN are in the field of explosives and fertilizers. As a fertilizer, it incorporates nitrogen in both of the forms taken up by crops: ammonia and nitrate ion. AN is the cheapest source of oxygen available in the condensed form for commercial explosives. AN is used by itself in conjunction with fuels or in admixture with solid fuels and sensitizers. Properties of AN, such as density and porosity also need to be tailored depending upon the application (Oommen et al., 1999).

AN must be considered a high explosive under the following three conditions: bolstering by a high velocity explosive, confinement at elevated temperatures, and in presence of oxidizable material. Although AN does not burn by itself, it is a strong oxidizer capable of supporting combustion (Oommen et al., 1999).

There are a kind of thermal decomposition where is studied the different phases of the compound. This means that the compound is decomposed, but does not originate new chemical products, only changes its phase. The crystal transformation of AN has been the subject of examination by numerous investigators. Under ordinary pressure AN occurs in no fewer than five stable polymorphic modifications. The mechanical strength of the AN prills is dependent on the phase transition behaviour, the phases are:

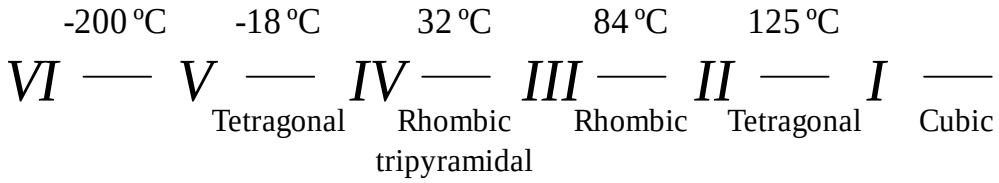

Many of the studies on the phase transformation support the generally accepted idea that the mechanical strength of the prill should be related to the AN *IV* –AN *III* polymorphic transition at 32 ºC (Oommen et al., 1999).

There are a kind of thermal decomposition where the increasing of temperature is enough to originate new chemical products. A simplified global mechanism is presented bellow. AN has been extensively studied. As for most energetic materials, the thermolysis of AN depends upon various factors like pressure, temperature, and experimental conditions like sample size, rate of heating, sample purity, monitoring techniques and presence of foreign substances. No single mechanism could explain all the aspects of its decomposition characteristics (Oommen et al., 1999).

$$NH_4NO_3 \rightarrow NH_3 + HNO_3 \quad (1)$$

$$NH_4NO_3 \rightarrow N_2O + 2H_2O \quad (2)$$

$$NH_4NO_3 \rightarrow 3/4N_2 + 1/2NO_2 + 2H_2O \quad (3)$$

$$NH_4NO_3 \rightarrow N_2 + 2H_2O + 1/2O_2 \quad (4)$$

$$8NH_4NO_3 \rightarrow 5N_2 + 4NO + 2NO_2 + 16H_2O \quad (5)$$

$$NH_4NO_3 \rightarrow 1/2\ N_2 + NO + 2H_2O \quad (6)$$

In spite of several favourable attributes, AN also presents some disadvantages. Besides its high hygroscopicity and phase transitions, the burning characteristics of AN are not comparable to the burning characteristics of ammonium perchlorate. Experimental

results, from decomposition processes of pure ammonium nitrate, show significant influence of endothermic dissociation above 169 ºC (reaction 1); exothermic elimination of N_2O on careful heating at 200 ºC (reaction 2); exothermic elimination of N_2 and NO_2 above 230 ºC (reaction 3); and exothermic elimination of nitrogen and oxygen, sometimes accompanied by detonation (reaction 4), in a good agreement with theoretical predictions (Durães et al., 1996). During detonation, reaction 5 has been suggested when AN undergoes explosion; when the salt is heated from 200 to 230 ºC, exothermic decomposition occurs (reaction 6) (Oommen et al., 1999); (Théorêt et al., 1964).

Model and experiments of combustion of ammonium nitrate based propellants also shown the influence of small concentrations of catalysers (Carvalheira et al., 1995). Other studies were focused on increasing the oxidiser effect and density of the mixtures, based in ammonium nitrate. This was the case of mixtures of ammonium nitrate (AN) and sodium nitrate (SN) that optimised the ratio of AN/SN to the constant value of 86/14 %, in mass (Campos et al., 1991; Pires et al., 1996). The mixture also use the same binder type (a polyurethane solution system) of the hydroxyl terminated polybutadiene of the classic ammonium perchlorate based composite propellants, very well justified in previous works (Marques et al., 2013).

2.3. Flame retardants

Fire retardancy requires the disruption of the burning process at one or more stages so that the process is terminated within an acceptable period of time (Singh et al., 2009).

In general, flame retardants act by preventing ignition or preventing the spread of a fire. First, the ignition susceptibility of a product lowers when the flame retardant increases the net heat capacity of the product. Second, once a fire has already begun, flame retardants can reduce the tendency of the fire to spread by reacting with the product and forming a less flammable char or noncombustible gaseous layer along the boundary of the fire (EPA, 2005).

There are five specific mechanisms by which flame retardancy may occur. Physical dilution, where he flame retardant can act as a thermal sink, increasing the heat capacity of the product or reducing the fuel content to a level below the lower limit of

flammability. Inert fillers such as glass fibers and microspheres and minerals such as talc act by this mechanism. Chemical interaction where the flame retardant dissociates into radical species that compete with chain propagating and branching steps in the combustion process. This is the general flame-retarding mechanism by which brominated flame retardants operate. Inert gas dilution, the flame retardant additives produce large volumes of noncombustible gases when the product decomposes during combustion. The gases dilute the oxygen supply to the flame or dilute the fuel concentration below the flammability limit. Metal hydroxides, metal carbonates and some nitrogen producing compounds function in this way when used as flame retardants. Thermal quenching, where the endothermic degradation of the flame retardant results in thermal quenching. Metal hydroxides and carbonates act in this way. Protective coatings, some flame retardants function by forming a protective liquid or char barrier that acts as an insulating layer to reduce the heat transfer from the flame to the combusting product. Phosphorous compounds that decompose to give phosphoric acid and intumescent systems operate by this mechanism (EPA, 2005).

Flame retardants are categorized as either additive or reactive. Additive flame retardant chemicals can be added to a manufactured product without bonding or reacting with the product. They are incorporated and dispersed evenly throughout the product, but are not chemically bound to it. Reactive flame retardant chemicals may be incorporated into the product during manufacture of the plastic raw materials. They are chemically bound to the raw materials that are used to make the final product. Additive and reactive flame retardant chemicals can be utilized in any of the mechanisms previously discussed, depending on the specific chemical. Most flame retardants are used as additive flame retardants, they react when heated and either emit substances that displace the oxygen needed for a fire to burn, form a protective coating on the surface of a flammable substrate, thereby limiting access of the fire to fuel sources, or do a combination of both. Additive flame retardants used in foam and other plastics are typically incorporated after manufacture of the polymer and during the manufacture of the end product. Reactive flame retardants are chemically bound to polymer products either by incorporating them into the polymer backbone during the polymerization reaction or by grafting them onto it (EPA, 2005).

This prevents them from bleeding out of the polymer, and their fire retardancy is thus retained. They have no plasticizing effect and do not affect the thermal stability of the foam structure (Singh et al., 2009).

A combination of reactive and additive fire retardants produces a synergistic effect (Singh et al., 2009). Reactive flame retardants are chemically bound to polymer products either by incorporating them into the polymer backbone during the polymerization reaction or by grafting them onto it. The presence of a synergist can dramatically increase the flame retardant's effectiveness, lowering the quantity of the flame retardant needed to meet the required standard. Since high levels of flame retardants often affect product quality, a synergist to reduce the amount of flame retardant is often used (EPA, 2005).

Synergists have achieved great importance because they are less expensive than actual fire retardants, and the addition of reactive fire retardant can be greatly reduced in the presence of a synergist, without any reduction of the fire-retardant effect (Singh et al., 2009).

For the extinguishing of accidental fires, water is always assumed as the ideal fire extinguishing material, but in the case of polyurethane foams it cannot be used because PU foams are an insulating material, and can react with pyrotechnic combustion products. In order to act as a flame retardant material, extinguishing powder can be added to the polyurethane solution system, but this kind of materials must be selected as a function of the burning material. Each extinguishing agent is adapted to one or more types of fires in different materials. It is advisable to select the extinguishing agents as a function of the burning material. There are polyvalent powder (ammonium dihydrogen phosphate), special powder (sodium chloride or talc, etc.), and normal powder (sodium bicarbonate or potassium) (Marques et al., 2013).

For this work was chosen the sodium bicarbonate as a flame retardant, because from all types of flame retardants this one belongs to the category that can reduce the flame in the kind of inflammation studied. In this particular case, the flame retardant material is based on sodium bicarbonate particles mixed in the original polyurethane material that is due to its influence on combustion temperatures. However, it has been proved that this kind of retardant flame particles loses its properties over long time period and there is a lack of knowledge how this process can occurs (Marques et al., 2013).

2.3.1. Sodium Bicarbonate

Fire suppression mechanisms of alkali bicarbonate particles, for example, sodium bicarbonate ($NaHCO_3$), have received considerable attention recently. From previous

studies it was evident that particle delivery rate and calibration are major obstacles in experiments, and, perhaps, the major cause for the experimental uncertainties observed. Another major factor that can contribute to experimental uncertainty, especially in low resident time flames, is the particle heating rate (which is directly related to the initial particle size and the flame structure) and the subsequent decomposition process (Chelliah et al., 2003).

$$NaHCO_3 \rightarrow 0.5Na_2CO_3 + 0.5CO_2 + 0.5H_2O \quad (7)$$

$$Na_2CO_3 \rightarrow Na_2O + CO_2 \quad (8)$$

$$Na_2O + H_2O \rightarrow 2NaOH \quad (9)$$

$$NaHCO_3 \rightarrow NaOH + CO_2 \quad (10)$$

$$NaOH + H \rightarrow H_2O + Na \quad (11)$$

$$Na + OH + M \rightarrow NaO — H + M \quad (12)$$

$$NaOH + OH \rightarrow H_2O + NaO \quad (13)$$

Thermal decomposition of SB particles is known to occur in two stages. However, the details and rates of these decomposition stages are not well established. In the first stage (reaction 7), SB decomposes to form solid sodium carbonate (Na_2CO_3) (Chelliah et al., 2003).

The particle temperature at which the first decomposition reaction occurs is not unique and is known to vary from 370 to 543 K, depending on the particle heating rate (for example, smaller particles are expected to heat rapidly when exposed to the flame environment, because of their higher surface area and volume ratios). In the second stage, (Na_2CO_3) is known to decompose/evaporate at 1123 K, leading to formation of liquid sodium oxide (Na_2O) and carbon dioxide (CO_2) (reaction 8), followed by the homogeneous reaction (9) to form sodium hydroxide (NaOH) (Chelliah et al., 2003).

The disodium oxide formed promotes catalytic recombination of the radical species that are needed for flame propagation, causing the flame to extinguish. As indicated earlier, the present bibliographic study is addressed to understand the effect of sodium bicarbonate particle size on flame extinction (Chelliah et al., 2003).

Although finite-rate reaction models have been proposed for the decomposition of SB, a finite-rate kinetic model was also developed for the overall decomposition of SB particles (reaction 10). As a first-step, a similar single-step global reaction model, but assuming fast decomposition of $NaHCO_3$ at a prescribed decomposition temperature

(between 543 and 1123 K), is studied here. Once the alkali hydroxide is formed, the catalytic radical scavenging cycle (reactions 11 to 13) is known to interact with homogeneous chemistry of the flame and be responsible for reduction of the radical pool (Chelliah et al., 2003).

The methane oxidation model employed includes 16 species in 39 elementary reactions, while the homogeneous chemistry model associated with Na species includes four additional species (Na, NaO, NaO_2, and NaOH) in 14 elementary reactions (Chelliah et al., 2003).

Although, there is a lack of knowledge about their phenomenological contribution in local PU flame propagation, sodium bicarbonate was mixed with polyurethane as a retardant flame material, due to its thermal decomposition, because it is produced water, when heated, that has the capacity to reduce temperature by consuming energy. (Marques et al., 2013).

2.4. Paint

In order to study the differences in ignition of polyurethane foams in different conditions, research was carried out on different kinds of paints that could be used to paint polyurethane foams. The cellulosic aluminium paint was chosen due to its components properties. The combustion of paints was previous described, as it seems to have a fundamental contribution in the *Hindenburg* disaster.

2.4.1. Aluminium

Cellulosic aluminium paint is a product that is applied with ease and good lacquer properties. It has good covering power, capable of producing an aluminium film with good weather resistance properties. It is a product designed for the industrial sector, and can be used in automotive refinishing jobs and used to paint polyurethane. Aluminium is sometimes added to increase the sensitiveness of explosives. Cellulosic aluminium paint can be a potential oxidant; this product have a very complex composition: toluene, xylene (isomers mixture), ethyl acetate, n-butyl acetate, acetone, isopropyl alcohol (isopropanol), light aromatic solvent naphtha (petroleum), ethyl alcohol (ethanol),

methyl ethyl ketone, aluminium powder, naphtha (petroleum), hydrotreated heavy (Barbot, 2012).

The components in highest quantity are toluene and xylene, which are both highly flammable, and are examples of organic compounds that evaporate readily to the atmosphere, the so called VOCs as characterised by the Environment Protection Agency (EPA). Toluene, xylene, and other secondary petrochemicals from various sources are pollutants that threaten human health (Pinto et al., 2012).

The other component is aluminium powder that can be found in explosives as fuel. It can be explosive when added to ammonium or potassium perchlorate, barium peroxide and magnesium powder and potassium permanganate and icing sugar. The mixture of aluminium and iron oxide powders generates enormous quantities of heat and is known as thermite (Brousseau et al., 2002).

Aluminium powder is a common ingredient in energetic materials. The aluminium is used to increase the energy and raise the flame temperature in rocket propellants. It is also incorporated in explosives to enhance air blast, increase bubble energies in underwater weapons, raise reaction temperatures and create incendiary effects. In explosives, it is generally assumed that combustion of aluminium particles occurs behind the reaction front (during the expansion of the gaseous detonation products), so that the particles do not participate in the reaction zone, but rather act as inert ingredients (Brousseau et al., 2002).

CHAPTER 3 – THEORETICAL APPROACH

3.1. THOR – Theoretical combustion prediction

The existing reactions in pyrolysis, combustion or detonation processes, generating intermediary chemical species and compounds, are very hard to follow by experiments, because these processes are very fast and proceed with increasing pressure and temperature. Studies concerning theoretical prediction of the probable pathways of pyrolysis or thermal decomposition of energetic materials are not numerous (Durães et al., 1998).

Design and production of energetic materials, propellants and explosives, requires the prediction of the thermodynamic properties of their combustion products. Theoretical prediction codes of combustion products properties are based in thermodynamic equilibrium of products for the minimum value the Gibbs free energy (Durães et al., 1995).

The method, here presented, of predicting reaction path and final compositions of combustion products, as function of temperature and pressure, uses a thermochemical computer code, named THOR (Durães et al., 1997).

THOR code is based on theoretical work of Heuzé et al., 1985, 1989, later modified by Campos, 1991, and Durães et al., 1995, in order to calculate the composition and thermodynamic properties of combustion products, assuming an isobar or isochor adiabatic combustion, or a Chapman-Jouguet detonation (Durães et al., 2000).

The reaction path is estimated for all the possible compounds, as a function of temperature and pressure, for the minimum Gibbs free energy, at thermodynamic equilibrium. In the THOR code, several equations of state may be used, namely Perfect Gas, Boltzmann, BKW, H_9, H_{12} and H_L. (Durães et al., 1998).

The prediction of combustion temperature and products was made using THOR code in the condition of isobaric combustion using the equation of state H_L.

This equation takes the general expression:

$$\frac{PV}{nRT} = \sigma(V, T, X_i)$$

where V represents the volume, T the temperature and X_i the mole number of i compound in reaction gaseous products. The second term, σ, presented by Heuzé et al., 1985, for H_α equations of state, is a fifth order polynomial obtained from virial expansion. It represents very well the behaviour of gaseous mixtures at high temperature and pressure:

$$\sigma(V,T,X_i) = 1 + x + 0.625x^2 + 0.287x^3 - 0.093x^4 + 0.014x^5$$

with,

$$x(V,T,X_i) = \frac{\Omega}{VT^{3/\alpha}}$$

$$\Omega = \sum_{i=1}^{s} X_i \omega_i$$

The term α represents the exponent of the repulsive part of the intermolecular potential. Heuzé et al., 1985, has proposed for α the values 9 and 12 (to deduce H_9 and H_{12} equations of state), based on theoretical and experimental final correlations. This parameter has great influence on the results and the preceding values are too low to represent the detonation gaseous products, which co-exist in equilibrium at very high pressure. In H_L equation of state, the intermolecular potential function considered is the Buckingham α-exp-6 function, where α takes the value 13.5 (Durães et al., 1995).
The ω_i values are dependent of each gas component,

$$x = \frac{\sum_{i=1}^{n} X_i \omega_i}{VT^{3/\alpha}}$$

and considering the Boltzmann EoS, this can be rewritten:

$$\frac{\sum_{i=1}^{n} X_i \omega_i}{VT^{3/\alpha}} = \frac{\sum_{i=1}^{n} X_i B_i}{V}$$

where B_i is the covolume of component i in reaction products. This is a valid procedure because, at low densities, the terms of higher order (fourth and fifth) in s expression are negligible, and then, numerically, H_L EoS reduces to a Boltzmann EoS (Durães et al., 1995).

Using a simplified rigid sphere model:

$$B_i = \frac{2}{3}\pi r_{0i}^3 N_{AV}$$

where r_{0i} is the intermolecular distance at minimum value of the intermolecular potential and N_{AV} the Avogadro number, can be obtained:

$$T = \theta \frac{\varepsilon}{k}$$

In these equations, θ is the adimensional temperature, k the Boltzmann constant ($k = 1.380\text{x}10^{-23}$ J.K^{-1}) and r_{0i} and ε_i/k the parameters of the Buckingham α-exp-6 intermolecular potential function, for each reaction gaseous product in the pure state (Durães et al., 1995).

Four calculating clusters are used in THOR code:

(i) the conservation equations (mass, atomic species, momentum and energy), being the thermodynamic equilibrium for $G = G_{min}$ (P, T, X_i), applying to the condensed phase the model proposed by Tanaka, 1983, or the equivalent function proposed by Gordon and McBride, 1994;

(ii) the thermal equation of state (EoS), using generally the H_L EoS (Durães et al., 1995);

(iii) the energetic equation of state, related to the internal energy $E = \sum X_i e_i(T) + \Delta e$, $e_i(T)$ being calculated from JANAF Thermochemical Tables, 1971, and polynomial expressions of Gordon and McBride, 1994;

(iv) the combustion condition regime, assumed like an isobare or isochore adiabatic combustion.

The thermodynamic modelling conditions are based on the calculation of the thermodynamic properties of the products of combustion, first, of a theoretical adiabatic combustion, assuming *P* and *T* conditions, and secondly, evaluating the decomposition reaction path, based in heat losses to the exterior (Durães et al., 1996).

The isobar adiabatic combustion is the basic theoretical combustion condition where $dP = 0$ and $dQ = 0$ imply $dH = 0$; this means that equal initial and final total enthalpy ${H_b}^{T_b} = {H_0}^{T_0}$. This expression is equivalent to ${H_b}^{T_b} - {H_b}^{T_0} = -\left({H_b}^{T_0} - {H_0}^{T_0}\right)$, also equivalent to $H_b|_{T_0}^{T_b} = -\Delta_r^{T_0} H$ (the total enthalpy from burned gases is equal to the module of the enthalpy of reaction). Considering now a global isobar adiabatic process, formed by one reactive system enclosed in a non resistant wall, working like an enthalpy absorber of value ΔH, the preceding equation takes the form $H_b|_{T_0}^{T_b} + \Delta H = -|\Delta_r^{T_0} H$, where the enthalpy of reaction is distributed to the heated burned gas and the wall, considering always $P = P_0$. Consequently, it is possible to consider $T_0 < T_1 < T_b$. The corresponding products composition can then be changed from the "basic" chemical components, when $T_1 = T_0$, to the final components, when $T_1 = T_b$, isobar adiabatic combustion temperature with the preceding condition. The Gibbs free energy, taking its minimum relative value for a (V, T ,X_i) group, is also reduced with increasing values of T_1, from T_0 to T_b (Durães et al., 1996).

Chemical equilibrium conditions: A classical combustion system is generally a CHNO system. It is possible to consider up to *m* atomic species and form *n* chemical components. The mass balance yields a linear system involving *m* equations. The *n-m* equilibrium equations, necessary to solve the problem, are determined by the method of Lagrange multipliers or the equilibrium constants. To determine the chemical concentration of *n* components, for imposed P and T conditions, the chemical affinity method, proposed by Heuzé et al., 1985, can be used, or the equations solved first the system composed by the *m* basic components, and secondly adding one by one more components, optimising the relative concentration inside the group related to the same atomic species, for the minimum value of global Gibbs free energy, $G = \sum x_i \mu_i$, whit the Gibbs free energy of each component being $\mu_i = G_{0i}(T) + RT \ln P + RT \ln(x_i)$ (Durães et al., 1996).

For a classical CHNO system an equilibrium composition is assumed of CO_2, H_2O, N_2, H_2, OH, CO, NH_3, O_2, NO, NO_2, H, C, N, O, CH_4, CH_2O_2 gases and two kinds of solid

carbon (graphite and diamond). In our case the Na element of sodium bicarbonate has been introduced in some pyrotechnic mixtures (Durães et al., 1997).

The selection of the Na components was made based on the decomposition equations of sodium bicarbonate found in the literature (Chelliah et al., 2003).

Thus, for our system $m = 5$, it was added the components Na_2CO_3, Na_2O, NaOH and NaO to the classical CHNO system components.

3.1.1. THOR results

These THOR predicting calculations took into account the combustion of the presented mixtures in air. Consequently, the equivalence ratio will take into account air concentration: the first calculations were calculated for an equivalence ratio from 0.8 to 1.5, for a constant concentration of polyurethane (plus polyethylene in the case of syntactic foam), changing the concentration of air. The calculations for the syntactic foam were performed for a constant ratio of polyurethane/polyethylene (85/15 %).

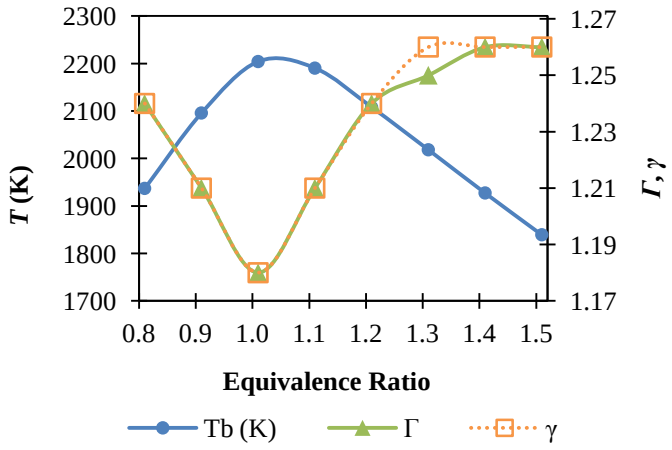

Figure 25 – Calculated values of *Tb*, *Γ* and *γ* as a function of *r* (equivalence ratio), for PU and air mixtures.

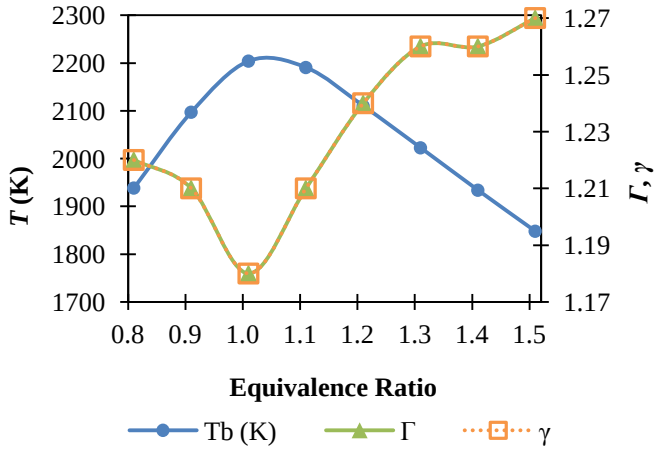

Figure 26 – Calculated values of *Tb*, *Γ* and *γ* as a function of *r* (equivalence ratio), for PU/PE and air mixtures.

Calculated results show the maximum calculated combustion temperatures (*Tb* ≈ 2200 K and for *r* = 1.0, showing *Γ* = *γ* = 1.18) for both kinds of foams (expanded polyurethane foam - Figure 25; syntactic polyurethane foam - Figure 26). Products composition as a function of isobare adiabatic combustion temperature for PU-air mixtures and for PU/PE-air are presented in Figure 148 and 149 (in Appendix A), respectively.

The mixtures of the maximum *Tb* values were recalculated adding increasing quantities of sodium bicarbonate (SB) and ammonium nitrate (AN).

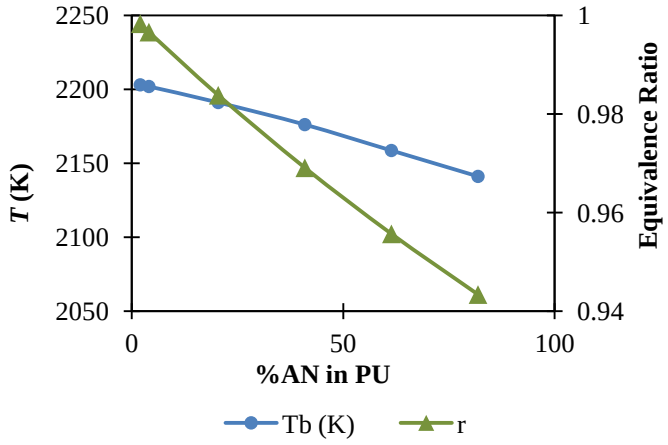

Figure 27 - Calculated values of *Tb* and *r* (equivalence ratio) as a function of % of AN in PU, for PU/AN and air mixtures.

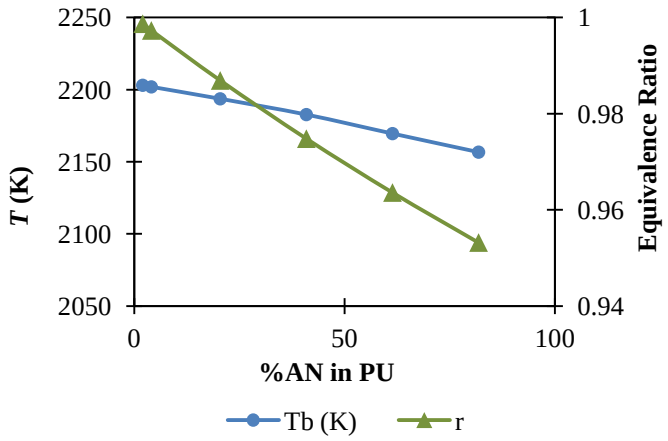

Figure 28 – Calculated values of *Tb* and *r* (equivalence ratio) as a function of % of AN in PU, for PU/PE/AN and air mixtures.

Small quantities of AN do not really increase calculated Tb. Strong AN concentrations decrease *Tb* values. Syntactic PU foams (Figure 28) have similar behaviour to the expanded PU foams (Figure 27) but the influence of AN concentrations is lower because this kind of mixtures have polyethylene as a supplementary combustible.

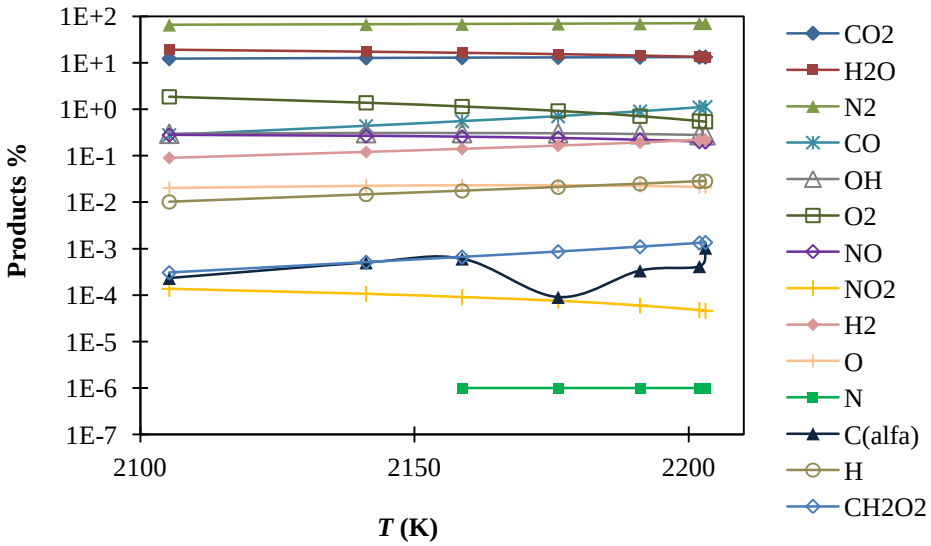

Figure 29- Products composition as a function of isobare adiabatic combustion temperature, for PU/AN and air mixtures.

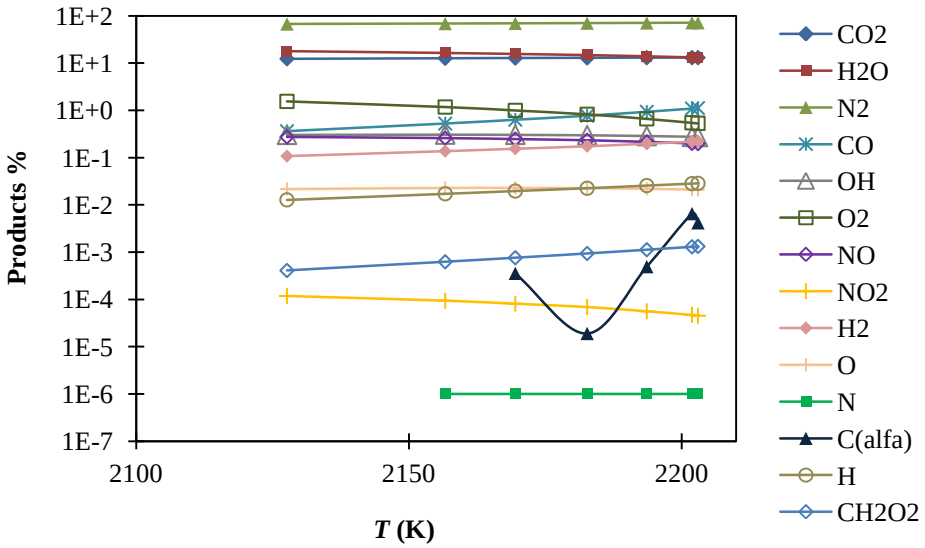

Figure 30 - Products composition as a function of isobare adiabatic combustion temperature, for PU/PE/AN and air mixtures.

In Figure 29 and 30 are represented the percentage of the products obtained for the isobare combustion of expanded and syntactic PU foams with AN and air mixtures.

In Figure 150 to 153 (in Appendix A) it is presented the same calculation that was made in Figure 27 to 30, but instead of ammonium nitrate, it was calculated with sodium bicarbonate. It was concluded that the addition of SB in high, with percentage almost equal to the percentage of polyurethane, the combustion temperature reaches 400 K and that the only product with Na was NaOH.

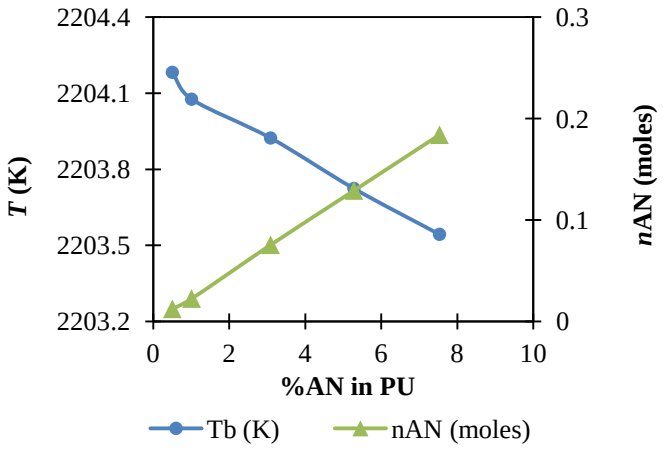

Figure 31 – Obtained values of *Tb* and number of moles of AN as a function of % of AN, for PU/AN and air mixtures.

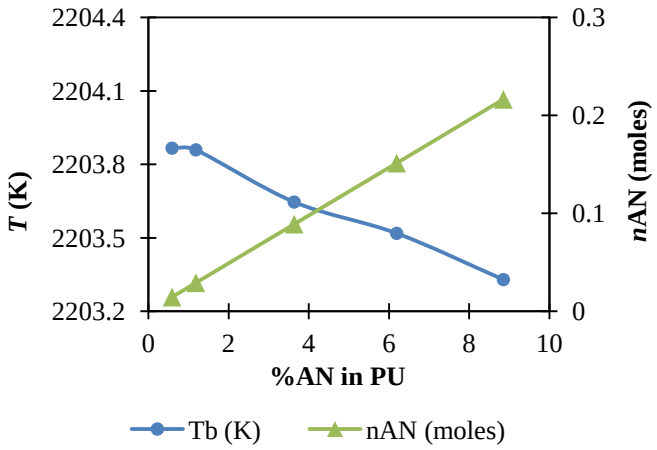

Figure 32 – Obtained values of *Tb* and number of moles of AN as a function of % of AN, for PU/PE/AN and air mixtures.

Figure 31 and 32 show results for mixtures of expanded and syntactic foams of $r = 1$ and different percentages of ammonium nitrate in polyurethane: 0.5, 1, 3, 5 and 7 %. It is seen that the combustion temperature decreases when the quantities of AN are higher and that the expanded foam has higher values of temperature than the syntactic foam. In the small range of temperature studied, the obtained products are the same.

Products composition as a function of isobare adiabatic combustion temperature for polyurethane, air and ammonium nitrate mixtures, and for polyurethane/polyethylene, air and ammonium nitrate mixtures are shown in Figure 154 e 155 (in Appendix A), respectively.

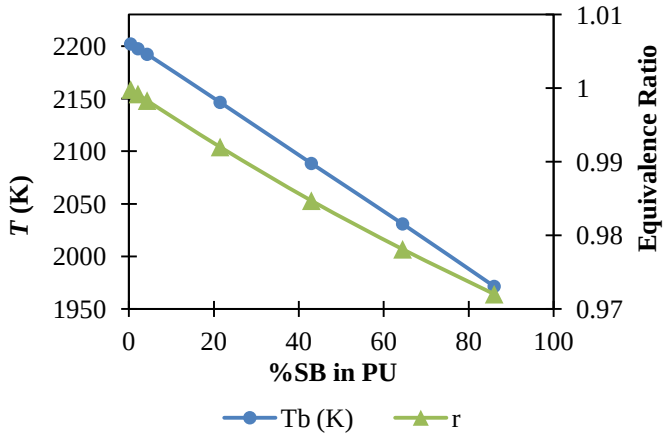

Figure 33 – Obtained values of *Tb* and *r* as a function of % of SB in PU, for PU/7 %AN (in PU) and air mixtures.

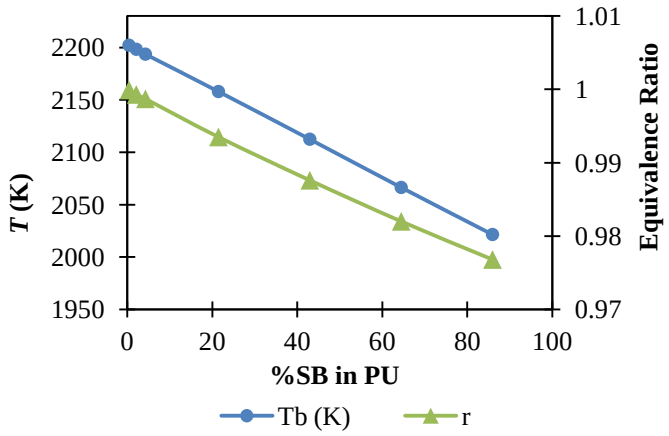

Figure 34 – Obtained values of *Tb* and *r* as a function of % of SB in PU, for PU/PE/7 %AN (in PU) and air mixtures.

In the case of the expanded foam (Figure 33) it was observed that the addition of sodium bicarbonate affects the combustion temperature of the mixture by lowering it. Small quantities of SB have low impact in the difference of the *Tb*. The same happened in the case of the syntactic foam (Figure 34).

The equivalence ratio value decreases in both foams, but the impact is higher in the expanded PU foam, because this does not have the presence of polyethylene, and the addition of SB increases the number of atoms of oxygen in the mixture.

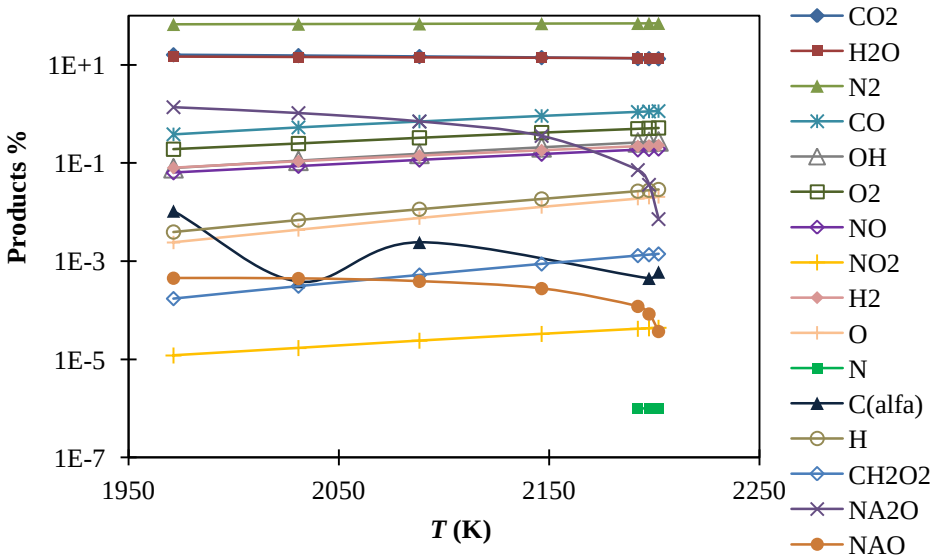

Figure 35 – Products composition as a function of isobare adiabatic combustion temperature, for PU/7 %AN (in PU)/air and SB mixtures.

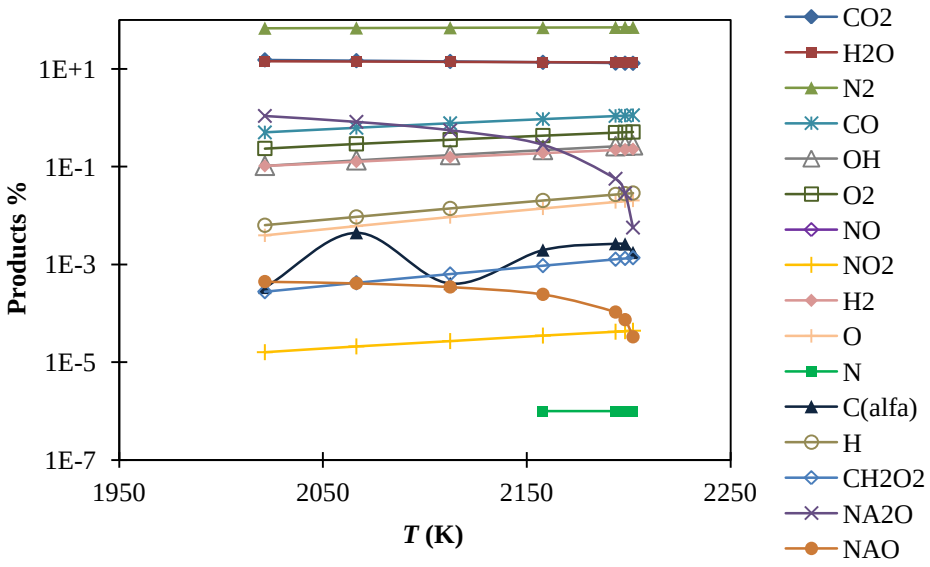

Figure 36 - Products composition as a function of isobare adiabatic combustion temperature, for PU/PE/7% AN (in PU)/air and SB mixtures.

Although there is no significant difference in the temperature values the products obtained are the same and approximately at the same proportion, the addition of SB leads to new products, NaO and Na_2O. This is seen in Figure 35 and 36.

From Figure 156**Error! Reference source not found.** to Figure 171**Error! Reference source not found.** (in Appendix A) it is shown the effect of different quantities of sodium bicarbonate, to expanded and syntactic foams with 0.5, 1, 3 and 5 % of ammonium nitrate. There is no big difference in the temperature values, but it is constant that in expanded foam the temperature is always lower than the syntactic foam. The products obtained, are always the same at the same proportion.

3.2. Prediction of temperature and ignition delay

3.2.1. Semenov model of thermal ignition

Semenov developed a model for thermal explosions, which demonstrated the principles of the thermal ignition phenomenon in a quantitative way. The thermodynamics within the system leads to a heat production term and a heat loss term (Wheatley, 2003).
When the heat flux and the heat production fluxes are graphically represented in a plot of heat flux against temperature, the following three cases can arise (Wheatley, 2003).

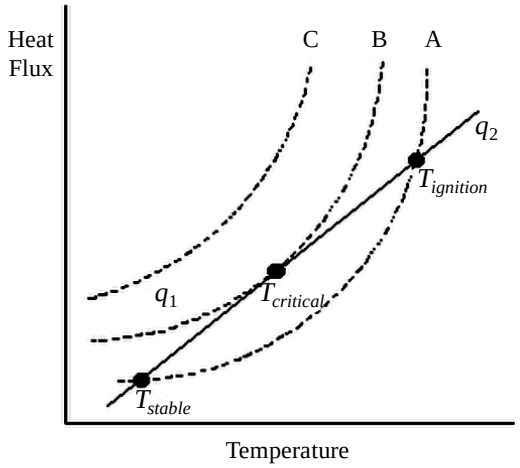

Figure 37 - Plot of the thermal fluxes against temperature (adapted from Wheatley, 2003).

Curves A, B and C are the heat gain curves (q_1). The straight line (q_2) that crosses the curves is the heat loss (Wheatley, 2003).
Curve A: The heat production is less than the heat lost. The reactants enter into the system at a low temperature and, because the heat production curve lies above the heat loss curve, they proceed to heat up until the temperature reaches the T_{stable}. Because this temperature is said to be a stable temperature, no further self-heating will take place, with the temperature remaining constant around this stable temperature. If the reactants in the system are now heated by some external source, then the temperature within the system will rise. If the temperature reaches $T_{ignition}$, which is an unstable point, and becomes greater than $T_{ignition}$ then the system becomes unstable and thermal runaway will occur. If however the external heat source is removed, then the reactants should

begin to drop in temperature and return back to T_{stable}, where the system will become stable again (Wheatley, 2003).

Curve B: The heat production is the same as the heat lost. This is the most important of the three curves in Figure 37. The three temperatures T_{stable}, $T_{critical}$, and $T_{ignition}$ are all at the same temperature. The heat loss curve is tangential to the heat gain curve. The temperature of the reactants in the system will slowly rise up to the critical temperature; at which point a rapid acceleration of the temperature will occur resulting in a thermal explosion (Wheatley, 2003).

Curve C: The heat production is greater than the heat lost. As can be seen from Figure 37, this curve is always going to have a heat gain flux that is always exceeding the heat loss flux. Therefore at whatever temperature the reactants are in the system, then a thermal explosion will take place (Wheatley, 2003).

The Semenov theory provides an easy method for calculating the critical temperature $T_{critical}$. (Bandyopadhyay et al., 1972).

$$q_1 = I_p \beta \rho_O \frac{273}{T_g} \left[\frac{0.01.[O_2]}{\frac{1}{Ae^{-E_a/RT_p}} + \frac{\lambda}{D_O \left(\frac{T_g}{273}\right)^2 Nu_\lambda}} \right]$$

$$q_2 = h\left(T_p - T_g\right) + \sigma\left(T_p{}^4 - T_g{}^4\right)$$

Equations of S. Bandyopadhyay and Bhaduri. In the system of equations:

$$q_1 \Big|_{T_i} = q_2 \Big|_{T_i}$$

$$\frac{dq_1}{dT} \Big|_{T_i} = \frac{dq_2}{dT} \Big|_{T_i}$$

by replacing q_1 and q_2 by the expressions above described, is obtained the system:

$$\begin{cases} I_p \beta \rho_O \dfrac{273}{T_g} \left[\dfrac{0.01.[O_2]}{\dfrac{1}{Ae^{-E_a/RT_p}} + \dfrac{\lambda}{D_O \left(\dfrac{T_g}{273}\right)^2 Nu_\lambda}} \right] = h(T_p - T_g) + \sigma({T_p}^4 - {T_g}^4) \\ I_p \beta \rho_O \dfrac{273}{T_g} \left\{ \dfrac{0.01.[O_2]}{\left[\dfrac{1}{Ae^{-E_a/RT_p}} + \dfrac{\lambda}{D_O \left(\dfrac{T_g}{273}\right)^2 Nu_\lambda} \right]^2} \right\} \dfrac{E_a e^{E_a/RT_p}}{A{T_p}^2} = h + 4\sigma {T_p}^3 \end{cases}$$

In this system the two unknown T_g and T_p are, to diameter λ given, linked by two relations of the form:

$$F(T_g, T_p) = 0$$

$$G(T_g, T_p) = 0$$

3.2.2. Prediction results

Numerical solutions were performed with *Excel* and the values of the constants used in the calculation are given in Table 10 (in Appendix B). The solution can be found by looking in the intersection of the curves *F* and *G* (Bandyopadhyay et al., 1972).

The method of finite differences was used, taking independent variable T_g from value T_{g_0} = 298 K and not a set of 1 K. It was tested for T_p 100 K higher than T_g because when the difference was only 1 K it was almost impossible to spot the differences. When the difference between both temperatures was 50 K, the differences were still very difficult to spot, which is why ΔT = 100 K was chosen.

There are sensitivities from the value of convective heat transfer coefficient (*h*) that can be obtained from the Nusselt number (*Nu*), and depends on the thermal conductivity (k_f) value which is obtained from the expression given in the literature, and on the diameter of the particle.

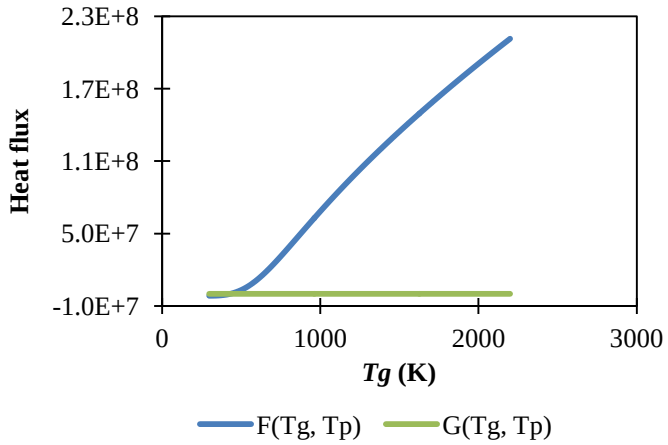

Figure 38 – Obtained plot of the thermal flux against temperature.

The curves *F* and *G* are tangential to each other. In addition, in this case, where the fuel is solid, the T_{g_l} upper limit of this zone, is well defined, because the two functions (*F* and *G*) after converging, diverging rapidly for $T_g > T_{g_l}$ values. (This indicates that $q_1 > q_2$, it means that the ignition has occurred). Figure 38 shows the heat flux vs. T_g for $F(T_g, T_p)$ and $G(T_g, T_p)$ for $\lambda = 3.51 \times 10^{-6}$ m. It was obtained $T_g = 434$ K and $T_p = 534$ K.

The solutions (T_g, T_p) obtained as a function of λ represent the minimum temperature desired in the gas to the particle can be currently ignited, and also the temperature of the particle, when ignited (Bandyopadhyay et al., 1972).

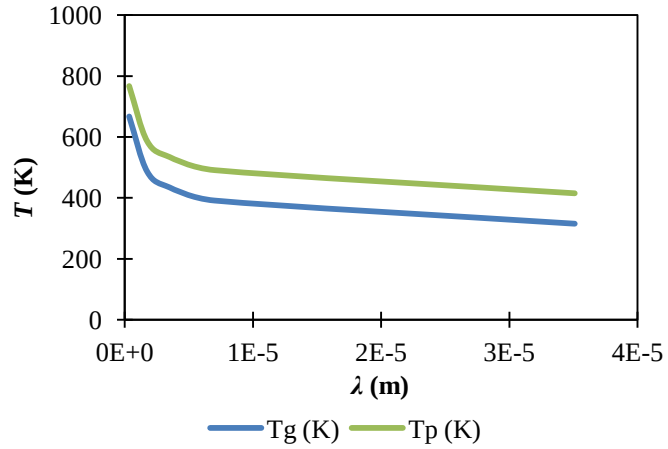

Figure 39 - Temperatures obtained for different particle diameters.

Figure 39 shows the temperatures obtained for different particle diameters. Diameter values studied and the obtained temperatures are presented on Table 1.

Table 1 – Values of *Tg* and *Tp* obtained for different diameters.

λ (m)	*Tg* (K)	*Tp* (K)
1.76×10^{-7}	795	895
3.51×10^{-7}	667	767
1.76×10^{-6}	486	586
3.51×10^{-6}	434	534
7.02×10^{-6}	391	491
3.51×10^{-5}	315	415

It can be concluded that the higher the diameter, the lower is the temperature's particle. That is due to the fact that particles with lower diameter have higher surface area.

3.2.3. Frank-Kamenetskii phenomenological approach

The Frank-Kamenetskii theory allows the temperature and time gradient to be taken into account. This is where there could be a considerable resistance to heat transfer in the reacting system, or the system has reactants with a low thermal conductivity and the system having highly conducting walls (Wheatley, 2003).

The heat balance of the particle is given by the equation:

$$\frac{1}{6}\lambda\rho C_p\frac{dT_p}{dt} = I_p\beta\rho_O\frac{273}{T_g}\left[\frac{0.01.[O_2]}{\frac{1}{Ae^{-E_a/RT_p}} + \frac{\lambda}{D_O\left(\frac{T_g}{273}\right)^2 Nu_\lambda}}\right] - h(T_p - T_g) - \sigma({T_p}^4 - {T_g}^4)$$

The integration of this equation was made of the form:

$$\frac{dT_p}{dt} = H(T_g, T_p, \lambda)$$

The evolution was made as a function of the time *t* and the temperature T_p of the particle.

The particle of diameter λ initially at temperature T_{p_0} = 298 K, was brought in contact with hot air in the instant $t = 0$ at constant temperature T_g. Time of ignition, t_i, for a particle with diameter λ, in air at T_g, is obtained during the previous integration, $T_p = T_{p_l}$ (Bandyopadhyay et al., 1972).

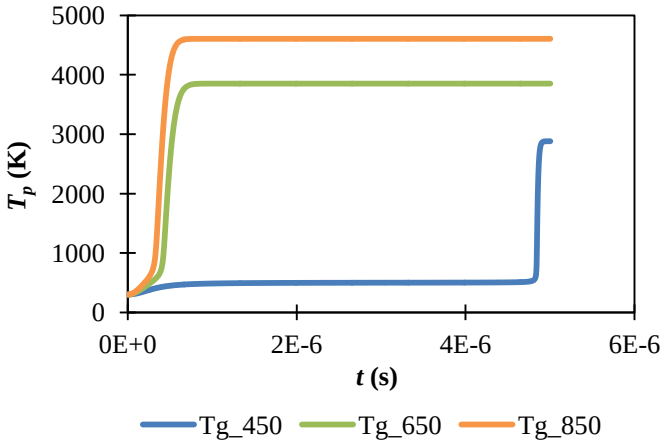

Figure 40 – Time vs. ignition temperature, at different oven temperatures.

This calculation was made for several air temperatures, always with ΔT = 100 K, at the same diameter, λ = 3.51 x 10^{-6} m. Figure 40 shows the time that it takes to ignite a sample, for different values of T_g.

It is observed that the previous system must have the solution $t_i = \infty$ limit, when $T_g = T_{g_l}$, so that the t_i function of T_g, for a given particle diameter λ must have a vertical asymptote for $T_g = T_{g_l}$.

For ΔT = 100 K values of T_g and T_p were obtained, which gave rise to certain values of k_f and h. This results in the same values of heat transmission for q_1 and q_2, which means that there is an inversion in the heat transmission with the same parameters.

It was predicted, for gas environmental temperature of 450 K, that the particle takes 5 x 10^{-6} s to ignite. For T_g = 650 K the particle takes 4 x 10^{-7} s to ignite, and for 850 K takes 3 x 10^{-7} s. The higher the T_g, the faster is the ignition of the particle .

CHAPTER 4 – MATERIALS CHARACTERISATION AND PROCEDURES

4.1. Thermal methodology

4.1.1. Differential Scanning Calorimetry (DSC) and Thermo-Gravimetric Analysis (TGA)

Differential scanning calorimetry (DSC) is a thermal technique that provides information about thermal changes in different kinds of materials (Gabbott, 2008).

A DSC analyser measures the energy changes that occur as a sample is heated, cooled or held isothermally, together with the temperature at which these changes occur. The energy changes give the possibility to find and measure the transitions that occur in the sample quantitatively, and to note the temperature where they occur. One of the big advantages of DSC is that samples are very easily encapsulated, usually with little or no preparation, ready to be placed in the DSC, so that measurements can be quickly and easily made (Gabbott, 2008).

The main property that is measured by DSC is heat flow, the flow of energy into or out of the sample as a function of temperature or time, and usually shown in units of $J.s^{-1}$.

Traditionally, with heat flux systems endotherms are shown as going down, since endothermic transitions result in a negative temperature differential. The value of measuring energy flow is that it allows the identification of the range of different transitions that may occur in the sample as it is heated (Gabbott, 2008).

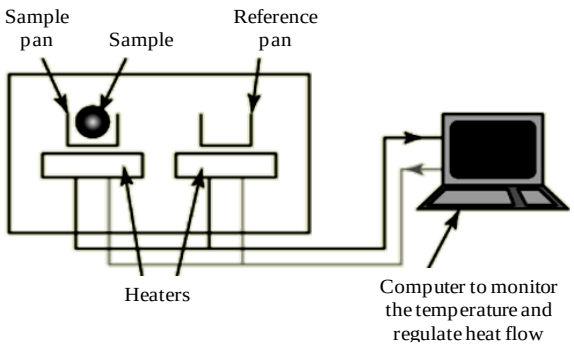

Figure 41 - Schematic principle of DSC measurement (adapted from Tarr, 2012).

Heat flux DSC involves a single furnace design with a temperature sensor (or multiple sensors) for each of the sample and reference pans located within the same furnace (Figure 41). Sample and reference pans are placed in their required positions and the furnace heated at the pre-programmed heating rate. When transitions in the sample are found, a temperature difference is created between sample and reference. On continued heating beyond the transition this difference in temperature decreases as the system reaches equilibrium in accordance with the time constant of the system. The difference in temperature or Δt signal is the basic parameter measured. Modern analysers are carefully calibrated so that the Δt signal is converted to a heat flow equivalent and this is displayed as a function of temperature or time (Gabbott, 2008).

The starting temperature should be well below the beginning of the first transition that is to be measured in order to see a clear flat baseline. This should take into account the period of the initial transient where the scan rate is not yet fully controlled and the baseline is not stable. With ambient DSC systems the starting temperature is often around 30 ºC. The upper temperature should be below the decomposition temperature of the sample. Decomposing a material in a DSC normally gives rise to a very noisy drifting response and the evolved volatiles will contaminate the system. It is good practice to establish the decomposition temperature first using a TGA analyser if available (Gabbott, 2008).
DTA (differential thermal analysis) is quite similar to DSC, but the measurement was performed to just one oven with the thermocouple system.

Thermo-gravimetric analysis (TGA) is an experimental technique in which the weight or the mass of a sample is measured as a function of sample temperature or time. In Figure 42 a scheme with the principle of TGA measurement is represented. The sample is typically heated at a constant heating rate (so-called dynamic measurement) or held at a constant temperature (isothermal measurement), but may also be subjected to non-linear temperature programs such as those used in sample controlled TGA experiments (Bottom, 2008).

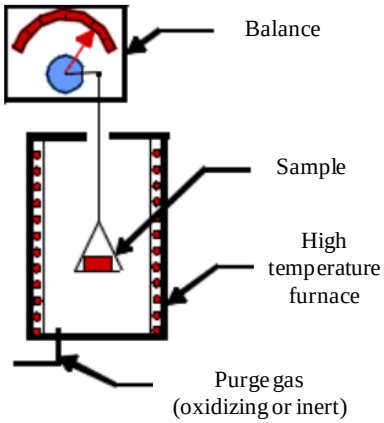

Figure 42 - Schematic principle of TGA measurement (adapted from Tarr, 2012).

The choice of temperature program will depend upon the type of information required about the sample. Additionally, the atmosphere used in the TGA experiment plays an important role and can be reactive, oxidising or inert. Changes in the atmosphere during a measurement may also be made. The results of a TGA measurement are usually displayed as a TGA curve in which mass or percent mass is plotted against temperature or time. Mass changes occur when the sample loses material in one of several different ways or reacts with the surrounding atmosphere. This produces steps in the TGA curve. Different effects can cause a sample to lose, or even gain, mass and so produce steps in the TGA curve (Bottom, 2008).
Various reactions may be included the thermal decomposition in an inert atmosphere with the formation of gaseous products, in which the case with organic compounds, this process is known as pyrolysis or carbonisation (Bottom, 2008).

DSC-TGA have advantages over other analytical methods, a sample can be studied over a very wide range of temperatures, using various heating programs; it is possible to study a sample in almost all the physical state (liquid, solid) using the appropriate accessories; the quantities tested are minimal (0.1 μg - 400 mg), although this fact may be mentioned as a disadvantage in the case of scale effect is important; the atmosphere is controlled, test conditions may be easily repeated; the time required for testing the material under study is relatively small and may take from a few minutes to a few hours; taking into account the capabilities of the equipment, its purchase price is not too high (Hatakeyama et al., 1999).

Differential scanning calorimetry and thermogravimetric analysis were made using the *Rheometric Scientific STA 1500* apparatus. In order to perform reliable experiment with DTA, an appropriate pan type was selected.

Polyol thermogravimetric analyses were made at a heating rate of 5 ºC.min^{-1} under nitrogen atmosphere until 700 ºC and at a heating rate of 10 ºC.min^{-1} also under nitrogen atmosphere until 750 ºC.

Thermogravimetric analysis of hollow plastic microspheres was made at a heating rate of 10 ºC.min^{-1} under nitrogen atmosphere until 600 ºC.

4.1.2. Infrared Spectroscopy

IR spectroscopy is a very important technique that yields both qualitative and quantitative information above chemical nature of different kinds of compounds such as structural repeating units, end groups, and branch units, additives and impurities. IR spectroscopy is also sensitive to change in the dipole moments of vibration groups in molecules (Saetung, 2009).

A compound that has a covalent bond and a dipole moment can absorb frequencies of electromagnetic radiation in the infrared region. To absorb energy, the bond must have a dipole moment that changes at the same frequency as the incoming radiation. Different molecules absorb at different energies/frequencies and thus have different absorption patterns. The absorbed energy increases the amplitude of the vibrational motion, exciting the molecule to a higher energetic state (Leikvoll, 2011).

Generally, there are two kind of fundamental vibrations for molecules: stretching, in which the distance between two atom increases or decreases, but the atoms remain in the same bond axis, and bending (or deformation), in which the position of the atom changes relative to original bond axis (Saetung, 2009).

The FTIR instrument, (Figure 43) uses an interferometer for generation of a spectrum. A chopper or beam splitter divides the radiation from the infrared source in two equal parts. Half of the light hits a fixed mirror and half of it hits a mirror that is moving at high speed. The beams will be out of phase to each other when they meet again. They will then be recombined and the result will be an interference pattern where a specific wavelength is reinforced at a specific time depending on the position of the moving mirror. The radiation that goes through the sample will contain light of all wavelengths

but because of the reinforcing of wavelengths, depending on the moving mirror, the detection signal can be transformed to a spectrum where transmittance or absorbance are plotted against the wavelength (Leikvoll, 2011).

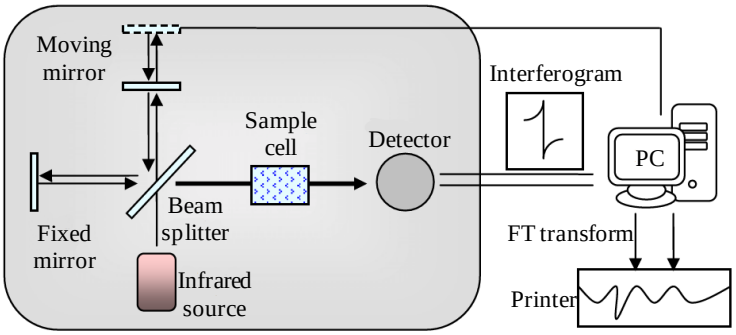

Figure 43 - Fourier transform infrared spectrometer (adapted from Leikvoll, 2011).

Benefits for FTIR as compared to a dispersive instrument are that a spectrum can be generated in a very short time, sometimes less than a second, and a mean can be calculated during series of measurements that improves the signal-to-noise ratio, and, hence, the sensitivity (Leikvoll, 2011).

Infrared spectra were recorded on a *Nicolet 6700 FTIR* Spectrometer, from *Thermo Scientific*, with a *DTGS (KBr)* detector, in the wavenumber range of 4000-400 cm^{1}.
Fresh and burned samples of expanded PU foam with and without ammonium nitrate and of syntactic PU foam with and without ammonium nitrate and sodium bicarbonate were analyzed by FTIR. Both additives, ammonium nitrate and sodium bicarbonate, were also analysed, separately.
To analyse the samples, pellets were made with KBr, because it is a transparent compound and usually does not have any peaks in the range that are acquire the IR spectrums in. Sample pellets with KBr were made using the appropriate die set, under a pressure of 10 tons during 5 minutes. The concentration of the sample in KBr was, approximately, in the range of 0.01 % to 1 %.

4.2. Experimental procedure

4.2.1. Mixture compositions and reactant thermodynamic properties

Energetic mixtures were defined taking in account polyurethane as the basic combustible reactant. Syntactic foam was formed by adding polyethylene hollow microspheres (*Q-cell*) to the original dense polyurethane.

AN and SB were added to the mixture in order to increase or decrease flame propagation.

In Table 2 the thermodynamic properties of reactants used in the mixture formulations are presented (ICT, 2005).

Table 2 - Thermodynamic properties of reactant.

Component	**Molecular global formula**	**Molecular weight (kg.mol^{-1})**	**ρ (kg.m^{-3})**	**H_f (kJ.mol^{-1})**
Polyurethane	$C_{10}H_{18.711}N_{0.273}O_{3.294}$	0.195	1000	-679.0632
Polyethylene	C_2H_4	0.0281	940	-53.80624
Air	$N_{1.5788}O_{0.4212}$	0.0289	1.205	0
Ammonium Nitrate	NH_4NO_3	0.0801	1725	-365.17952
Sodium Bicarbonate	$NaHCO_3$	0.0801	2159	-950.814

As it was explained before, it is assumed that the polyurethane formation is followed by the scheme:

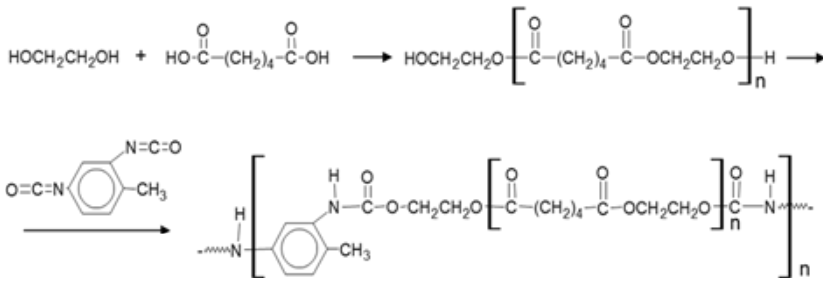

Figure 44 – Formation of polyurethane (adapted from Portugal et al., 2000).

Some samples were painted with aluminium cellulosic paint, before running the experimental tests.

This kind of paint has a very complex composition, the properties of the components are presented in Table 3 (Barbot, 2012).

Table 3 - Thermodynamic properties of components present in cellulosic aluminium paint.

Component	**%**	**Molecular global formula**	**Molecular weight (kg.mol^{-1})**	***ρ* (kg.m^{-3})**	***H_f* (kJ.mol^{-1})**
Toluene	10 < 25	C_7H_8	0.0921	867	12.17544
Xylene (isomers mixture)	10 < 25	C_8H_{10}	0.1062	864	-25.35504
Ethyl acetate	2.5 < 10	$C_4H_8O_2$	0.0881	900	-480.57424
n-butyl acetate	2.5 < 10	$C_6H_{12}O_2$	0.1162	883	-609.6088
Acetone	2.5 < 10	C_3H_6O	0.0581	790	-249.3664
Isopropanol	2.5 < 10	C_3H_8O	0.0601	786	-318.06768
Solvent naphtha (petroleum), light aromatic	2.5 < 10	Hydrocarbon mixture	≈ 0.120	870 at specific gravity	
Ethanol	2.5 < 10	C_2H_6O	0.0461	789	-277.90128
Methyl ethyl ketone	2.5 < 10	C_4H_8O	0.0721	805	273.46624
Naphtha (petroleum) hydrotreated heavy	< 2.5	Hydrocarbon mixture		760-790	
Aluminium powder	< 2.5	Al	0.0270	2702	0

4.2.2. Sample preparation

The expanded PU foam was made with a formulated commercial product from *Luís Falcão Simões de Carvalho* dealer, of two liquid solutions, one containing the prepolymer (*polyfoam A 100 %*) and the other the isocyanate solution (*polyfoam B 110 %*).

Samples of expanded PU foam, without any additive, were prepared by measuring 4×10^{-3} L of the prepolymer solution into a plastic cup of 8×10^{-2} L with a sterile syringe of 5×10^{-3} L, following which was added 4.4×10^{-3} L of the isocyanate solution measured with a different sterile syringe of 5×10^{-3} L. Then the two components were mixed with a plastic spatula for a few seconds; when the mixture was homogeneous it was put inside the plastic cup a PVC made cylinder of 0.032 x 0.032 m diameter, and the sample was left to self free expanded process. After the expansion phase had occurred the excess of expanded sample was removed with a cutter, leaving only the cylinder filled with the sample of polyurethane.

The procedure for making the samples of expanded PU foam with an additive was similar. The ammonium nitrate was previously micronized in a mill and then was mixed with the prepolymer solution, and only after that it was added the isocyanate solution, the following steps of the procedure were the same. Some expanded PU foam samples were painted with aluminium cellulosic paint. The process of painting the samples was very simple, stirring the ink that was in the can, and then painting the samples with an appropriate brush.

Syntactic PU foam was made with a formulated commercial dense (without voids) PU product, from *Luís Falcão Simões de Carvalho* dealer, similar to the previous one, also formed from of two liquid solutions, prepolymer (*polydur 50 %*) and isocyanate (*polyflow 100 %*) solutions.

Samples of syntactic PU foam were prepared by measuring 1×10^{-3} L of the prepolymer solution into a plastic cup of 0.28 L with a sterile syringe of 5×10^{-3} L, after which hollow plastic microspheres (polyethylene microspheres of 6×10^{-5} m size) were added; both components were mixed using an original screw mixing system, a wimble with a spiral metal drill of 8×10^{-3} m diameter. Then it 2×10^{-3} L of the isocyanate solution was added with a sterile syringe of 5×10^{-3} L, and the mixing process continued. When the mixture was well mixed it was put inside the test confinement (also a PVC made cylinder of 0.032 x 0.032 m diameter).

The procedure for making the samples of syntactic PU foam with an additive was similar. The additives were mixed with the prepolymer solution, and only after that it was added the HPM, the following steps of the procedure were the same. Some syntactic PU foam samples were painted with aluminium cellulosic paint, using the same process that was used in the expanded polyurethane samples.

Several samples (Table 4) were made to optimize the production method.

Table 4 - Percentage of the components used in mixtures.

Mixture	% Polyurethane	% *Q-cell*	% Ammonium nitrate	% Sodium bicarbonate
1	100	0	0	0
2	80	0	0	20
3	50	0	0	50
4	40	0	0	60
5	30	0	0	70
6	25	0	0	75
7	97	0	3	0
8	95	0	5	0
9	93	0	7	0
10	80	0	20	0
11	88	0	7	5
12	75	0	20	5
13	94	6	0	0
14	90	10	0	0
15	85	15	0	0
16	82	15	3	0
17	80	15	5	0
18	78	15	7	0
19	77	15	3	5
20	75	15	5	5
21	73	15	7	5

First six mixtures were made with expanded PU foam and an additive (sodium bicarbonate) that does not react with PU, the objective was to optimize the percentages between both components to get to know the right quantity of additive used, to let the polyurethane expand in the right conditions.

It was observed that when the amount of additive is over 50 mass percent the expansion of polyurethane does not occurred or there was a considerably weaker expansion.

In the optimizing procedure of syntactic PU foam, 6 and 10 mass percent of hollow plastic microspheres were first added to the dense polyurethane, this samples turned out to have a very high density (in average, 273 and 136 $kg.m^{-3}$, respectively), and the objective was to make samples with a density more similar to the density of expanded

PU foam without any additive (in average, 52.3 $kg.m^{-3}$). The quantity of HPM used at most of syntactic PU foam samples was 15 mass percent, it has a bulk density of 129.5 $kg.m^{-3}$, is not very close to the density of expanded PU foam, but with higher quantity of HPM the mixture is not very homogeneous.

Final selected and experimentally tested compositions were the mixtures: 1, 10, 15, 18 and 21. These are samples without any additive, and others with ammonium nitrate (oxidizer). In the case of syntactic PU foams mixtures were experimentally tested with both additives (AN and SB). One of each type were analysed on the microscope *Apex microscopes* which was connected to a computer by a USB cable. In the computer was installed the program *Minisee* (Figure 45). Some of the experimental tests involved the mixtures 1, 10, 18 and 21 painted with cellulosic aluminium paint.

Figure 45- Optical microscope apparatus.

4.2.3. Sample configuration

Both kinds of polyurethane foams were tested using the original cylindrical sample configuration (Figure 46) horizontally and vertically, with and without being painted with aluminium cellulosic paint.

The possibility of flame extinction was experimentally tested for the composition of expanded PU foam material. Ignition of such compositions implied a small modification from the original cylindrical shape. One of those configurations was to open one tunnel for the continuous ignition a PMMA slab of $5 \times 10^{-3} \times 5 \times 10^{-3}$ m, (Figure 47), a driven flame configuration. In the other different configuration sample, seven tunnels were

opened to give the sample a higher surface area (Figure 48). The tunnels of the modified expanded PU foam samples, and the holes in the PVC test-tube (for the thermocouples) were opened with a wimble with a spiral metal drill.

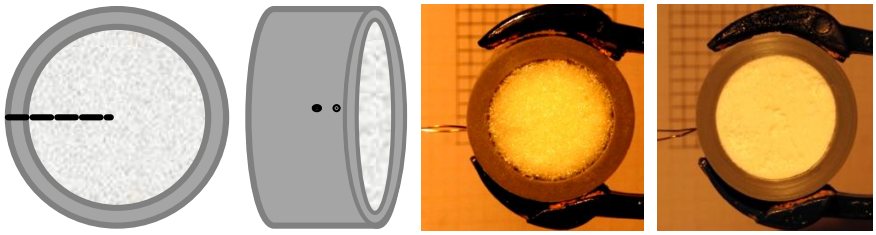

Figure 46 - Original cylindrical sample configuration (scheme and photo – lines indicate thermocouple position).

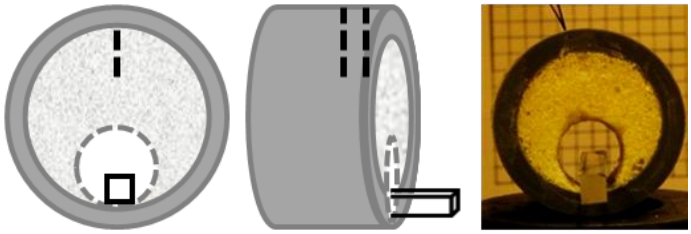

Figure 47 - Modified cylindrical sample configuration with PMMA continuous ignition device (scheme and photo – lines indicate thermocouple position).

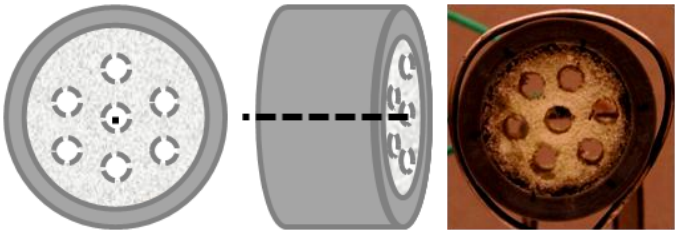

Figure 48 - Modified cylindrical sample configuration with seven tunnels (scheme and photo – lines indicate thermocouple position).

4.2.4. Burning tests procedures

The experimental apparatus used (Figure 50) allows the recording of temperature and thermal determination of regression velocities. Two Cr/Al thermocouples (*Thermocoax TKI 10/10/NN*) were used, connected to an electronic amplifier for thermocouples (having an integrated circuit for cold junction). The amplified signal was recorded by a digital signal analyzer (*Tektronix TDS 320*). Independently, videocrono-photography

(*Casio Excilim*), having recording speed up to 1000 fps, allows the real time flame records.

The tests made most recently were made using an electronic balance (*Kern PCB* with readability of 0.001 g and maximum weighing range of 250 g) that was connected to a computer by a RS232 cable with a USB entry. In the computer the program *PuTTY* was installed that is a digital recording system (Figure 49), allowing the direct measurement of sample mass while being tested.

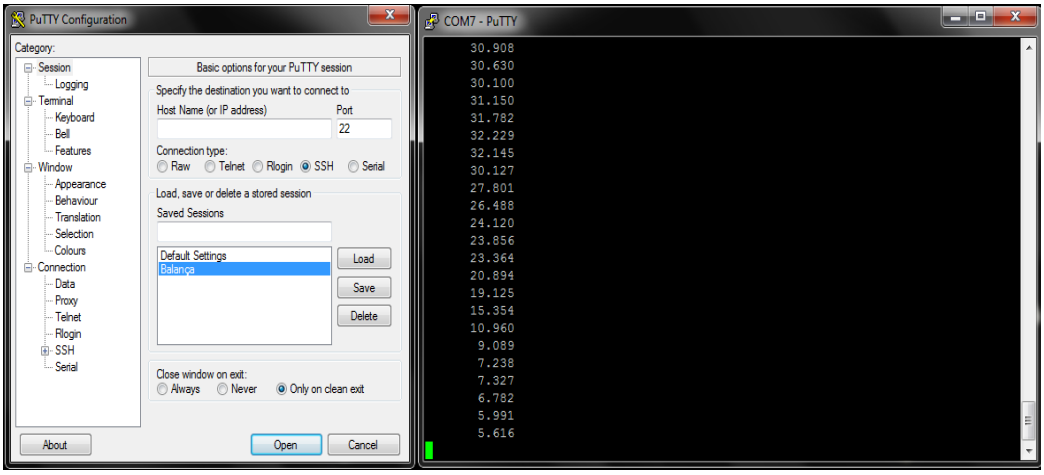

Figure 49 – Example of the operation of program *PuTTY*.

PuTTY is an SSH and telnet client, developed originally by Simon Tatham for the Windows platform. *PuTTY* is open source software that is available with source code and is developed and supported by a group of volunteers (Jackson, 2011).

In all the tests made with this procedure, the samples were ignited three times, to obtained the mass depletion during the combustion and to see if there is a big difference in the mass after the first burning test.

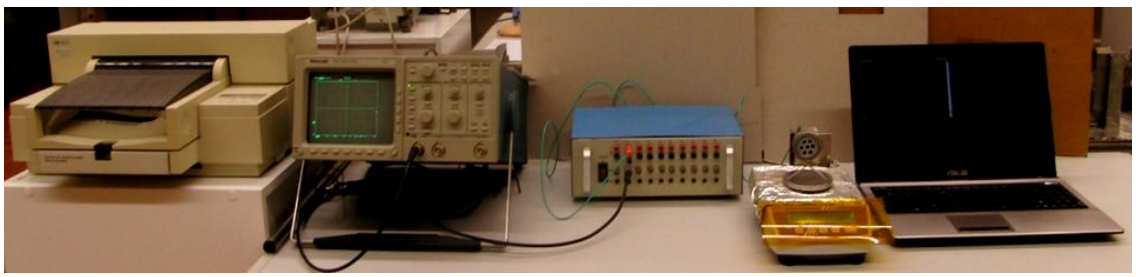

Figure 50 - Recording equipment.

Calibration of the thermocouple, temperature measurements and time delay, connected to the recording equipment, was done using a pyrotechnical cord having standard flame velocities of 1 $cm.s^{-1}$ (Figure 51). This procedure allows confirming the measurement of flame velocity, based in time delay between the two thermocouples. Temperature record of the calibration procedure is shown Figure 52.

Figure 51 - Thermocouples assembly for calibration of temperature equipment and flame velocity measurement.

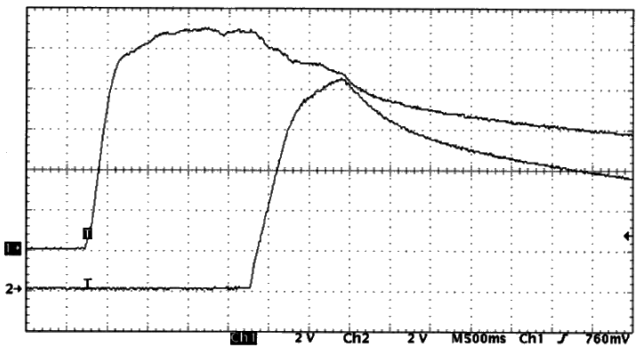

Figure 52 - Temperature records showing thermocouples delay allowing flame velocity measurement (2 V/div. ↔ 200 ºC/div.) as a function of time (500 ms/div.) of calibration.

Results of calibration: obtained values correspond to the maximum of the signal obtained by both thermocouples, including the Δt.

Thermocouple 1: 11 V = 1100 ºC (1 V ≈ 100 ºC)

Thermocouple 2: 10.6 V = 1060 ºC (1 V ≈ 100 ºC)

Δt = 1 s for $\Delta L = 1 \times 10^{-2}$ m between thermocouples.

After the calibration conclusion, all the apparatus were ready to proceed to the burning tests. Samples were put in a respective support with the thermocouples in the right position. A common lighter was used to initiate the samples ignition. Figure 53 illustrates a sample in horizontal position on the balance ready to be tested. In Figure 54

a sample is shown in vertical position being inflamed. Samples tested with electronic balance apparatus were ignited three times if extinction occurs.

Figure 53 - Experimental preparation of a burning test on a horizontal sample.

Figure 54 - Experimental assembly of a burning test on a vertical sample.

CHAPTER 5 – EXPERIMENTAL OF RESULTS

5.1. DSC-TGA

The results from a thermogravimetric run are presented by as both loss of weight versus temperature curve.

Polyol

The thermal stability of the polyol used in the syntactic PU foam was determined by TGA and DSC. TGA is used to analyse the decomposition, and DSC is used to determine the thermal transitions. DSC-TGA was made with two different temperature rates, 5 ºC.min^{-1} and 10 ºC.min^{-1}.

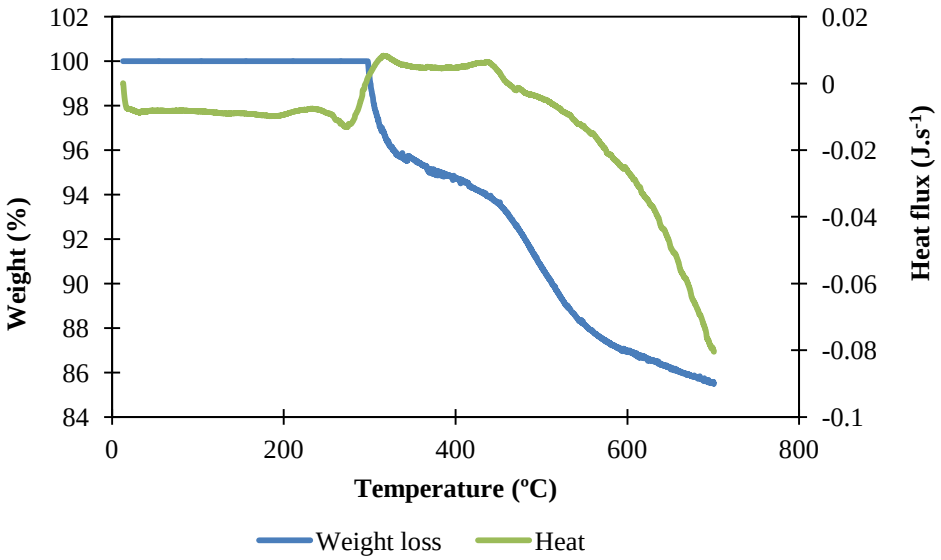

Figure 55 – DSC-TGA results for polyol used in syntactic PU foam heated at 5 ºC.min^{-1} under nitrogen atmosphere (60 mg).

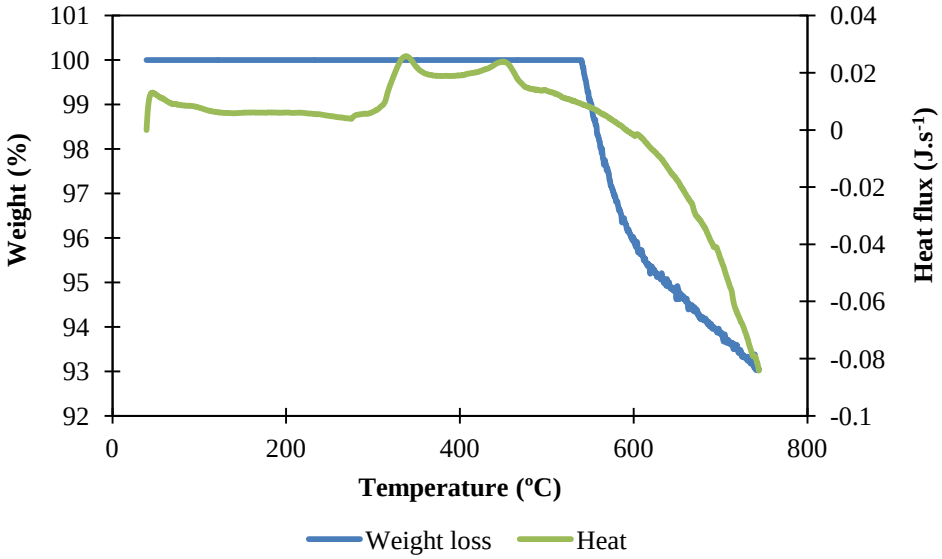

Figure 56 – DSC-TGA results for polyol used in syntactic PU foam heated at 10 ºC.min^{-1} under nitrogen atmosphere (34.3 mg).

For the chart with temperature rate of 5 ºC.min^{-1} (Figure 55), the sample was substantially decomposed in two temperature ranges, the first one between 300 and 315 ºC, and the second one between 440 and 540 ºC. The decomposition process of polyol covered a larger temperature range, between 250 and 700 ºC, though at temperatures lower than 315 ºC only 95 % was decomposed,, and by the end of the process only 85 % was decomposed, producing charcoal as the final product. This result implied that the degradation of polyol occur at temperatures higher than 700 ºC. Two endothermic peaks are seen, the first at 315 ºC and the second one at 435 ºC.

For the thermogram with heating rate of 10 ºC.min^{-1} (Figure 56), the sample was substantially decomposed in one temperature range that started at 540 ºC, but can be seen that this was more accentuated from 540 to 600 ºC, until 96 % of weight loss was observed. The decomposition process of polyol with a heating rate of 10 ºC.min^{-1} covered a smaller temperature range than the decomposition process of the polyol with a heating rate of 5 ºC.min^{-1}. By the end of the process only 93 % of the sample was decomposed. Two endothermic peaks are seen, the first at 338 ºC and the second one at 450 ºC. The polyol that was heated at 10 ºC.min^{-1} has lower percentage of weight loss, because the heat rate was faster.

In both DSC-TGA results for polyol the total % of weight loss is very low, this is due to the encapsulation of the sample in the pan. The top of the sample, that is the exterior part of all the sample inside the pan, suffered pyrolysis and the products cover the rest

of the sample and did not let the sample lose weight. The complete pyrolysis of the sample only occurs inside the pan, and only left carbon, as seen in the curve of heat flux. The fact that the difference in temperature between sample and reference decreased means that the system reached equilibrium.

The onset temperatures seen in the TGA and DSC thermograms of the polyol are presented earlier, for the lower heating rate. The onset temperature corresponds to the temperature of initiation of the thermal effect, and. is obtained by the intersection of the baseline before the effect occurs (extrapolated) with the tangent to the curve produced by the thermal effect. This is due to the fact that the sample is heated more uniformly during the slower heating. In fact, the heating rate significantly influences the DSC line of the thermogram. For slower rates, reaction peaks appear earlier.

The type of polyol analysed by this method is unknown, but literature studies have shown the differential thermal analysis, with heating rate of 10 ºC.min^{-1}, of polyurethane foam made with different kinds of polyol, polyether polyol and polyester polyol. These studies detected a small mass loss of the order of 6 %, from 435 ºC in the case of foams based on polyether polyol and from 525 ºC to foams based on polyester polyol (Neves, 2010). It is possible to compare these literature results with the results obtained (Figure 56), and conclude that probably the polyol studied in this work is a polyester polyol.

Hollow plastic microspheres

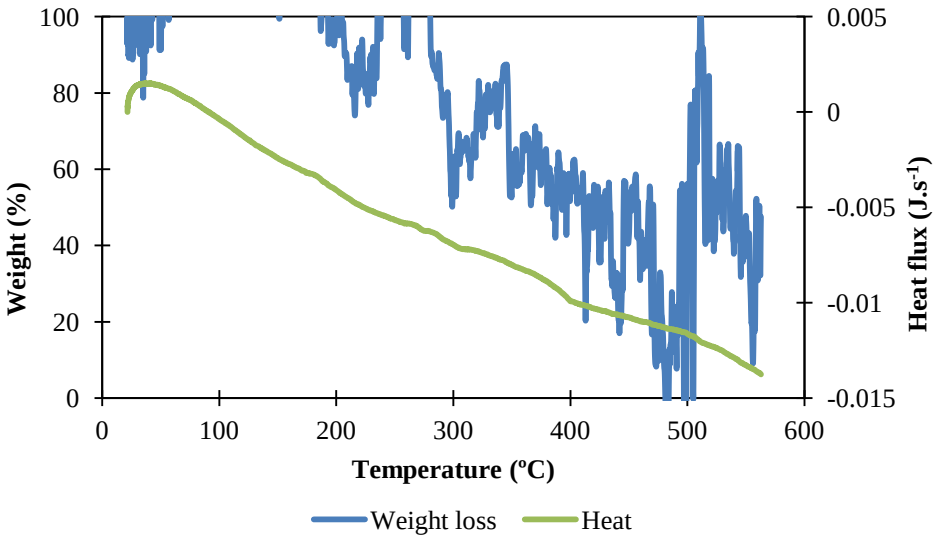

Figure 57 – DSC-TGA results for hollow plastic microspheres used in syntactic PU foam heated at 10 ºC.min^{-1} under nitrogen atmosphere (0.7 mg).

The thermal stability of the hollow plastic microspheres used in the syntactic PU foam was determined by TGA and DSC. TGA is used to analyse the decomposition, and DSC is used to determine the thermal transitions. DSC-TGA was made in the temperature rate of 10 ºC.min^{-1}.

It has already been indicated during this work, that the hollow plastic microspheres are made of polyethylene. Polyethylene was completely pyrolysed. The mass of the sample tested is almost insignificant, and HPM has a very low density, that is why the TGA curve is so inconstant. As the material has a low density, the HPM pyrolysis process is constrained due to the occurrence of pyrolysis of the nearest spheres.

It is probable that the HPM was completely decomposed before the temperature reaches 480 ºC, which is where the weight loss curve reaches the value 0 (zero) for the first time.

The endothermic transition happened at 40 ºC, this is due to a particular endothermic transition, called the glass transition. This is a second-order transition that does not give a peak but leads to a change in the rate of heat flux. The glass transition is related to a variation of the rigidity (as measured by viscoelastic properties) of the sample and is detected by a variation of the DSC slope. This variation corresponds to a change in the heat capacity of the sample.

It is seen in the curve of heat flux that there is a continuous heat absorption during the changes in the sample's pyrolysis, because the difference in temperature between sample and reference decreased, which means that the system reached equilibrium, so the sample was completely decomposed.

5.2. Infrared

Ammonium Nitrate

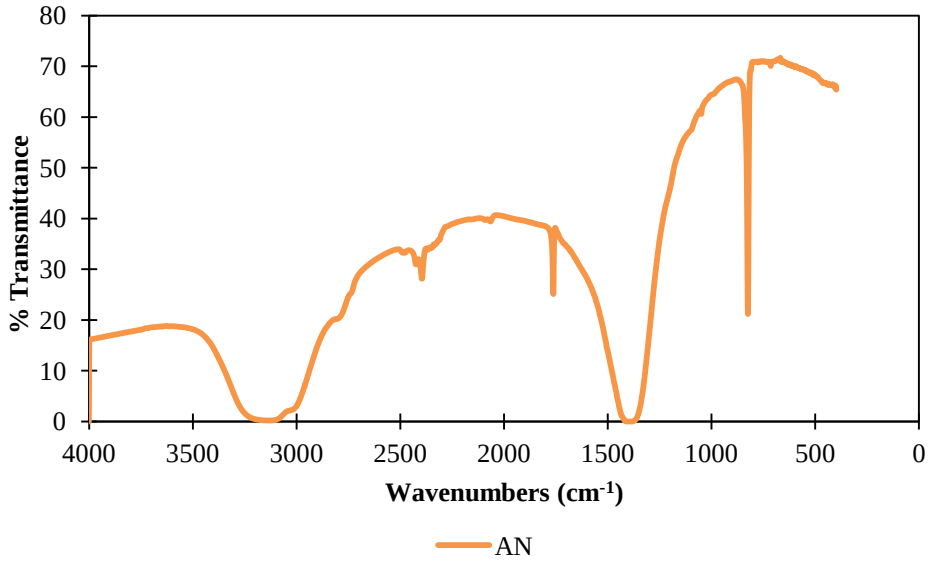

Figure 58 – Infrared spectra of ammonium nitrate.

Table 5 – Infrared absorption bands of ammonium nitrate.

Functional class	Wavenumber (cm^{-1})	Assignment
Amines	3125	ν NH_4^+ asym
Carbon dioxide	2400	CO_2
Amines	1760	ν NO_3^- sym; NO_3^- in-plane deformation
Amines and nitro compounds	1380	ν NO_3^- asym; NH_4^+ asym deformation
Nitro compounds	825	ν NO_3^- out of plane deformation

The different solid phases of AN crystals exhibit different physical and thermodynamic properties such as solubility, specific volume and heat capacity, phase *IV* is stable at the tropospheric temperature and is the only phase considered in current atmospheric chemical models.

The band at 2400 cm^{-1} arises from the presence of atmospheric carbon dioxide molecules in the path of the IR beam, between the source and the detector.

Strong band between, approximately, 3300-2800 cm^{-1} is due to NH_4^+ asymmetric stretch and deformation. Medium intensity band at 1760 cm^{-1} is the combination of NO_3^- symmetric stretch and NO_3^- in-plane deformation. Strong band between

1500-1300 cm^{-1} is the overlap of NH_4^+ asymmetric deformation with NO_3^- asymmetric stretch. A very intense band at 825 cm^{-1} is due to NO_3^- out-of-plane deformation.

Sodium Bicarbonate

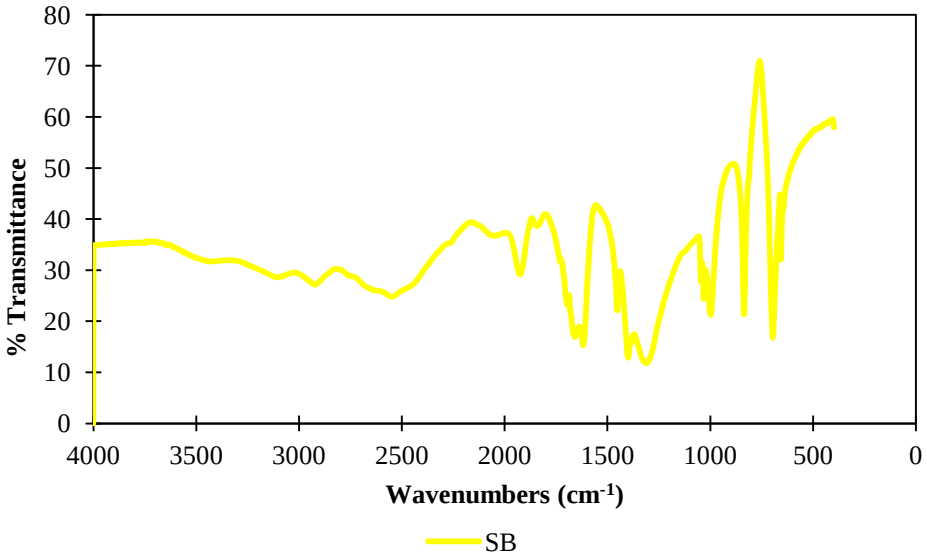

Figure 59 – Infrared spectra of sodium bicarbonate.

Table 6 – Infrared absorption bands of sodium bicarbonate.

Functional class	Wavenumber (cm^{-1})	Assignment
Hydroxyl	3000-3500	ν OH
Carbon dioxide	2550	CO_2
Carbonate	1620	ν CO_2 asym
Carbonate	1450-1400	ν C-O symmetric
Bicarbonate	1310	δ COH
Bicarbonate	1050-1000	ν C-OH
Carbonate	840	CO_3 out-of-plane
Carbonate	700-650	δ CO_2

Very broad band at, approximately, 3000-3500 cm^{-1} is due to OH stretching. Very intense band at 1620 cm^{-1} is CO_3 asymmetric stretching. Two bands between 1450-1400 cm^{-1} is the overlap C-O asymmetric stretching. Very strong and broad band at 1310 cm^{-1} corresponds to the bending of COH. The last two intense and sharp bands 840 and 700-650 cm^{-1} are the CO_3 out-of-plane and the bending of CO_2, respectively.

Expanded PU foam fresh and burned

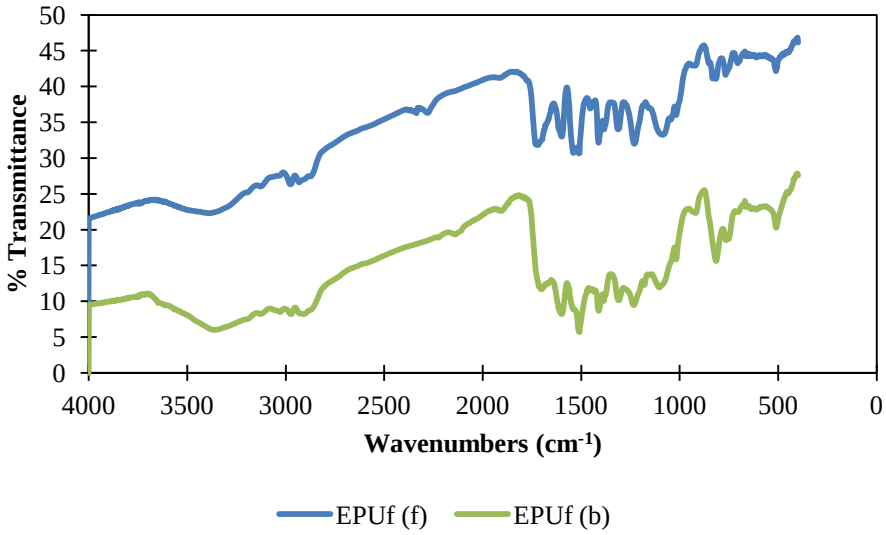

Figure 60 – Infrared spectra of expanded PU foam before (fresh) and after (burned) the burning test.

Table 7 – Infrared absorption bands of Expanded PU foam.

Functional class	Wavenumber (cm^{-1})	Assignment
Amines	3400-3300	ν N-H (secondary amines)
Alcohol	3580-3200	ν O-H (H-bonded)
Alkanes	3000-2850	ν C-H (2 bands)
Isocyanates	2270-2100	ν –N=C=O
Carboxylic acid and derivatives	1725-1700	ν C=O (acids)
Aromatics	1600	ν C=C
Amines	1510	δ N-H scissoring
Carboxylic acid and derivatives	1410-1360	δ C-O-H
Carboxylic acid and derivatives	1310	ν C-O (acids)
Amines	1230	ν C-N
Carboxylic acid and derivatives	1100	ν C-O-C (ether)
Aromatics	815-765	δ C-H and ring puckering

The difference in the transmission % in both curves is due to the different concentrations of the samples. Both samples present the bands related to the stretching of N-H, O-H and C-H. It is seen that in the fresh sample the band correspondent to the stretching of N=C=O (isocyanate) is more intense, it means that some hard segments

were decomposed. The wide range between 1725-1000 cm^{-1} is quite similar between both samples. The bending vibration of C-H is more intense in the burned sample.

Ammonium Nitrate and fresh samples of expanded PU foam with and without 20 mass percent of AN

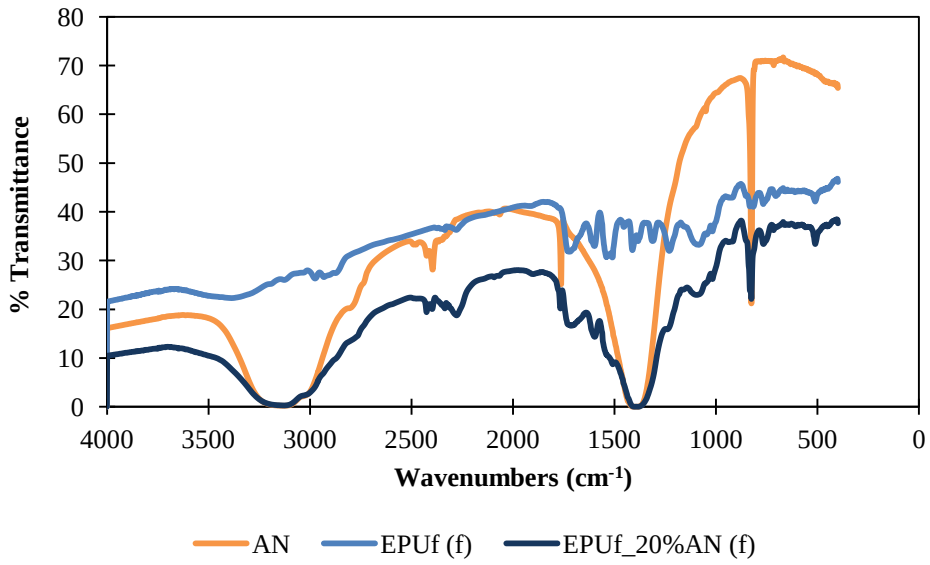

Figure 61 – Infrared spectra of ammonium nitrate, fresh expanded PU foam and fresh expanded PU foam with 20 mass percent of AN.

After the analysis of ammonium nitrate and of both fresh expanded polyurethane foams (with and without AN), it is possible to make to a comparison of the spectra. It is clear which one is the sample of expanded PU foam that has ammonium nitrate. Between 3300-3000 cm^{-1}, in 1380 cm^{-1} and in 825 cm^{-1} it is visible the effect of AN in the EPUf_20%AN sample, the presence of NH_4^+ and NO_3^- it is seen.

Ammonium Nitrate and burned samples of expanded PU foam with and without 20 mass percent of AN

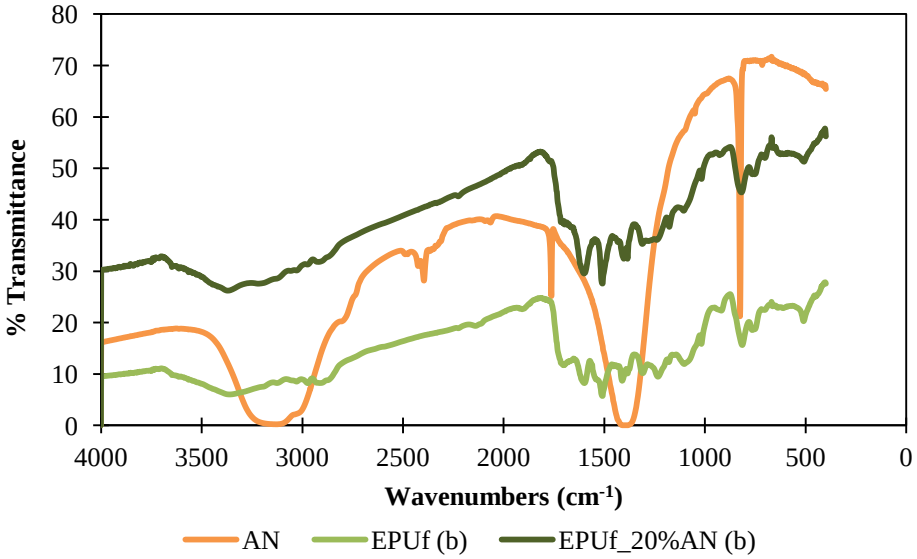

Figure 62 – Infrared spectra of ammonium nitrate, burned expanded PU foam and burned expanded PU foam with 20 mass percent of AN.

Proceeding to the comparison of the spectra of AN and the two burned samples of expanded PU foams (with and without AN), are no clear indications which one is the sample of expanded PU foam that has ammonium nitrate. After the burning process the ammonium nitrate present in the EPUf_20%AN was completely decomposed.

The difference in the transmission % in the curves of fresh and burned samples of expanded PU foam with 20 mass percent of AN, is due to the different concentrations of the samples. The two samples present the bands related to the stretching of N-H and O-H. The band between 3000-2850 cm^{-1} only appears in the curve of the burned sample, and is very weak. The band correspondent to the stretching of N=C=O (isocyanate) is only presented in the fresh sample curve, it means that the hard segments were decomposed. The wavelength of 1765-1700 cm^{-1}, in the fresh samples presents two bands with a relatively weak intensity, in the burned sample there is only slight evidence of this signal. The band in 1600 cm^{-1} is much more intense in the burned sample. While in the burned sample the range between 1410-1310 cm^{-1} the spectra appears in the form of three sharp bands, in the fresh sample appears in the form of only one broad band. The bands at 1180 and 1095 cm^{-1} are presented in both spectra at very low, almost insignificantly intensity.

Dense polyurethane and Syntactic PU foam (15 % HPM) fresh and burned

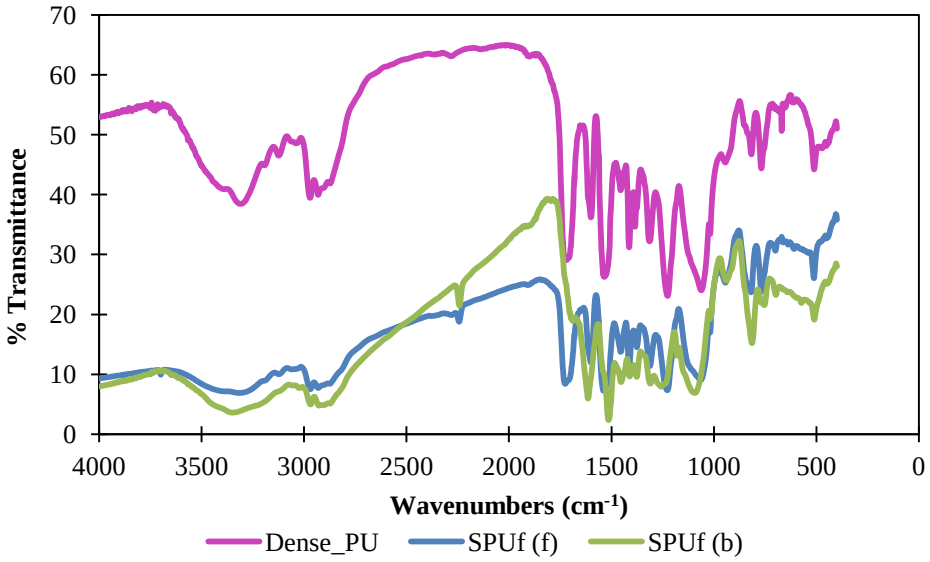

Figure 63 – Infrared spectra of dense PU and for the same PU with 15 mass percent of HPM (SPUf).

Table 8 – Infrared absorption bands of dense PU and syntactic PU foam.

Functional class	Wavenumber (cm^{-1})	Assignment
Amines	3400-3300	ν N-H (secondary amines)
Alcohol	3580-3200	ν O-H (H-bonded)
Alkanes	3000-2850	ν C-H (2 bands)
Isocyanates	2270-2100	ν –N=C=O
Carboxylic acid and derivatives	1725-1700	ν C=O (acids)
Aromatics	1600	ν C=C
Amines	1510	δ N-H scissoring
Alkanes	1450	δ CH_2 deformation
Carboxylic acid and derivatives	1410-1360	δ C-O-H
Carboxylic acid and derivatives	1310	ν C-O (acids)
Amines	1230	ν C-N
Carboxylic acid and derivatives	1100	ν C-O-C (ether)
Aromatics	815-765	δ C-H and ring puckering

In Table 9 are demonstrated the infrared absorption of the more intense bands of polyethylene (HPM) studied in the literature. It is seen that the only band that is not

present in syntactic PU foam is that corresponding to the CH_2 rocking vibration (731-720 cm^{-1}).

Table 9 – Main absorptions of polyethylene in the IR region and their assignment (adapted from Gulmine et al., 2002).

Wavenumber (cm^{-1})	Intensity	Assignment
2919	Strong	ν CH_2 asymmetric
2851	Strong	ν CH_2 symmetric
1473-1463	Strong	δ deformation
731-720	Medium	Rocking deformation

There are no significant differences between the dense polyurethane and the same PU with 15 mass % of hollow plastic microspheres, (polyethylene). The major difference is that in the dense PU curve it is easier to observe the bands in the region 3400-3300 cm^{-1} and 3580-3200 cm^{-1}, due to the fact that the syntactic polyurethane foam has the presence of polyethylene in its composition. The presence of polyethylene reduces the percentage of the atom oxygen in the mixture, so the percentage of hydrocarbons is higher. That is the reason why the dense PU has better resolution between the band of the stretching of the amine (N-H) and the band of stretching of the alcohol (O-H), because in this case the percentage of oxygen is higher.

The band 1725-1700 cm^{-1} corresponding to the stretching of C=O, is the only significant difference between the fresh and the burned sample of syntactic polyurethane foam. In the fresh sample an intense band appears in this region and in the burned sample it is only weakly evident.

The differences in infrared absorption of the two kinds of polyurethane foams, expanded and syntactic, (Figure 60 and 63, respectively) are interesting, because the composition of the compounds used in the formation of the foam are unknown, and they used different commercial solutions. Due to the fact that the infrared spectrums are from two polyurethanes without any additive there are no significant differences.
Syntactic PU foam presents a more significant band at 1450 cm^{-1} and between 1250-1000 cm^{-1}, corresponding to the bending deformation of CH_2 and to amine

stretching (N-C), respectively, this is explained by the presence of polyethylene (HPM) that increases the percentage of hydrocarbons in the mixture.

Ammonium Nitrate and fresh samples of syntactic PU foam with and without 7 mass percent of AN

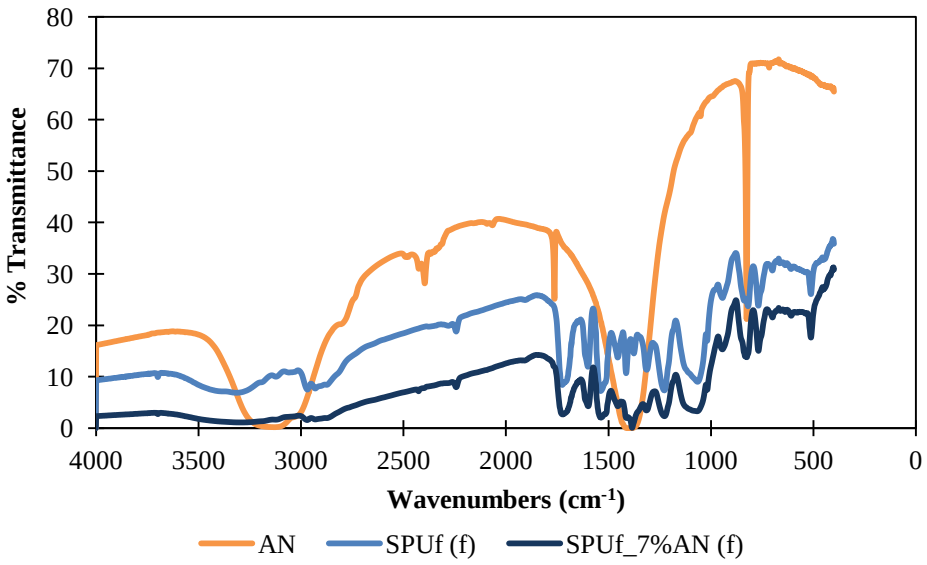

Figure 64 – Infrared spectra of ammonium nitrate, fresh syntactic PU foam and fresh syntactic PU foam with 7 mass percent of AN.

After the analysis of ammonium nitrate and of both fresh syntactic polyurethane foams (with and without AN), it is possible to provide a comparison of the spectra. It is not obvious (as was in the case of expanded PU foams) which is the sample of syntactic PU foam that has ammonium nitrate; this is due to the fact that only 7 mass percent of ammonium nitrate is present. Normally with mixtures unless one component has a very intense band, it is only possible to characterize compounds in quantities exceeding 10 % (m/m) by FTIR. It is only with the 1380 cm^{-1} band that there can be seen a slight higher intensity in the syntactic PU foam with 7 mass percent of AN compared with the syntactic PU foam without any additive.

Ammonium Nitrate and burned samples of syntactic PU foam with and without 7 mass percent of AN

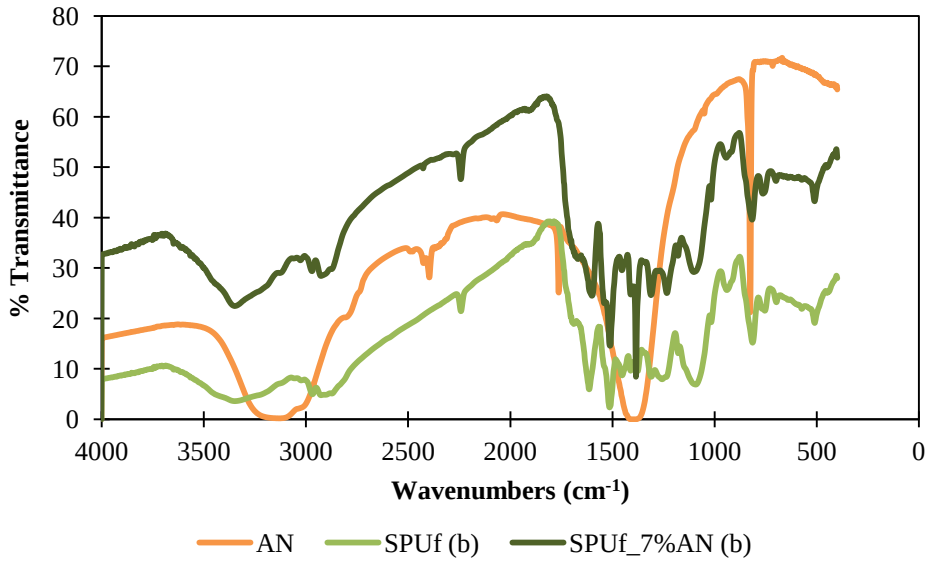

Figure 65 – Infrared spectraof ammonium nitrate, burned syntactic PU foam and burned syntactic PU foam with 7 mass percent of AN.

As it was indicated earlier, the quantity of ammonium nitrate in the mixture did not affect the infrared spectrum, such that there is no obvious results from the decomposition of AN after the burning process of the sample.

Between the infrared absorption of both syntactic PU foams the only significant difference that can be seen is in the transmission %, and this is due to the different concentrations of the samples. In 1380 cm^{-1} band, the burned sample has a more intense band attributed to bending of the C-O-H, possibly with a very small contribution from ions from AN.

Ammonium Nitrate, Sodium Bicarbonate and fresh samples of syntactic PU foam with and without 7 and 5 mass percent of AN and SB

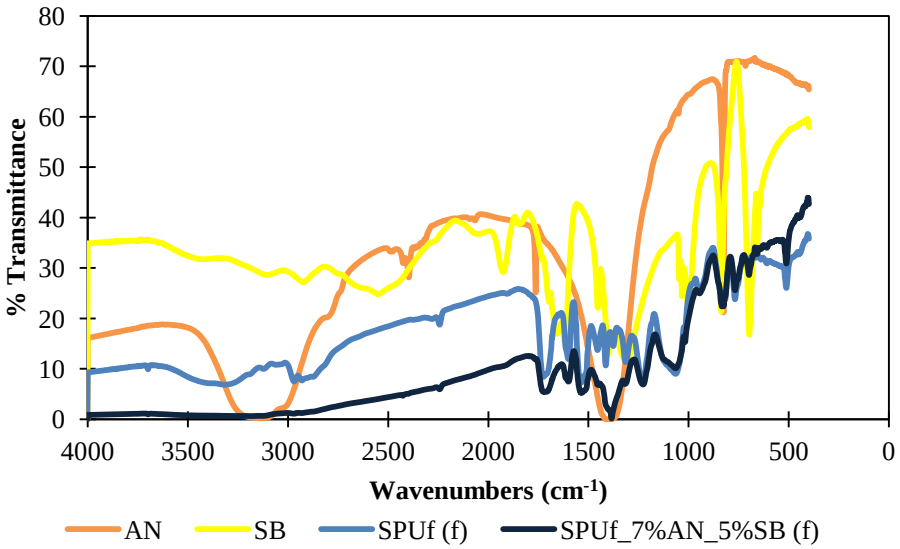

Figure 66 – Infrared spectra of ammonium nitrate, fresh syntactic PU foam and fresh syntactic PU foam with 7 mass percent of AN and 5 mass percent of SB.

After the analysis of the FTIR spectra of ammonium nitrate, sodium bicarbonate and of both fresh syntactic polyurethane foams (with and without AN and SB), it is possible to proceed to a comparison. As indicated earlier, the sensitivity of FTIR in mixtures generally limits detection of compounds in mixtures to concentrations exceeding 10 % (m/m), when it comes to mixtures. With only 5 mass percent of sodium bicarbonate and 7 mass percent of ammonium nitrate, FTIR is not able to detect them in the mixture. Comparing the IR absorptions of both syntactic foams, the same is seen as was observed in Figure 64, the sample with additives, in this case, AN and SB have a more intense band around 1380 cm^{-1}. In this case can be due to the detection of AN and SB simultaneously, since in total, the syntactic PU foam has 13 mass percent of additives.

Ammonium Nitrate, Sodium Bicarbonate and burned samples of syntactic PU foam with and without 7 and 5 mass percent of AN and SB

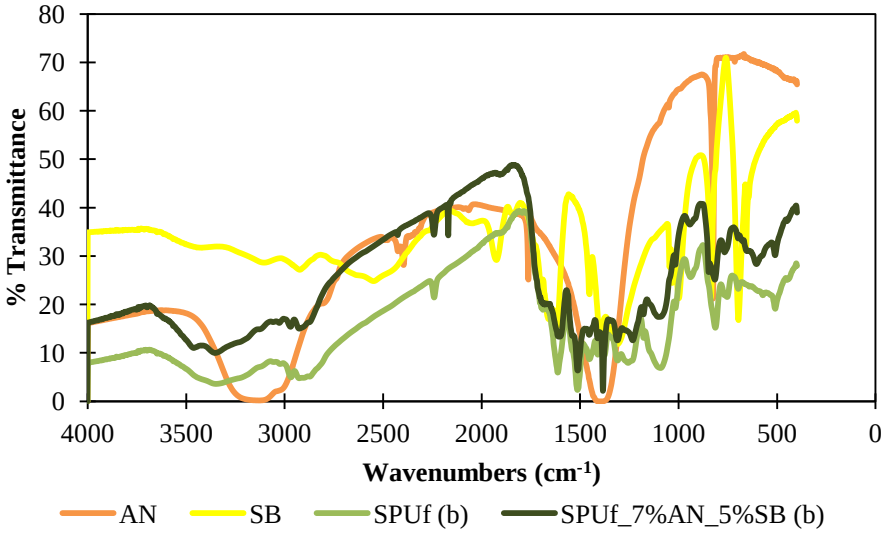

Figure 67 – Infrared spectra of ammonium nitrate, burned syntactic PU foam and burned syntactic PU foam with 7 mass percent of AN and 5 mass percent of SB.

As it was indicated earlier, the quantity of ammonium nitrate in the mixture was too small affect the infrared spectrum, so there is no obvious results from the decomposition of AN and SB after the burning process of the sample.

Between the infrared absorption of both syntactic PU foams the only significant difference that can be seen is in the transmission %, and this is due to the different concentrations of the samples. In the wavenumber region of 1380 cm^{-1} the burned sample has a more intense band associated with the bending of the C-O-H with a very small amount of ions from AN and SB.

5.3. Burning tests

The results presented bellow, were chosen from all the experiments made during this work. The remaining results are presented in Appendix C.

5.3.1. Expanded PU foam

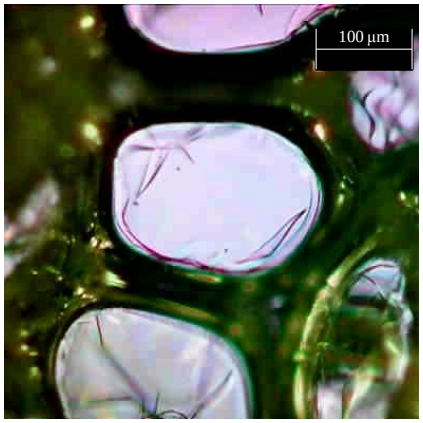

Figure 68 - Photography of microscopic investigation of expanded PU foam.

Figure 69 - Photography of microscopic investigation of expanded PU foam painted with cellulosic aluminium paint.

In the microscopy studies of expanded polyurethane foam (Figure 68) without any additive it is seen that the diameter of the pores in the sample are effectively constant, approximately 200 µm, and the foam itself is ≈ 50 µm. The diameter used to perform prediction of temperature and ignition by Semenov and Frank-Kamenetskii theories was $\lambda = 3.51 \times 10^{-6}$ m, because account was taken of the surface walls of the sample, this is where the sample starts its ignition.

Figure 69 shows the same kind of sample, with a different scale and painted with cellulosic aluminium paint. Due to the thickness of the paint the width of the sample is no clear, because there is reflection from the top light of the microscope.

Original cylindrical configuration horizontal position

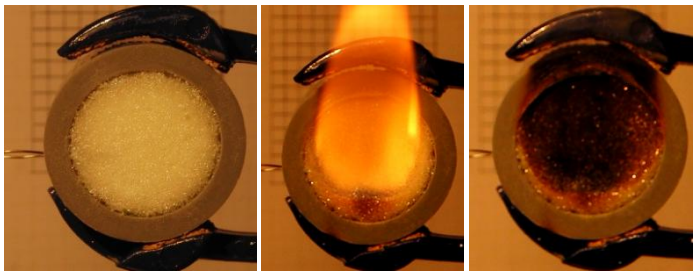

Figure 70 – Burning test of expanded PU foam, horizontal position.

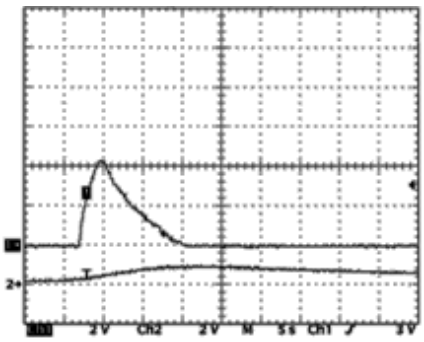

Figure 71 - Temperature records showing thermocouples delay allowing flame velocity measurement (2 V/div. ↔ 200 ºC/div.) as a function of time (5 s/div.).

Thermocouple 1: 4.4 V = 440 ºC

Thermocouple 2: no signal

$\Delta L = 3 \times 10^{-3}$ m

First thermocouple had a 2×10^{-3} m distance from the surface of the sample, the second thermocouple had 5×10^{-3} m.

$m_i = 29.452$ g

$m_f = 29.402$ g

It is visible in Figure 70 that only the surface was burned, the ignition of the sample only lasted about 5 to 10 seconds. The fast extinguishing of the sample is confirmed by the Δm, which is very low (0.05 g). The second thermocouple was not able to get the signal because the ignition of the sample happened only at the surface.

Modified cylindrical configuration with the seven tunnels horizontal position

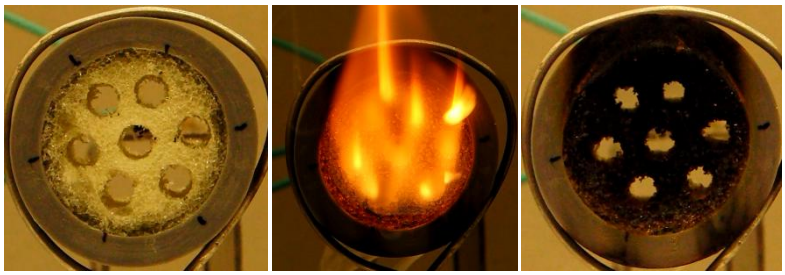

Figure 72 – Burning test of expanded PU foam with the 7 holes, horizontal position.

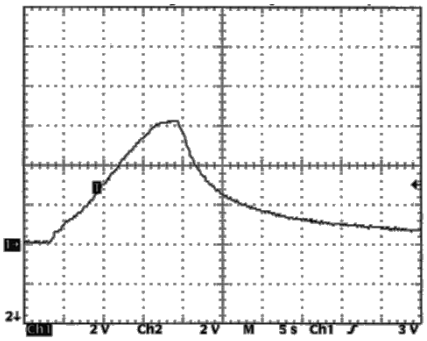

Figure 73 - Temperature records showing thermocouples delay allowing flame velocity measurement (2 V/div. ↔ 200 ºC/div.) as a function of time (5 s/div.).

Thermocouple 1: 6.4 V = 640 ºC

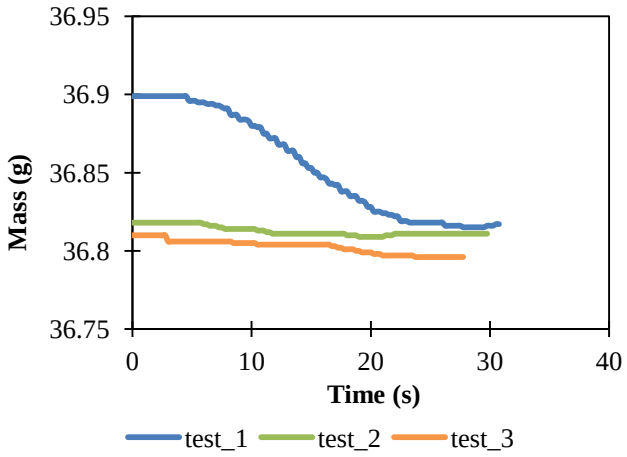

Figure 74 – Mass depletion of the sample during the burning tests.

Only one thermocouple was used in this assay. However, three burning tests were taken of to the same sample; only one graph is shown corresponding to the temperature records showing the thermocouples delay allowing flame velocity measurement. The

three measurments are all similar, due to the fact that the extremity of the thermocouple is near to the point where the sample is ignited. This means that with this configuration the temperature detected is of to the lighter used to ignite the samples.

Only the front and the interior of the holes, until effectively the middle of the sample, were burned superficially. In the first test the flame takes ≈ 10 seconds to extinguish, producing a lot of smoke during the inflammation. The second and third tests were quicker, because the sample almost did not ignite. The production of smoke decreased from test to test.

The total of mass loss was 0.103 g, approximately 80 % of the mass lost process occurred during the first test.

Modified cylindrical configuration with the seven tunnels horizontal position with paint

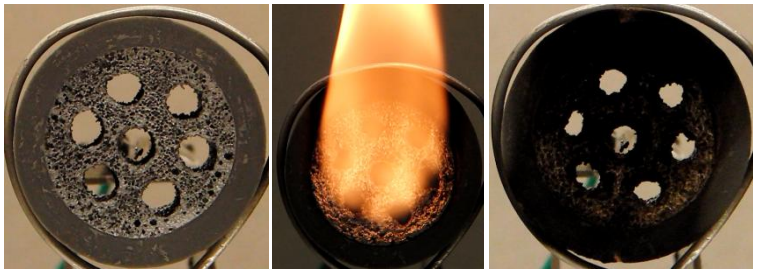

Figure 75 – Burning test of expanded PU foam with the 7 holes with cellulosic aluminium paint, horizontal position.

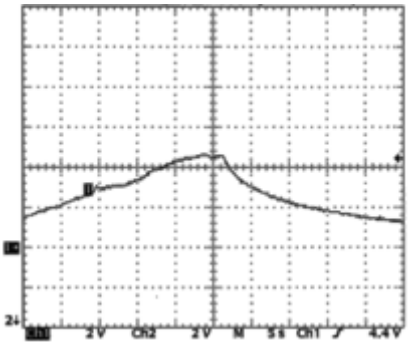

Figure 76 - Temperature records showing thermocouples delay allowing flame velocity measurement (2 V/div. ↔ 200 ºC/div.) as a function of time (5 s/div.).

Thermocouple 1: 4.8 V = 480 ºC

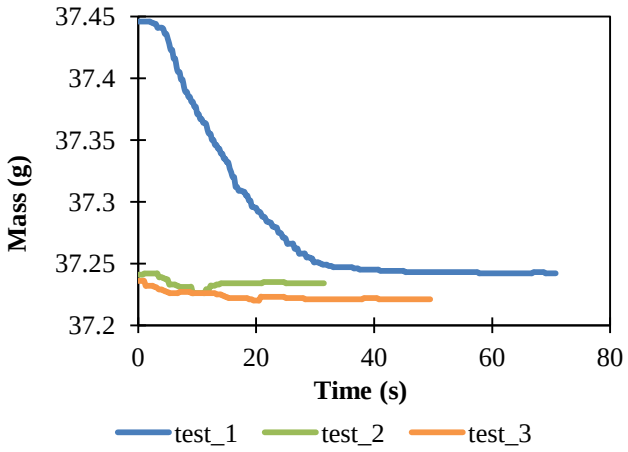

Figure 77 – Mass depletion of the sample during the burning tests.

Only the front and the interior of the holes, until effectivelly the middle of the sample, were burned superficially. In the first test the flame takes ≈ 30 seconds to extinguish, it was produced a lot of smoke during the inflammation. It was possible to see some bubbles at the top of the sample, from the paint. The second and third tests were quicker, because the sample almost did not ignite. The production of smoke decreased from test to test. Due to the presence of the paint, this sample produced more smoke than the sample, with the same configuration, that was not painted.

The total of mass loss was 0.225 g, approximately 90 % of the mass lost process occurred during the first test.

Original cylindrical configuration vertical position

Figure 78 – Burning test of expanded PU foam, vertical position.

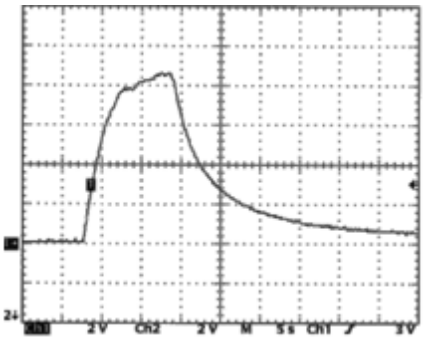

Figure 79 - Temperature records showing thermocouples delay allowing flame velocity measurement (2 V/div. ↔ 200 ºC/div.) as a function of time (5 s/div.).

Thermocouple 1: 8.8 V = 880 ºC

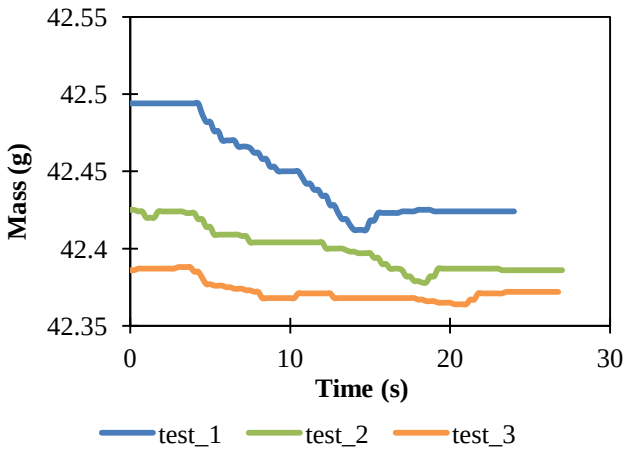

Figure 80 – Mass depletion of the sample during the burning tests.

Only one thermocouple was used in this assay, in the bottom of the sample, as can be seen in Figure 78. Only the bottom was burned superficially. In the first test the flame takes ≈ 10 seconds to extinguish, it did not produce a large quantity of smoke. The second and third tests were quicker, because the flame extinguished immediately.

The total of mass loss was 0.123 g, approximately 60 % of the mass lost process occurred during the first test.

Modified cylindrical configuration with the seven tunnels vertical position

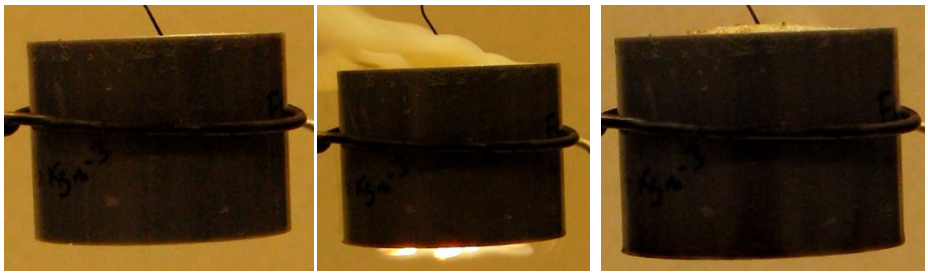

Figure 81 – Burning test of expanded PU foam with the 7 holes, vertical position.

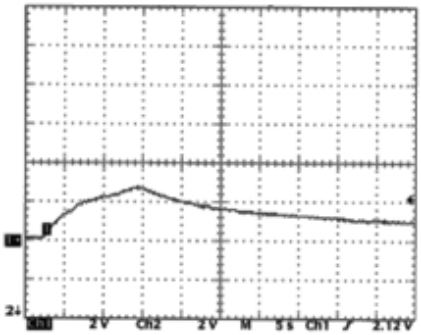

Figure 82 - Temperature records showing thermocouples delay allowing flame velocity measurement (2 V/div. ↔ 200 ºC/div.) as a function of time (5 s/div.).

Thermocouple 1: 3 V = 300 ºC

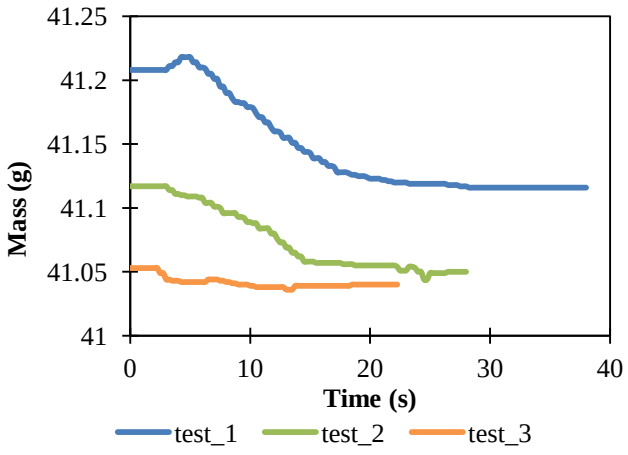

Figure 83 – Mass depletion of the sample during the burning tests.

Only one thermocouple was used in this assay, inside the central hole from the top of the sample. In the first test the flame takes ≈ 15 seconds to extinguish, it did produce a large quantity of smoke. In the second and third tests the flame extinguishes

immediately, the production of smoke is always decreasing from test to test. During the tests a small expansion of the foam was observed in the top of the test tube, when the next test was at the beginning, the expansion is not visible, but after burning the sample the expansion was visible again.

The total of mass loss was 0.168 g, almost 60 % of the mass lost process occurred during the first test.

Modified cylindrical configuration with the seven tunnels vertical position with paint

Figure 84 – Burning test of expanded PU foam with the 7 holes with cellulosic aluminium paint, horizontal position.

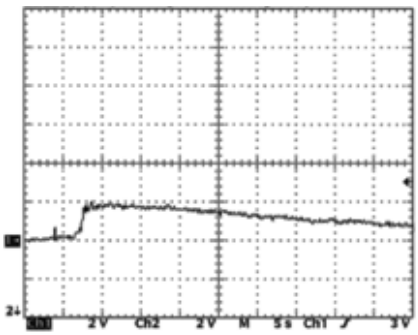

Figure 85 - Temperature records showing thermocouples delay allowing flame velocity measurement (2 V/div. ↔ 200 ºC/div.) as a function of time (5 s/div.).

Thermocouple 1: 2 V = 200 ºC

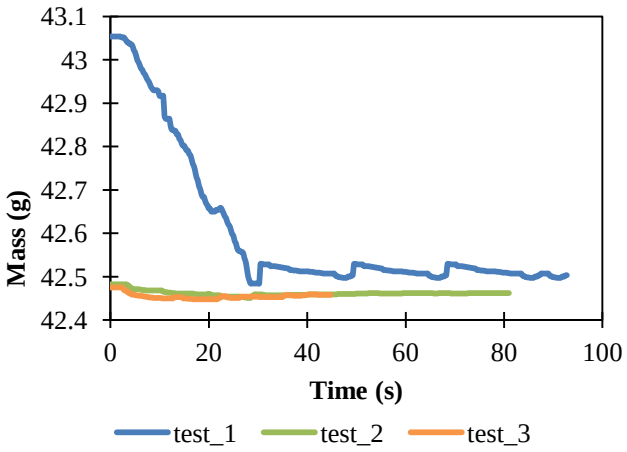

Figure 86 – Mass depletion of the sample during the burning tests.

Only one thermocouple was used in this assay, inside the central hole from the top of the sample. In the first test the flame takes more than 1 minute to extinguish, it did produce a large quantity of smoke, more than the sample that was not painted. In the video it is not possible to see the flame, but the sample was burning in the holes, due to the presence of the paint. In the second and third tests the flame extinguish immediately, the production of smoke is always decreasing from test to test.

The total of mass loss was 0.596 g, more than 90 % of the mass lost process occurred during the first test.

5.3.2. Expanded PU foam with 20 mass % of AN

Figure 87 - Photography of microscopic investigation of expanded PU foam with 20 mass percent of AN.

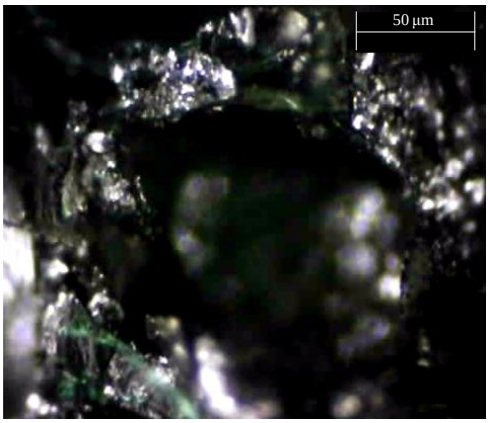

Figure 88 - Photography of microscopic investigation of expanded PU foam with 20 mass percent of AN, painted with cellulosic aluminium paint.

In the microscopy studies of expanded polyurethane foam with 20 mass percent of ammonium nitrate it is seen that the diameter of the pores in the sample are considerably constant, approximately 200 µm, and the foam itself is ≈ 50 µm. One of the pores in Figure 87 has a particle of ammonium nitrate. The particle is surrounded with smaller pores, resolved microparticles. This is the presence of water, due to the high hygroscopicity of the ammonium nitrate and its recrystallization. Comparing both microscope images of expanded PU foam with and without ammonium nitrate (Figure 68 and Figure 87) it is visible that the first one does not have the presence of this much smaller pores.

Figure 88 shows the expanded PU foam with 20 mass percent of ammonium nitrate, with a different scale and painted with cellulosic aluminium paint. Due to the thickness of the paint the width of the sample is not clear, neither is the presence of ammonium nitrate, but it can be seen that this sample presents higher roughness than the expanded PU foam without AN (Figure 69).

Without test tube

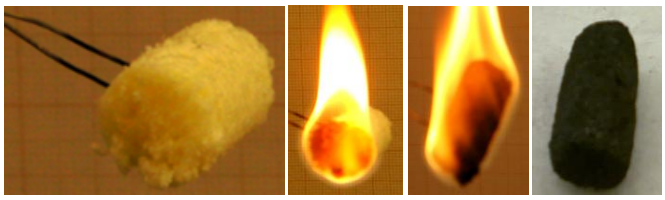

Figure 89 – Burning test of expanded PU foam with 20 mass of AN) without test tube.

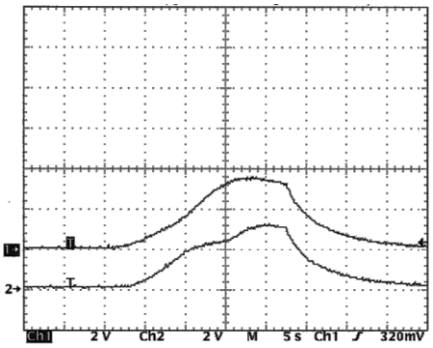

Figure 90 - Temperature records showing thermocouples delay allowing flame velocity measurement (2 V/div. ↔ 200 ºC/div.) as a function of time (5 s/div.).

Thermocouple 1: 3.6 V = 360 ºC

Thermocouple 2: 3.2 V = 320 ºC

Δt = 3 s for ΔL = 1 x 10^{-3} m

First thermocouple had a 1 x 10^{-2} m distance from the surface of the sample, the second thermocouple had 1 x 10^{-2} m.

m_i = 0.498 g

m_f = 0.126 g

The sample burned completely, in about 30 seconds, this happened because the sample was free, without test tube, there was plenty oxygen for the ignition be successfully.
Δm is 0.372 g; Δt is very close to 0, because when the trigger get the signal, the flame had already reached both thermocouples, due to the velocity of the sample's ignition.

Original cylindrical configuration horizontal position

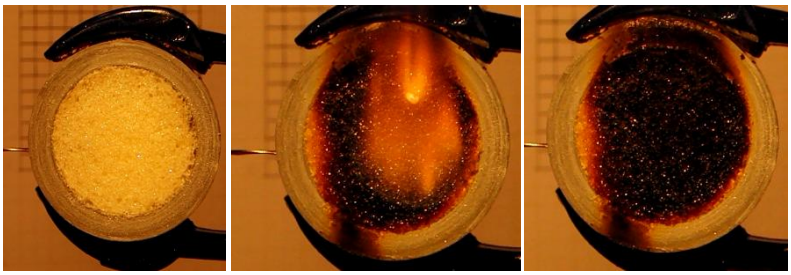

Figure 91 – Burning test of expanded PU foam with 20 mass percent of AN, horizontal position.

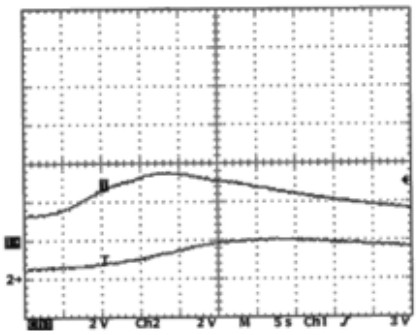

Figure 92 - Temperature records showing thermocouples delay allowing flame velocity measurement (2 V/div. ↔ 200 ºC/div.) as a function of time (5 s/div.).

Thermocouple 1: 3.6 V = 360 ºC

Thermocouple 2: 2 V = 200 ºC

Δt = 8 s for ΔL = 3 x 10^{-3} m

First thermocouple had a 4 x 10^{-3} m distance from the surface of the sample, the second thermocouple had 7 x 10^{-3} m.

m_i = 30.464 g

m_f = 30.372 g

It is visible in Figure 91 that only the surface was burned, the ignition of the sample only lasted about 20 seconds. The fast extinguishing of the sample is confirmed by the Δm, which is low (0.92 g). The signal from the second thermocouple is very low because the ignition of the sample only happened at the surface.

Modified cylindrical configuration with PMMA continuous ignition device

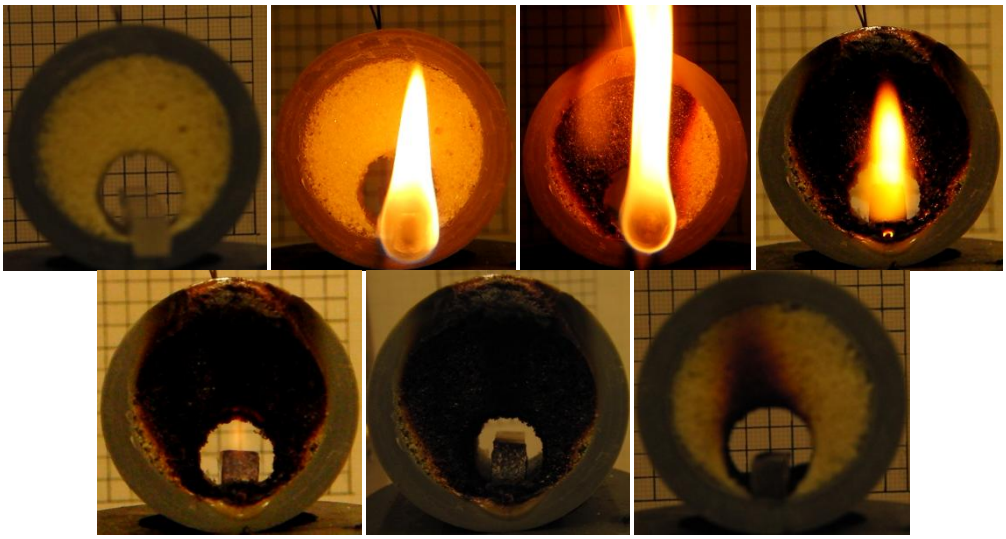

Figure 93 – Burning test of expanded PU foam with 20 mass percent of AN, with PMMA slab.

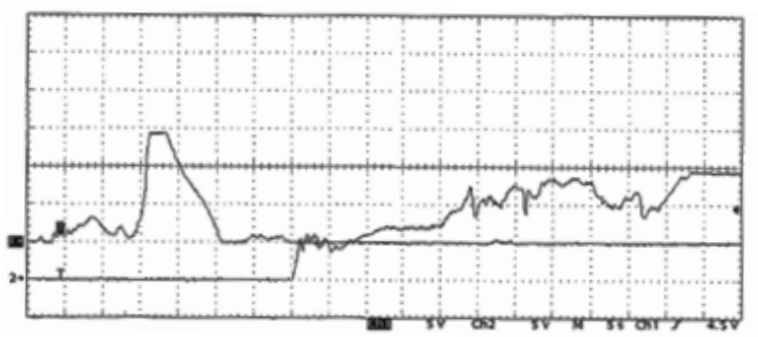

Figure 94 - Temperature records showing thermocouples delay allowing flame velocity measurement (5 V/div. ↔ 500 ºC/div.) as a function of time (5 s/div.).

Thermocouple 1: 14 V = 1400 ºC

Thermocouple 2: 14 V = 1400 ºC

Δt = 75 s for ΔL = 3 x 10^{-3} m

First thermocouple had a 5 x 10^{-3} m distance from the surface of the sample, the second thermocouple had 8 x 10^{-3} m.

m_i = 29.924 g

m_f = 28.761 g

$\Delta m_{(PMMA)}$ = 1.359 g

The measured temperature close to PMMA upper surface is 530 ºC. In the middle position between PMMA surface and PU upper tunnel surface it is 430 ºC. Close to the upper surface of tunnel (stagnation convection surface) it is 530 ºC.

Thermocouples records (Figure 94) show burning temperatures (when PU/AN burns and do not present partial pyrolysis) up to ≈1400 ºC and flame propagation on the level of $mm.s^{-1}$.

Pyrolysis is observed before flame propagation. The burning test lasted more than 6 minutes. The flame was carried out through the interior of the tunnel made in the sample, has it can be observed in Figure 93, even the back of the sample was a little burned at the end of the experiment.

Flame propagation, driven by PMMA slab, allows a more complete pyrolysis and burning of PU/AN material it is confirmed by Δm = 1.163 g, which is higher than in the sample testes in original configuration.

Modified cylindrical configuration with the seven tunnels horizontal position

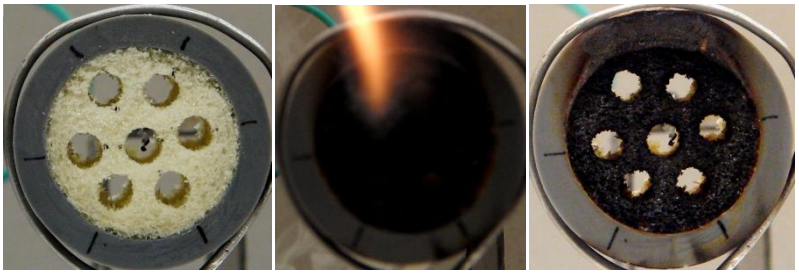

Figure 95 – Burning test of expanded PU foam with 20 mass percent of AN, with the 7 holes, horizontal position.

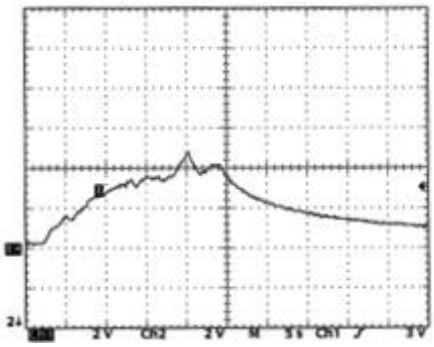

Figure 96 - Temperature records showing thermocouples delay allowing flame velocity measurement (2 V/div. ↔ 200 ºC/div.) as a function of time (5 s/div.).

Thermocouple 1: 4.8 V = 480 ºC

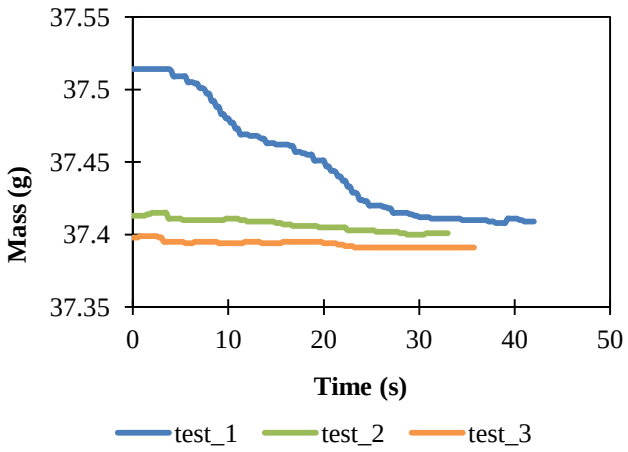

Figure 97 – Mass depletion of the sample during the burning tests.

Only the front and the interior of the holes, until effectivelly the middle of the sample, were burned superficially. In the first test the flame takes ≈ 10 seconds to extinguish, a lot of smoke was produced during the inflammation, more than the tests of the samples that used the tunnel ventilating configuration with the PMMA ignition slab. In the second picture of Figure 95 the holes cannot be seen due to the amount of smoke produced by the burning process. The second and third tests were quicker, because the sample almost did not ignite. The production of smoke decreased from test to test.

The total of mass loss was 0.123 g, approximately 85 % of the mass lost process occurred during the first test.

<u>Original cylindrical configuration horizontal position with paint</u>

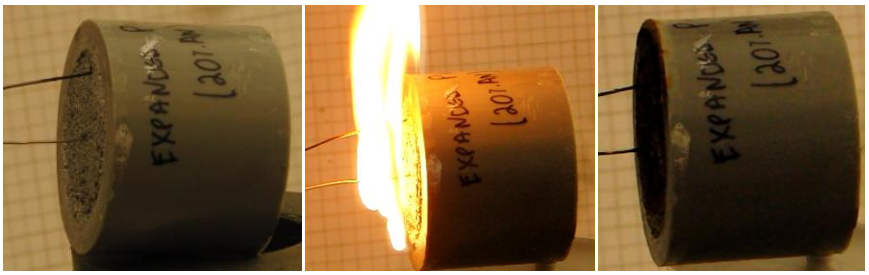

Figure 98 – Burning test of expanded PU foam with 20 mass percent of AN, painted with cellulosic aluminium paint, horizontal position.

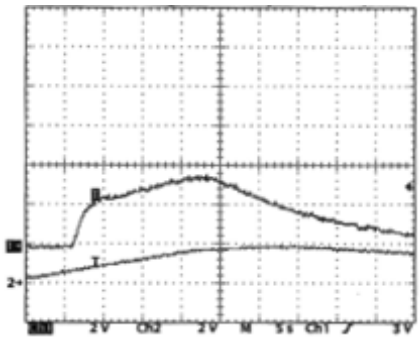

Figure 99 - Temperature records showing thermocouples delay allowing flame velocity measurement (2 V/div. ↔ 200 ºC/div.) as a function of time (5 s/div.).

Thermocouple 1: 3.6 V = 360 ºC

Thermocouple 2: 2 V = 200 ºC

Δt = 7 s for ΔL = 5 x 10^{-3} m

First thermocouple had a 3 x 10^{-3} m distance from the surface of the sample, the second thermocouple had 8 x 10^{-3} m.

m_i = 30.687 g

m_f = 30.422 g

Only the front of the sample was burned superficially. The flame took ≈ 25 seconds to extinguish, not a lot of smoke was produced during the inflammation. It was possible to see some bubbles at the top of the sample, from the paint. Due to the presence of the paint, this sample produced more smoke than the sample, with the same configuration, that was not painted. The fast extinguishment of the sample is confirmed by the Δm, which is very low (0.652 g).

Modified cylindrical configuration with PMMA continuous ignition device with paint

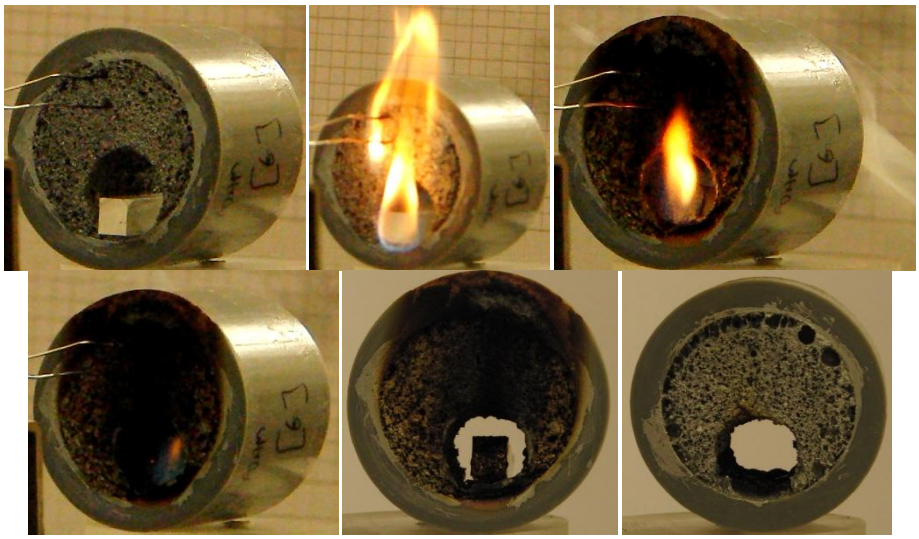

Figure 100 – Burning test of expanded PU foam with 20 mass percent of AN painted, with PMMA slab.

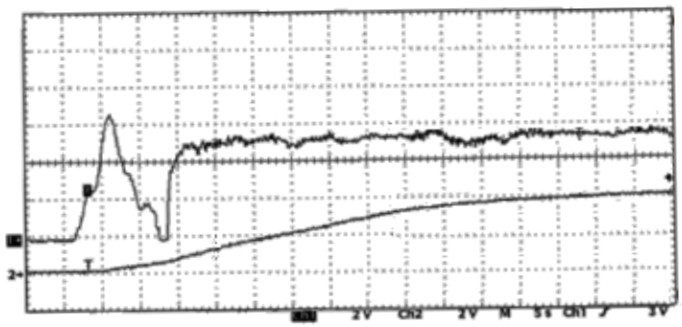

Figure 101 - Temperature records showing thermocouples delay allowing flame velocity measurement (2 V/div. ↔ 200 ºC/div.) as a function of time (5 s/div.).

Thermocouple 1: 4.8 V = 480 ºC

Thermocouple 2: 4 V = 400 ºC

Δt = 40 s for ΔL = 5 x 10^{-3} m

First thermocouple had a 3 x 10^{-3} m distance from the surface of the sample, the second thermocouple had 8 x 10^{-3} m.

m_i = 30.872 g

m_f = 29.707 g

$\Delta m_{(PMMA)}$ = 0.658 g

In the test using the tunnel ventilating configuration with the PMMA ignition slab, pyrolysis is observed before flame propagation. The burning test lasted approximately 10 minutes. The amount of smoke produced can be observed in Figure 100, which was high. At the beginning it is possible to see the paint boiling.

Flame propagation in a painted sample, driven by PMMA slab, allows a more complete pyrolysis and burning of PU/AN material it is confirmed by $\Delta m = 1.165$ g, which is higher than in the sample testes in original configuration with paint.

Modified cylindrical configuration with the seven tunnels horizontal position with paint

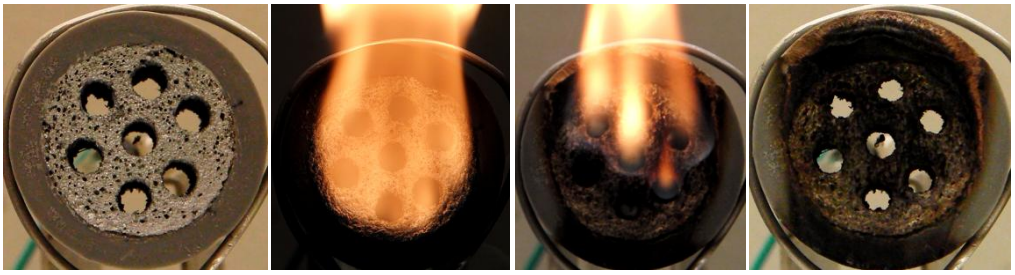

Figure 102 – Burning test of expanded PU foam with 20 mass percent of AN, with the 7 holes, painted with cellulosic aluminium paint, horizontal position.

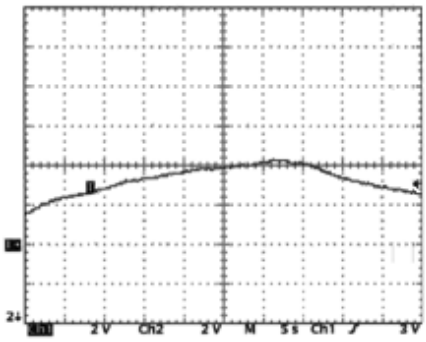

Figure 103 - Temperature records showing thermocouples delay allowing flame velocity measurement (2 V/div. ↔ 200 ºC/div.) as a function of time (5 s/div.).

Thermocouple 1: 4.4 V = 440 ºC

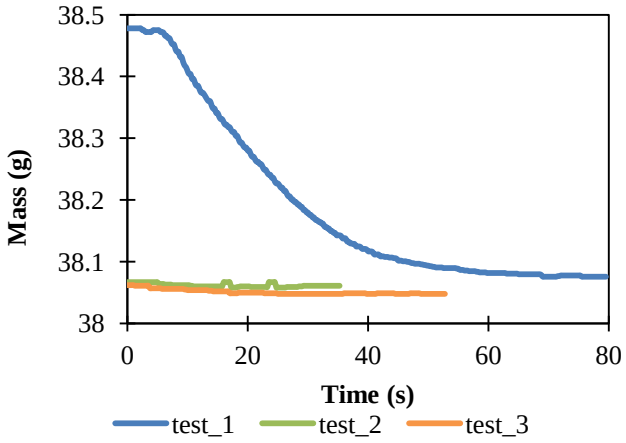

Figure 104 – Mass depletion of the sample during the burning tests.

Only the front and the interior of the holes, until effectivelly the middle of the sample, were burned superficially. In the first test after the flame reaches the sample it is seen that the paint starts to boil and it practically closes the small free spaces of the foam. The flame takes ≈ 50 seconds to extinguish, a lot of smoke was produced during the inflammation, more than the tests of the samples that used the tunnel ventilating configuration with the PMMA ignition slab.

The second and third tests were quicker, because the sample almost did not ignite. The production of smoke decreased from test to test.

The total of mass loss was 0.43 g, more than 90 % of the mass lost process occurred during the first test.

Original cylindrical configuration vertical position

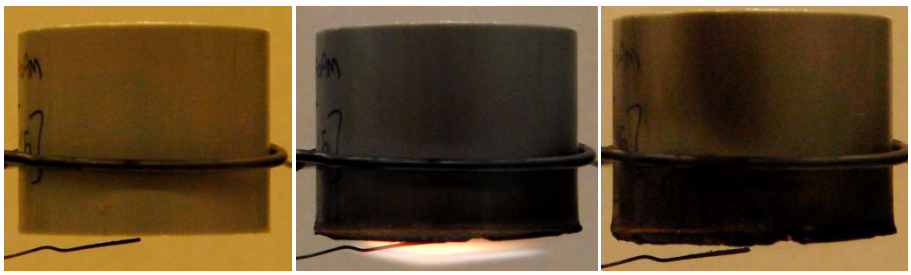

Figure 105 – Burning test of expanded PU foam with 20 mass percent of AN, vertical position.

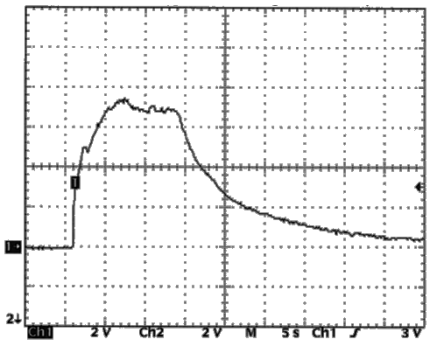

Figure 106 - Temperature records showing thermocouples delay allowing flame velocity measurement (2 V/div. ↔ 200 ºC/div.) as a function of time (5 s/div.).

Thermocouple 1: 9.2 V = 920 ºC

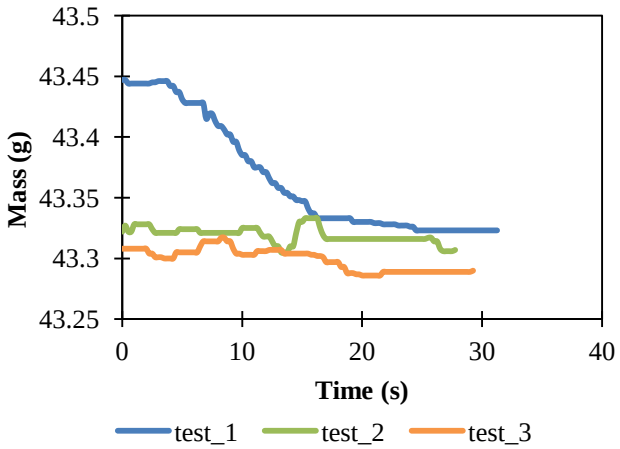

Figure 107 – Mass depletion of the sample during the burning tests.

Only one thermocouple was used in this assay, in the bottom of the sample, as can be seen in Figure 105. Only the bottom was burned superficially. In the first test the flame takes ≈ 10 seconds to extinguish, it did not produce a large quantity of smoke. The second and third tests did not burn.

The total of mass loss was 0.157 g, almost 80 % of the mass lost process occurred during the first test.

Modified cylindrical configuration with the seven tunnels vertical position

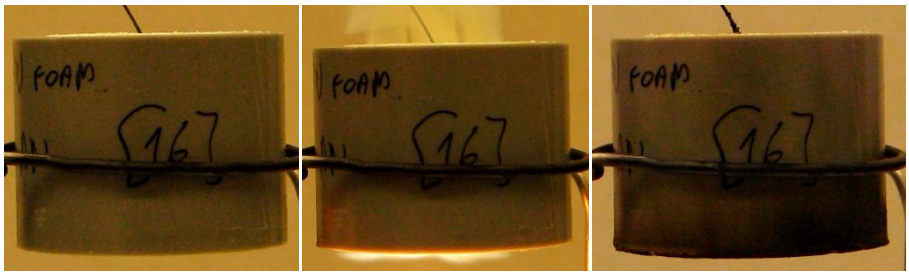

Figure 108 – Burning test of expanded PU foam with 20 mass percent of AN, with the 7 holes, vertical position.

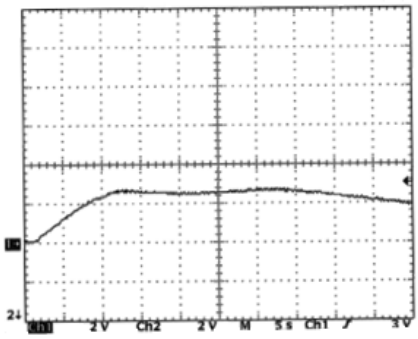

Figure 109 - Temperature records showing thermocouples delay allowing flame velocity measurement (2 V/div. ↔ 200 ºC/div.) as a function of time (5 s/div.).

Thermocouple 1: 2.8 V = 280 ºC

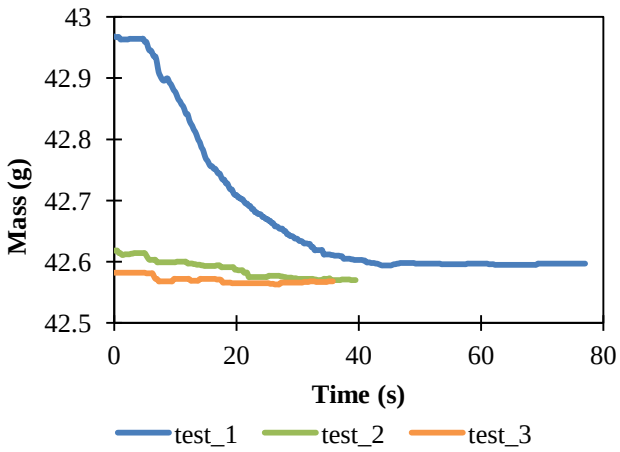

Figure 110 – Mass depletion of the sample during the burning tests.

Only one thermocouple was used in this assay, inside the central hole from the top of the sample. In the first test the flame takes ≈ 10 seconds to extinguish, it produced a lot

of smoke. During the videos the flame cannot be seen, but it is burning inside the holes made in the sample. In the second and third tests the flame extinguishes immediately, the production of smoke is always decreasing from test to test. During the tests it was observed a small expansion of the foam in the top of the test tube, when the next test was at the beginning, the expansion is not visible, but after burning the sample the expansion was visible again.

The total of mass loss was 0.4 g, more than 90 % of the mass lost process occurred during the first test.

Modified cylindrical configuration with the seven tunnels vertical position with paint

Figure 111 – Burning test of expanded PU foam with 20 mass percent of AN, with the 7 holes, painted with cellulosic aluminium paint, vertical position.

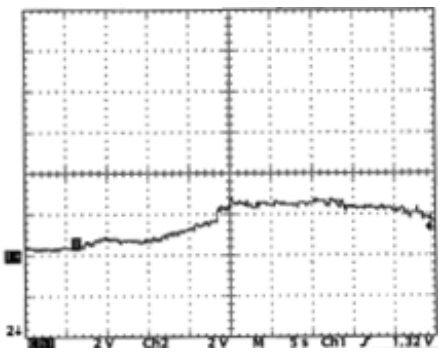

Figure 112 - Temperature records showing thermocouples delay allowing flame velocity measurement (2 V/div. ↔ 200 ºC/div.) as a function of time (5 s/div.).

Thermocouple 1: 3.2 V = 320 ºC

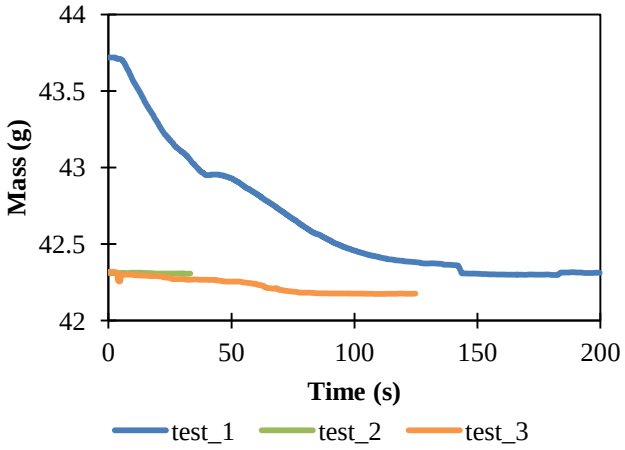

Figure 113 – Mass depletion of the sample during the burning tests.

Only one thermocouple was used in this assay, inside the central hole from the top of the sample. In the first test the flame takes more than 1 minute to extinguish, it did produce a high quantity of smoke, more than the sample that was not painted, and more than the painted sample in the horizontal position. In the video the flame is not possible to see, but the sample was burning in the holes, due to the presence of the paint. In the second and third tests the flame extinguished very quickly, the production of smoke is always decreasing from test to test.

The total of mass loss was 1.542 g, approximately 90 % of the mass lost process occurred during the first test.

5.3.3. Syntactic PU foam with 15 mass % of HPM

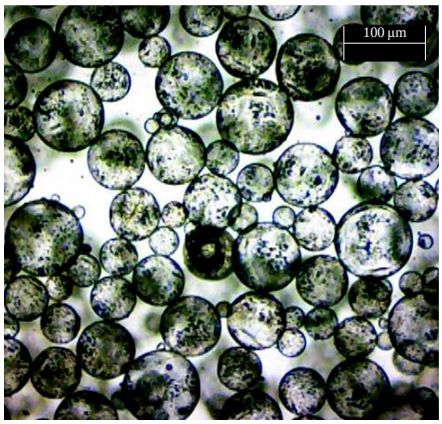

Figure 114 - Photography of microscopic investigation of hollow plastic microspheres.

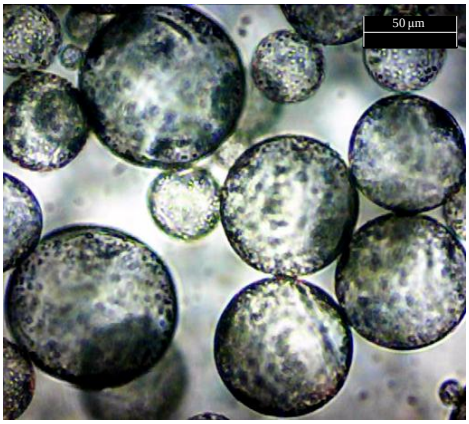

Figure 115 - Photography of microscopic investigation of hollow plastic microspheres.

In the microscopy studies of hollow plastic microspheres it is seen that the diameter is effectively constant, approximately 60 µm.

Figure 116 - Photography of microscopic investigation of syntactic PU foam (15 %HPM).

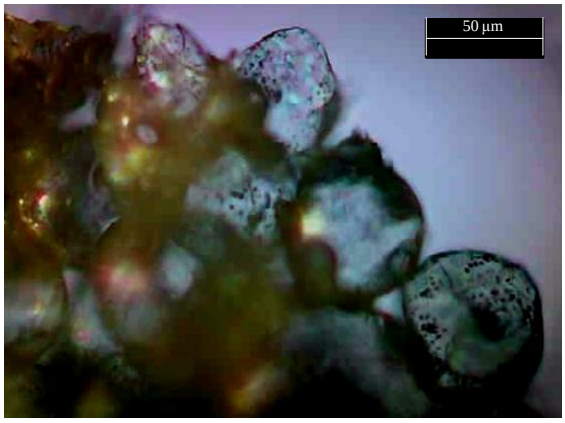

Figure 117 - Photography of microscopic investigation of syntactic PU foam (15 %HPM).

In the microscopy studies of syntactic polyurethane foam without any additive it is also seen the diameter of the hollow plastic microspheres still effectively constant, there are no destruction of HPM by the polyurethane components. All the hollow plastic microspheres are linked by the solution of dense polyurethane. In Figure 117 it can be observed that the foam itself is ≈ 50 µm. The diameter used to perform prediction of

temperature and ignition by Semenov and Frank-Kamenetskii theories was the same used in the expanded PU foam, it was $\lambda = 3.51 \times 10^{-6}$ m, because it was take in account the superficial walls of the sample, this is where the sample starts its ignition.

Original cylindrical configuration horizontal position

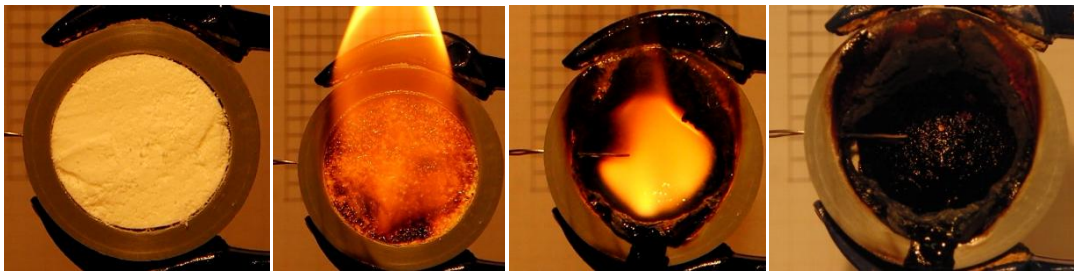

Figure 118 – Burning test of syntactic PU foam, horizontal position.

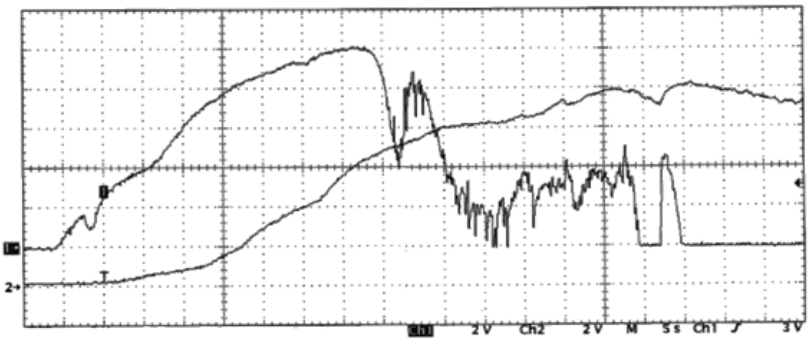

Figure 119 - Temperature records showing thermocouples delay allowing flame velocity measurement (2 V/div. ↔ 200 ºC/div.) as a function of time (5 s/div.).

Thermocouple 1: 10 V = 1000 ºC

Thermocouple 2: 10 V = 1000 ºC

$\Delta t = 35$ s for $\Delta L = 3 \times 10^{-3}$ m

First thermocouple had a 2×10^{-3} m distance from the surface of the sample, the second thermocouple had 5×10^{-3} m.

$m_i = 30.553$ g

$m_f = 29.128$ g

It is visible in Figure 118 that half of the sample was burned. The ignition of the sample had the duration of more than 4 minutes. During the pyrolysis of the sample some bubbles were seen, due to the high quantity of polyethylene (from the HPM) in the mixture. The total of mass loss was 1.425 g. Thermocouples records show burning temperatures up to ≈1000 ºC and flame propagation on the level of $mm.s^{-1}$.

5.3.4. Syntactic PU foam with 15 mass % of HPM and 7 mass % of AN

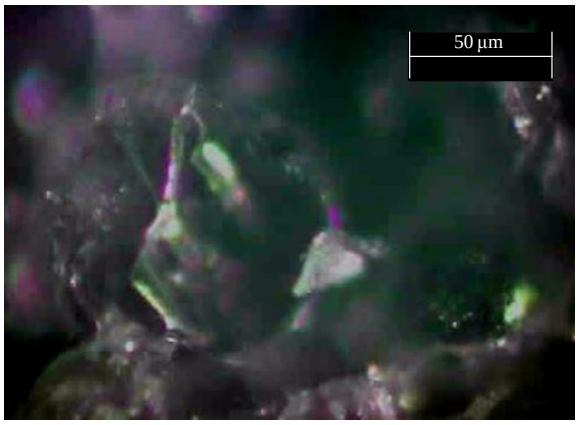

Figure 120 - Photography of microscopic investigation of syntactic PU foam (15 %HPM) with 7 mass percent of AN.

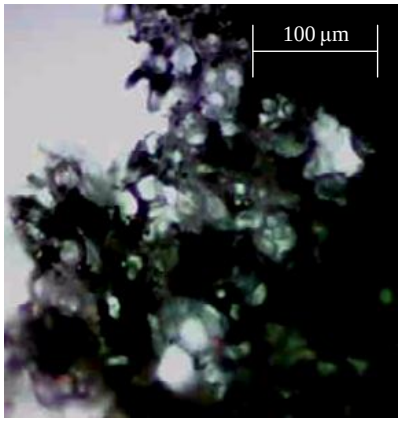

Figure 121 - Photography of microscopic investigation of syntactic PU foam (15 %HPM) with 7 mass percent of AN painted with cellulosic aluminium paint.

In Figure 120 a little particle of ammonium nitrate can be observed, this is smaller than the one present in the microscopic picture of the expanded PU foam with 20 mass percent of ammonium nitrate (Figure 87), this is, probably, because this particle was better micronized. In the microscopy studies of syntactic polyurethane foam with 7 mass % of AN it is seen in Figure 121 that the samples are slightly denser the sample without any additive, this is also due o the fact that the sample presented in this figure is painted with cellulosic aluminium paint.

Without test tube

Figure 122 – Burning test of syntactic PU foam (7 % AN) without test tube.

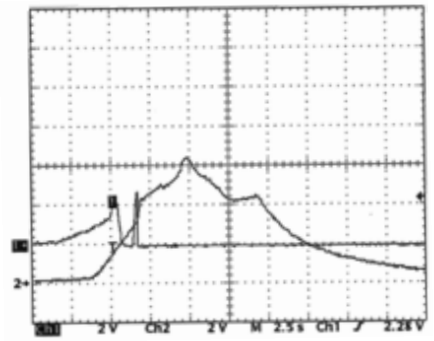

Figure 123 - Temperature records showing thermocouples delay allowing flame velocity measurement (2 V/div. ↔ 200 ºC/div.) as a function of time (5 s/div.).

Thermocouple 1: no signal

Thermocouple 2: 6.2 V = 620 ºC

$\Delta L = 1 \times 10^{-3}$ m

First thermocouple had a 1×10^{-3} m distance from the top of the sample, the second thermocouple had 2×10^{-3} m. The flame was too fast, and sample fell of both thermocouples, which is why the first thermocouple could not get the signal.

The flame burned all the surface first, reached both thermocouples at the same time and a signal was only obtained by one, because the sample separate from the other one. The sample continued to burn until it was separated from the two thermocouples. All this process lasted only ≈20 seconds.

Original cylindrical configuration horizontal position

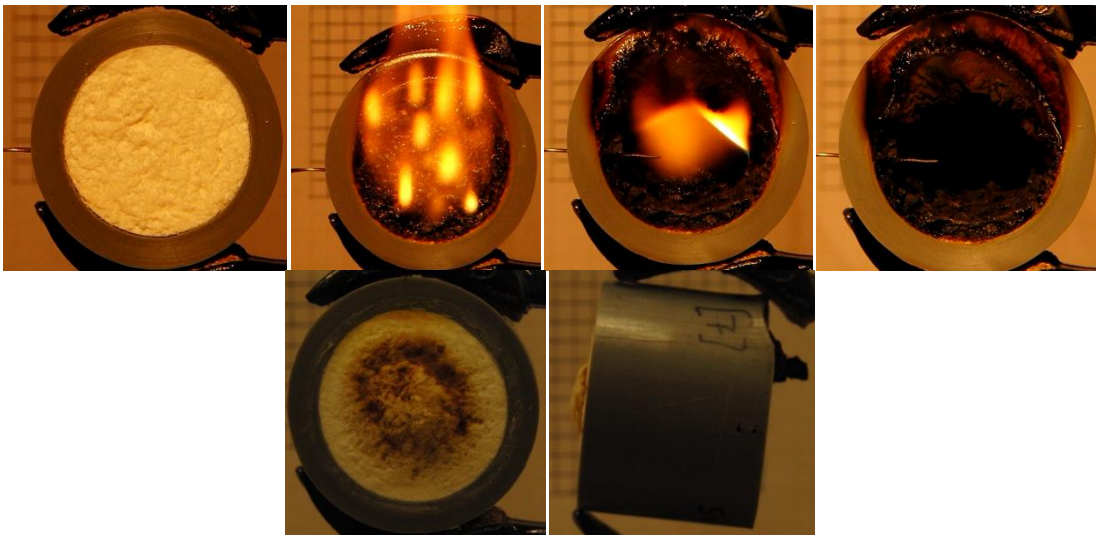

Figure 124 – Burning test of syntactic PU foam with 7 mass % of AN, horizontal position.

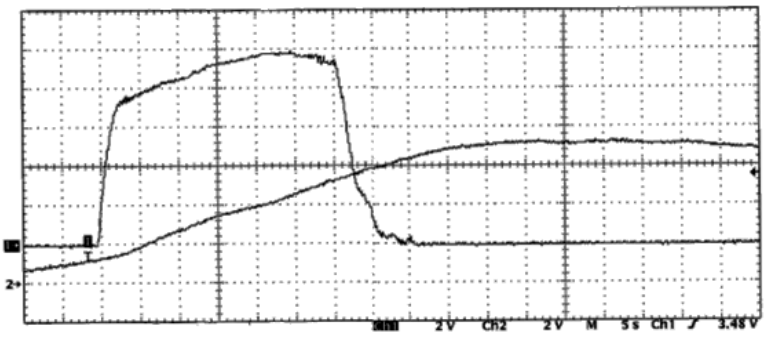

Figure 125 - Temperature records showing thermocouples delay allowing flame velocity measurement (2 V/div. ↔ 200 ºC/div.) as a function of time (5 s/div.).

Thermocouple 1: 10 V = 1000 ºC

Thermocouple 2: 7 V = 700 ºC

Δt = 35 s for ΔL = 3 x 10^{-3} m

First thermocouple had a 2 x 10^{-3} m distance from the surface of the sample, the second thermocouple had 5 x 10^{-3} m.

m_i = 30.983 g

m_f = 29.063 g

It is visible in Figure 124 that half of the sample was burned. The ignition of the sample had the duration of approximately 7 minutes. During the pyrolysis of the sample, some bubbles were seen, it is due to the high quantity of polyethylene (from the HPM) in the mixture. The total of mass loss was 1.92 g. It can be seen that in Figure 124 the back side of the sample expanded after the test was carried out.

Original cylindrical configuration horizontal position with paint

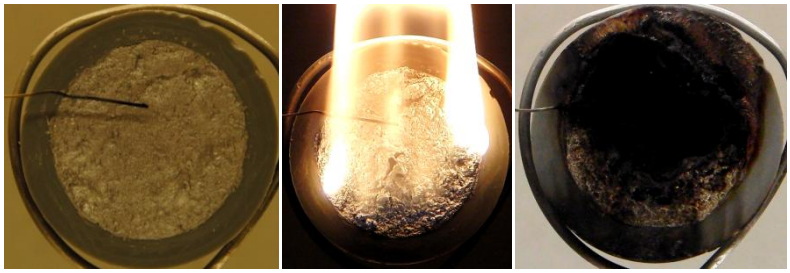

Figure 126 – Burning test of syntactic PU foam with 7 mass % of AN, painted with cellulosic aluminium paint, horizontal position.

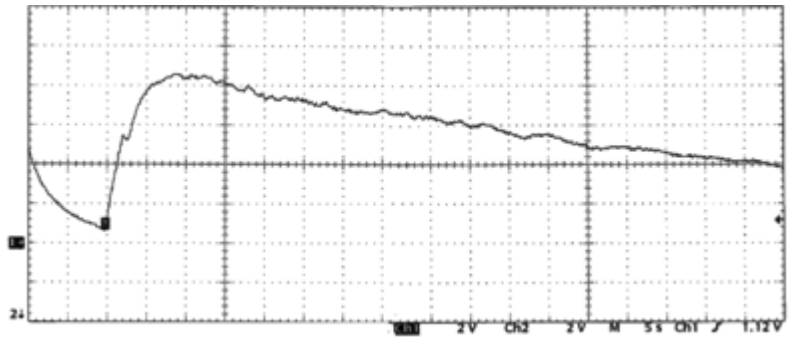

Figure 127 - Temperature records showing thermocouples delay allowing flame velocity measurement (2 V/div. ↔ 200 ºC/div.) as a function of time (5 s/div.).

Thermocouple 1: 8.4 V = 840 ºC

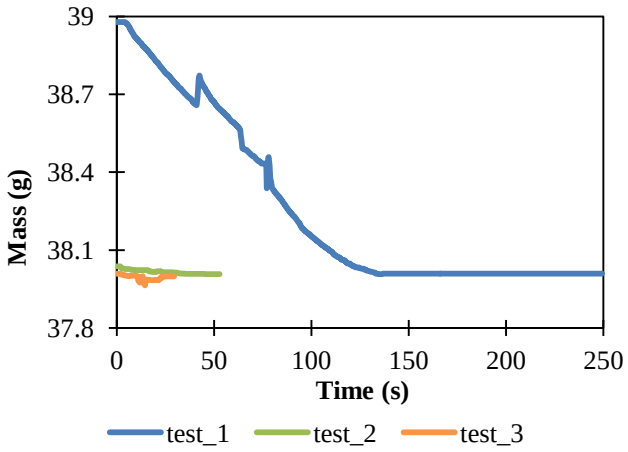

Figure 128 – Mass depletion of the sample during the burning tests.

It is visible in Figure 126 that half of the sample was burned. The first ignition of the sample had the duration of more than 4 minutes. The second test extinguished immediately, after spending almost 30seconds with the lighter. The third test sample did not burn at all.

The total of mass loss was 0.979 g, almost 99 % of the mass lost process occurred during the first test.

Original cylindrical configuration vertical position

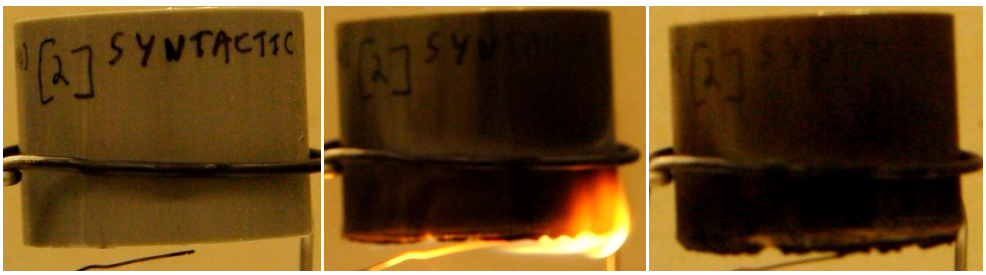

Figure 129 – Burning test of syntactic PU foam with 7 mass % of AN, vertical position.

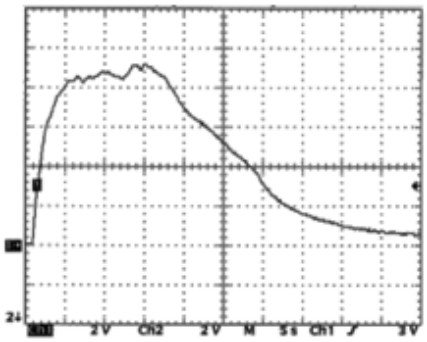

Figure 130 - Temperature records showing thermocouples delay allowing flame velocity measurement (2 V/div. ↔ 200 ºC/div.) as a function of time (5 s/div.).

Thermocouple 1: 8.8 V = 880 ºC

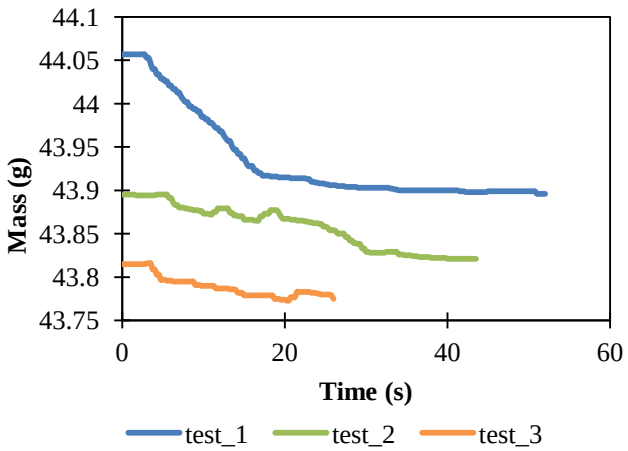

Figure 131 – Mass depletion of the sample during the burning tests.

Only one thermocouple was used in this assay, in the bottom of the sample, as it can be seen in Figure 129. In the first test the flame takes ≈ 1 minute to extinguish, it produced a significant quantity of smoke. The second and third tests did not ignite, but still produced a small quantity of smoke.

The total of mass loss was 0.282 g, almost 60 % of the mass lost process occurred during the first test.

Original cylindrical configuration vertical position with paint

Figure 132 – Burning test of syntactic PU foam with 7 mass % of AN, painted with cellulosic aluminium paint, vertical position.

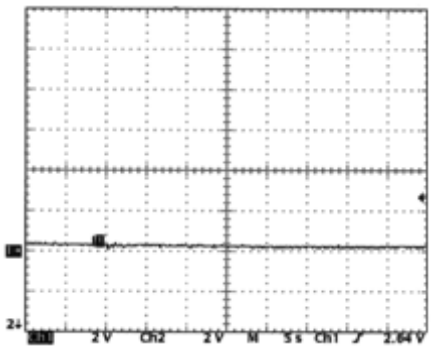

Figure 133 - Temperature records showing thermocouples delay allowing flame velocity measurement (2 V/div. ↔ 200 ºC/div.) as a function of time (5 s/div.).

Thermocouple 1: no signal

The thermocouple did not record the signal because it was put on top of the sample and the flame did not get there.

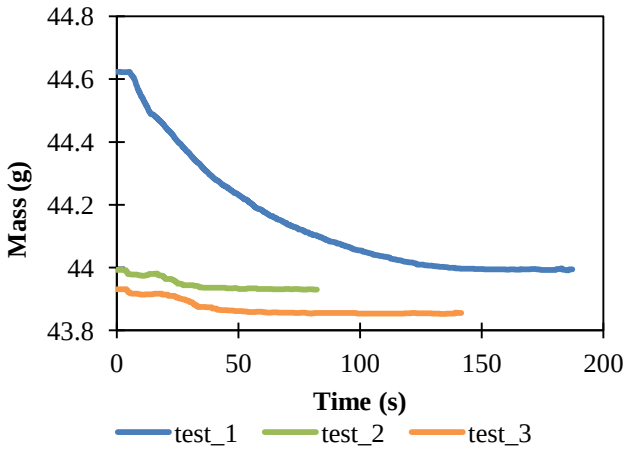

Figure 134 – Mass depletion of the sample during the burning tests.

This was actually the first test made in the vertical position with only one thermocouple, and this one was put on the top of the sample, as it did not recorded a signal, from this test on, the thermocouple was always put on the bottom of the sample, for samples with this configuration.

In the first test the flame takes ≈ 3 minutes to extinguish, it produced a significant quantity of smoke, more than the sample without paint. The second and third tests did not ignited, but still produced a small quantity of smoke.

The total of mass loss was 0.693 g, more than 90 % of the mass lost process occurred during the first test.

5.3.5. Syntactic PU foam 15 mass % of HPM, 7 mass % of AN and 5 mass % of SB

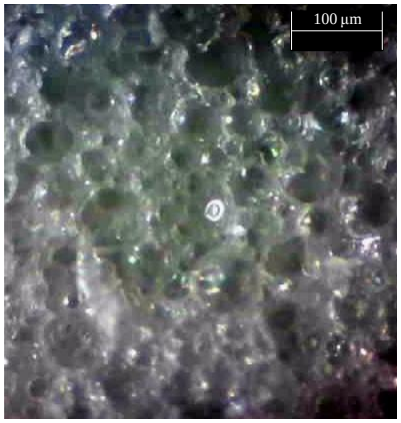

Figure 135 - Photography of microscopic investigation of syntactic PU foam (15 %HPM) with 7 and 5 mass percent of AN and SB, respectively.

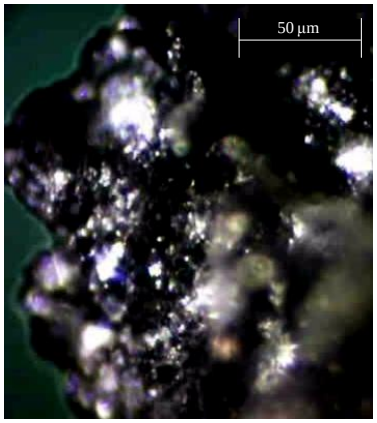

Figure 136 - Photography of microscopic investigation of syntactic PU foam (15 %HPM) with 7 and 5 mass percent of AN and SB, respectively, painted with cellulosic aluminium paint.

In the microscopy studies of syntactic polyurethane foam with 7 and 5 mass % of AN and SB, respectively, it is seen in Figure 135 that the samples are even denser than sample with only 7 mass % of SB. In Figure 136 it can be observed that in the sample

painted with cellulosic aluminium paint, the format of the microspheres is visible through the paint.

Original cylindrical configuration horizontal position

Figure 137 – Burning test of syntactic PU foam with 7 and 5 mass % of AN and SB, horizontal position.

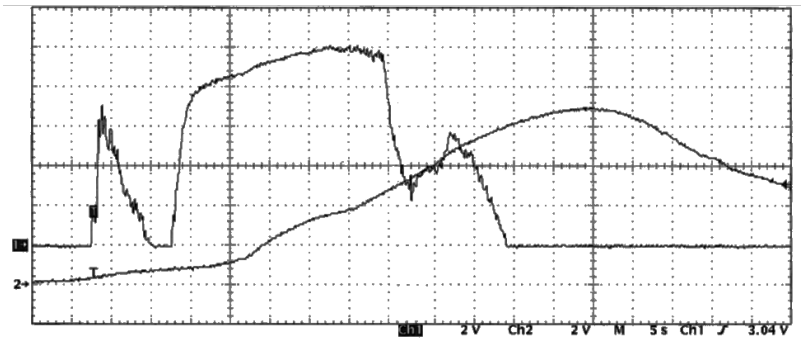

Figure 138 - Temperature records showing thermocouples delay allowing flame velocity measurement (2 V/div. ↔ 200 ºC/div.) as a function of time (5 s/div.).

Thermocouple 1: 10 V = 1000 ºC

Thermocouple 2: 8.8 V = 880 ºC

Δt = 35 s for ΔL = 3 x 10^{-3} m

First thermocouple had a 2 x 10^{-3} m distance from the surface of the sample, the second thermocouple had 5 x 10^{-3} m.

m_i = 30.981 g

m_f = 29.190 g

It is visible in Figure 137 that half of the sample was burned. The ignition of the sample had the duration of more than 5 minutes. During the pyrolysis of the sample some bubbles were seen, due to the high quantity of polyethylene (from the HPM) in the mixture. The total mass loss was 1.791 g. It can be seen that in Figure 137 the back of the sample was a little bit burned, and suffered a small expansion.
This assay was very similar to that taken in the syntactic PU foam with 7 mass % of AN and without sodium bicarbonate.

Original cylindrical configuration horizontal position with paint

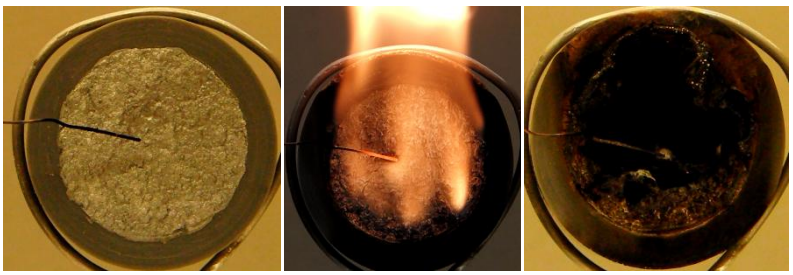

Figure 139 – Burning test of syntactic PU foam with 7 and 5 mass % of AN and SB, painted with cellulosic aluminium paint, horizontal position.

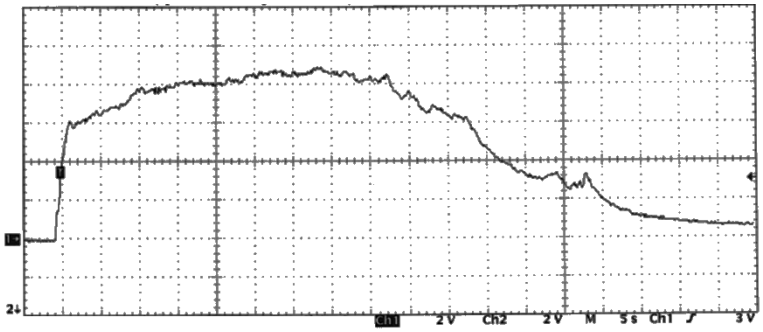

Figure 140 - Temperature records showing thermocouples delay allowing flame velocity measurement (2 V/div. ↔ 200 ºC/div.) as a function of time (5 s/div.).

Thermocouple 1: 8.4 V = 840 ºC

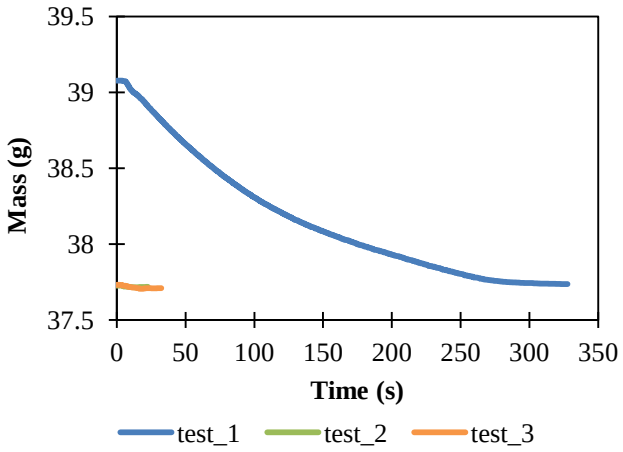

Figure 141 – Mass depletion of the sample during the burning tests.

It is visible in Figure 139 that almost half of the sample was burned. The first ignition of the sample had the duration of more than 4 minutes. The boiling of the paint at the surface of the sample was visible. The second and the third tests did not burn, there was almost no smoke produced in these last two tests.

The total of mass loss was 1.367 g, almost 99 % of the mass lost process occurred during the first test.

Original cylindrical configuration vertical position

Figure 142 – Burning test of syntactic PU foam with 7 and 5 mass % of AN and SB, vertical position.

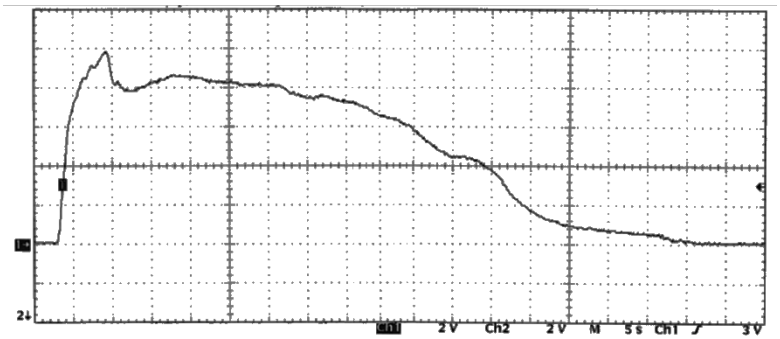

Figure 143 - Temperature records showing thermocouples delay allowing flame velocity measurement (2 V/div. ↔ 200 ºC/div.) as a function of time (5 s/div.).

Thermocouple 1: 8.4 V = 840 ºC

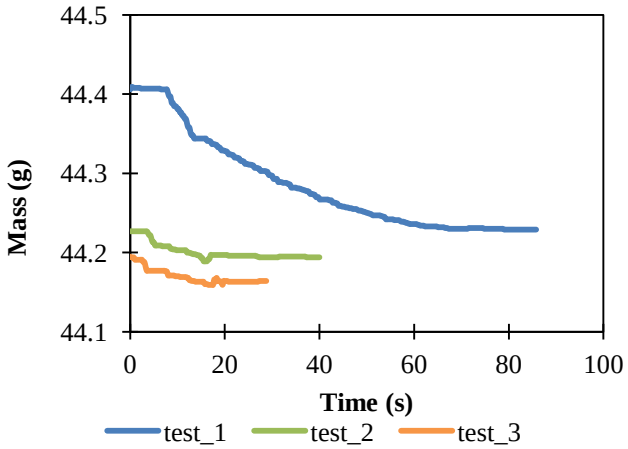

Figure 144 – Mass depletion of the sample during the burning tests.

Only one thermocouple was used in this assay, in the bottom of the sample, as can be seen in Figure 142. In the first test the flame takes ≈ 1 minute to extinguish, it produced a significant quantity of smoke. The second and third tests did not ignite, but still produced a small quantity of smoke.

The total of mass loss was 0.242 g, more than 70 % of the mass lost process occurred during the first test.

Original cylindrical configuration vertical position with paint

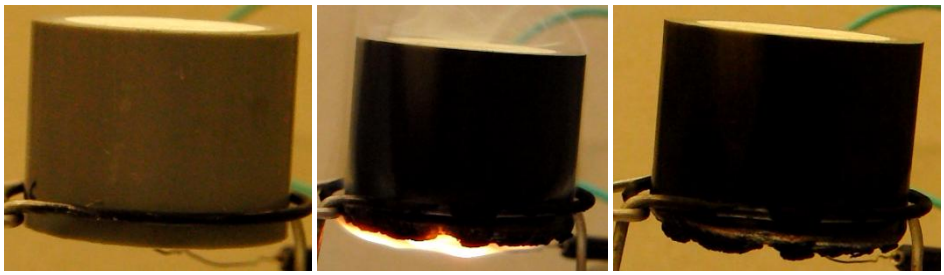

Figure 145 – Burning test of syntactic PU foam with 7 and 5 mass % of AN and SB, painted with cellulosic aluminium paint, vertical position.

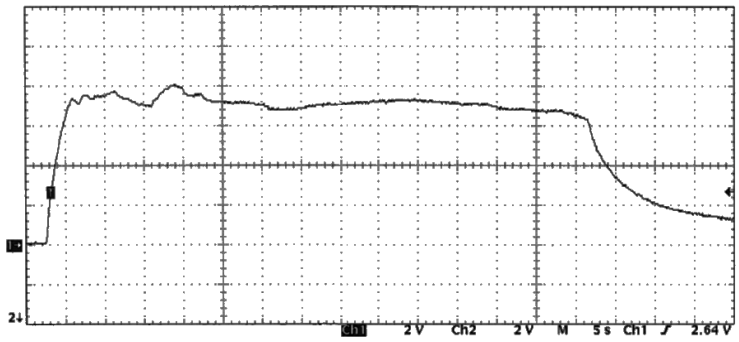

Figure 146 - Temperature records showing thermocouples delay allowing flame velocity measurement (2 V/div. ↔ 200 ºC/div.) as a function of time (5 s/div.).

Thermocouple 1: 8 V = 800 ºC

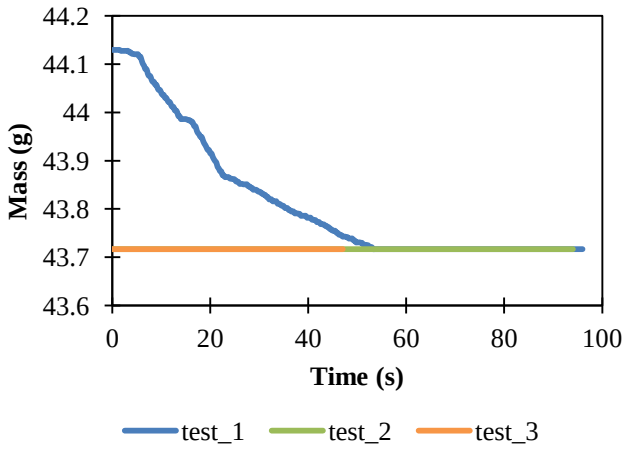

Figure 147 – Mass depletion of the sample during the burning tests.

In the first test the flame takes more than 1 minute to extinguish, it produced a significant quantity of smoke, more than the sample without paint. The second

extinguished after almost 30 seconds, and third test did not ignite, but still produced a small quantity of smoke. The production of smoke decreased from test to test.

The total of mass loss was 0.191 g, 100 % of the mass lost process occurred during the first test.

CHAPTER 6 – CONCLUSIONS

In this work were studied combustion properties, ignition and detection of two different kinds of polyurethane foams, expanded and syntactic (dense polyurethane with hollow plastic microspheres). To this two types of polyurethane foams were added ammonium nitrate and sodium bicarbonate as additive in small concentrations.

First of all, it were predicted their combustion properties using THOR code. The obtained results showed that adding ammonium nitrate, to polyurethane and air mixture, the combustion temperature decreases, and that adding sodium bicarbonate to polyurethane, air and ammonium nitrate the combustion temperature is also decreased.

The temperature was also predicted by Semenov's theory. It was studied the temperature values for different diameters and has been concluded that the higher the diameter, the lower is the temperature's particle. That is due to the decreasing of the surface area of the particle when the diameter is higher. For an equivalent particle diameter of 3.51×10^{-6} m the temperature obtained was 534 K. This reduced value was obtained for an "eternal" stay to obtain ignition and makes the boundary temperature limit of thermal ignition.
The ignition delay was predicted by Frank-Kamenetskii phenomenological approach. For gas environmental temperature of 450 K, the particle takes 5×10^{-6} s to ignite, for 650 K takes 4×10^{-7} s, and for 850 K takes 3×10^{-7} s. The higher the T_g, the faster is the ignition of the particle (that is because the heating rate is faster, so the particle takes less time to ignite).

Thermal decomposition of polyol in N_2 atmosphere heated at 5 ºC.min^{-1} occurs in two steps (300-315 ºC and 440-540 ºC), while the polyol with heat rate of 10 ºC.min^{-1} occurs in a single step at higher temperatures (540-600 ºC). In both DSC-TGA results for polyol the total percentage of weight loss is very low, this is due to the encapsulation of the sample in the pan. That is why the one that was heated at 10 ºC.min^{-1} has lower percentage of weight loss, because the heat rate was faster. Comparing with the results from the literature it was concluded that this is a polyol polyester. Due to hollow plastic microspheres (low density) the thermogram presents a very inconstant curve. It can be

concluded that in a N_2 atmosphere, heated at 10 ºC.min^{-1}, the polyethylene made microspheres were completely pyrolysed, but this process is constantly modified by the pyrolysis of the nearest spheres.

FTIR analysis showed that in expanded polyurethane foam the spectrums of fresh and burned samples do not have significant differences. Consequently the burned sample was not completely burned out. In the spectra of the fresh sample of expanded polyurethane foam, with 20 mass percent of ammonium nitrate, it can be seen the presence of ammonium nitrate. The same sample burned does not have ammonium nitrate in presence, during the ignition of the sample, the ammonium nitrate was reacted. Dense polyurethane, polyethylene and syntactic polyurethane foam were compared by infrared analysis. The major difference is that dense polyurethane presents more intense region of the functional groups with atoms of oxygen and/or nitrogen. This is due to the fact that the syntactic polyurethane foam has the presence of polyethylene in its composition. The presence of polyethylene reduces the percentage of the atom oxygen in the mixture, so the percentage of hydrocarbons is higher. Syntactic polyurethane foams, with 7 mass percent of ammonium nitrate, does not shows significant differences comparing to the one that has no additives. No differences were not observed also for the syntactic polyurethane foam, with 7 mass percent of ammonium nitrate and 5 mass percent of sodium bicarbonate, that is because the device only detects the compounds in quantities exceeding 10 % (m/m), when it comes to mixtures.

It was studied expanded polyurethane foam without any additive, and expanded polyurethane foam with 20 mass percent of ammonium nitrate.

In the burning tests for expanded polyurethane foam, various configurations were tested: filled cylindrical test samples, samples where seven tunnels were open, and samples where one tunnel was open parallel to the central axis, where it was placed a 5x5 mm PMMA slab working like a permanent ignition line. Measured temperature close to PMMA upper surface until the upper surface of tunnel (stagnation convection surface) is around 550 ºC. Some of these samples were painted with cellulosic aluminium paint and were tested in horizontal and vertical positions.

It was concluded that the flame propagation, driven by PMMA slab, was the configuration where the mass loss was more important. PMMA slab allows a more complete pyrolysis and burning of polyurethane material (with and without ammonium

nitrate). The samples painted with cellulosic aluminium presented an easier ignition and flame propagation. Also, the mass loss is generally higher, but the extinction of the flame is quicker than in the configuration with driven flame by PMMA slab. Comparing only the different position of the sample (horizontal and vertical) for the same configuration, the vertical test presented a more complete pyrolysis. As it was expected the samples with 20 mass percent of ammonium nitrate in its composition were ignites most successfully.

It was not added sodium bicarbonate to the expanded polyurethane foam due to the flame extinction observed in the tests presented.

The burning tests of syntactic polyurethane foam were performed for four configurations, cylindrical test samples, horizontal and vertical, and with or without cellulosic aluminium. It was concluded that samples with increased concentrations of ammonium nitrate burn quite well. The sodium bicarbonate has a very small influence in these reactive materials, because for concentrations less than 5 mass percent samples still burn quite well. The difference of mass loss between syntactic polyurethane foams with AN and with AN and SB is not very significant. The measurement of temperatures of these samples is quite similar. This is also due to the fact that the thermocouple were near to the ignition point, so the thermocouple captured the signal of the lighter. In the samples painted with cellulosic aluminium paint the ignition was not as easy as in the other samples, and the mass loss is lower. Tests taken in horizontal position presented a flame propagation more efficient than the vertical position tests.

Influence of hollow plastic microspheres in polyurethane foam changes combustion phenomena, generating micro continuous hot spots, from spheres. Polyethylene microspheres increase thermal insulation of foam, reducing the thickness between existing flame and internal ignition layer, do not increase flame velocity, but ensure more regular flame propagation, it allows flame propagation in syntactic polyurethane foams (when expanded polyurethane foam present extinction).

BIBLIOGRAPHIC REFERENCES

AkzoNobel (2011). "Expancel DE", *AkzoNobel*. http://www.akzonobel.com/expancel/products/expancel_de/ [November, 2012].

Bandyopadhyay, S., Bhaduri, D. (1972). "Prediction of Ignition Temperature of a Single Coal Particle", *Combustion and Flame*. Vol. 18. pp. 411-415.

Barbot (2012). "Alumínio Celuloso", *Ficha de dados de segurança*. Version 6. pp. 1-10.

Bottom, R. (2008). "Principles and Applications of Thermal Analysis: Thermogravimetric Analysis", *Blackwell Publishing*. Oxford, UK. pp. 87-118.

Brousseau P., Dorsett, H. E., Cliff, M. D., Anderson, C. J. (2002). "Detonation Properties of Explosives Containing Nanometric Aluminum Powder", *12th Symposium(International) on Detonation*. San Diego, California. pp. 1-10.

Busker, R. W., Hammer, A. H., Kuijpers, W. C., Poot, C. A. J., Bergers, W. W. A., Bruijnzeel, P. L. B. (1999). "Toxicity Testing of Combustion Products of Polyurethane and Polyvinylchloride", *TNO report*. Netherlands. pp. 1-30.

Campos, J. L. A. (1982). "Risco de Explosão em Instalações de Transporte Pneumático", *Seminário Sobre Transporte Pneumático*. F.C.T.U.C., Coimbra. pp. 97-143.

Campos, J., (1991). "Thermodynamic Calculation of Solid and Gas Combustion Pollutants Using Different Equations of State", in *Proc. of 1st International Conference on Combustion Technologies for a Clean Environment*, Vilamoura, Algarve, Portugal, pp. 30.4-1-30.4-11.

Carvalheira, P., Campos, J., Gadiot, G. (1995). "Burning Rate Modifiers for NA/HTPB-IPDI Composite Solid Propellants for Gas Generators", *Proc. of the 26th International Annual Conference of ICT*, Fraunhofer-Institut für Chemische Technologie. Karlsruhe, Germany. pp. 69.1-69.14.

Chattopadhyay, D. K., Webster, D. C. (2009). "Thermal Stability and Flame Retardancy of Polyurethanes" *Progress in Polymer Science*. Vol. 34. pp. 1068-1133.

Chattopadhyay, D.K., Raju, K. V. S. N., (2007). "Structural Engineering of Polyurethane Coatings for High Performance Applications", *Progress in Polymer Science*. Vol. 32.- pp. 352-418.

Chelliah H.K., Wanigarathne, P.C., Lentati, A.M., Krauss, R.H., Fallon, G.S. (2003). "Effect of Sodium Bicarbonate Particle Size on the Extinction Condition of Non-premixed Counterflow Flames", *Combustion and Flame*. Vol. 134. pp. 261-272.

Dessler A. J., Overs D. E., Appleby W. H. (2005). "The Hindenburg Fire: Hydrogen or Incendiary Paint?", *Buoyant Flight*. Vol. 52. pp. 1-11.

Durães L., Campos J., Portugal A. (1998). "Reaction Path of Energetic Materials Using THOR Code", *American Institute of Physics*. Woodbury, NY. Vol. 429. pp. 341-344.

Durães, L., Campos J. (1995). "Thermodynamic Predictions of Pollutants Using a New Equation of State", *Proc. of the 3rd International Conference on Combustions Technologies for a Clean Environment*. Lisboa, Portugal. Vol. II. pp. 116-123.

Durães, L., Campos, J., Góis, J. C. (1995). "Deflagration and Detonation Predictions Using a New Equation of State." *Proc. of the 26th International Annual Conference of ICT*, Fraunhofer-Institut für Chemische Technologie. Karlsruhe, Germany. pp. 67.1-67.13.

Durães, L., Campos, J., Góis, J. C. (1996). "New Equations of State for the Detonation Products of Explosives", *American Isntitute of Physics*. Woodbury, NY. Vol. 370. pp. 385-388.

Durães, L., Campos, J., Portugal A. (1997). "Combustion and Detonation Modelling Using THOR Code", *Proc. of the 28th International Annual Conference of ICT*, Fraunhofer-Institut für Chemische Technologie. Karlsruhe, Germany. pp. 89.1-89.10.

Durães, L., Campos, J., Portugal, A. (1996). "Thermal Decomposition of Energetic Materials Using THOR Code", Proc. *of the 22nd International Pyritechnics Seminar*. Fort Collins, CO. pp. 496-508.

Durães, L., Campos, J., Portugal, A. (2000). "Thermodynamical Prediction of Combustion and Detonation Properties Using Modified THOR Code", *Proc. of the 31st International Annual Conference of ICT*, Fraunhofer-Institut für Chemische Technologie. Karlsruhe, Germany. pp. 129.1-129.14.

EPA, Environmental Protection Agency (2005). "Furniture Flame Retardancy Partnership: Environmental Profiles of Chemical Flame-Retardant Alternatives for Low-Density Polyurethane Foam", *EPA report*. USA. pp. 2.1-2.4.

Ezinwa, J. U. (2009). "Modeling Full-Scale Fire Test Behaviour of Polyurethane Foams Using Cone Calorimeter Data", *MSc Thesis*, University of Saskatchewan, Saskatoon.

Gabbott, P. (2008). "Principles and Applications of Thermal Analysis: A Practical Introduction to Differential Scanning Calorimetry", *Blackwell Publishing*. Oxford, UK. pp. 1-50.

Gordon, S., McBride, B.J., (1994). "Computer Program for Calculation of Complex Chemical Equilibrium Compositions and Aplications, Part I and II", *NASA Report SP1311*, NASA Lewis Research Center, Cleveland OH), USA.

Gulmine, J.V., Janissek, P. R., Heise, H. M., Akcelrud, L. (2002). "Polyethylene Characterization by FTIR", *Polymer Testing*. Vol. 21. pp. 557-563.

Hatakeyama, T., Quinn, F.X. (1999). "Thermal Analysis Fundamentals and Applications to Polymer Science", *John Wiley & Sons*. England.

Heuzé, O. (1989). "Cálculo Numérico das Propriedades das Misturas Gasosas em Equilíbrio Termodinâmico", Universidade de Coimbra, Portugal.

Heuzé, O., Bauer, P., Presles, H., Brochet, C. (1985). "The Equations of State of Detonation Products and Their Incorporation into the Quatuor Code", *Proc. of the 8th Symposium (International.) on Detonation*. Albuquerque, New Mexico. pp. 762-769.

ICT (2005) "Database of Thermochemical Values", Fraunhofer-Institut für Chemische. Karlsruhe, Germany, 2005.

Ionescu, M. (2005). "Chemistry and Technology of Polyols for Polyurethanes", *Rapra Technology Limited*. UK.

Jackson, I. (2011). "PuTTY: A Free Telnet/SSH Client for Windows", *Chiark*. http://www.putty.org/ [May 20, 2013].

JANAF (1971). "Janaf Thermochemical Tables", 2nd Ed., *National Bureau of Standards*, Washington DC.

Leikvoll, L. T. (2011). “Development of FTIR and HPLC Methods for Analysis of Substances Extracted from Hydrophilic Urinary Catheters”, *MSc Thesis*. Chalmers University of Technology.Göteborg, Sweden.

Liu, H., Liu, D., Yao, F., Wu, Q. (2010). “Fabrication and Properties of Transparent Polymethylmethacrylate/cellulose Nanocrystals Composites”, *Bioresource Technology*. Vol. 101. pp. 5685-5692.

Marques, J. (2013). “Incêndio na Discoteca "Kiss": Materiais Pirotécnicos, Espuma de Isolamento e Intoxicações”, *Monografia de Seminários*. F.C.T.U.C., Coimbra. pp. 1-35.

Marques, J., Campos, J., Quaresma, J., Góis, J. C., Durães, L. (2013). “Ignition and Combustion of Syntactic and Expanded Polyurethane Foam with Ammonium Nitrate and Sodium Bicarbonate Additives”, *Proc. of the 44th International Annual Conference of ICT*, Fraunhofer-Institut für Chemische Technologie. Karlsruhe, Germany. pp. 28.1-28.16.

Naka, R., Kobayashi, I., Tanaka, K., Gotoo, K., (1990). “Rigid Polyurethane Foam and Process for Producing the Same”, *Patent*. EP 0 443 158 B1.

Neves, A. C. C., (2010). “Comportamento de Espumas de Poliuretano no Processo de Colagem à Chama”, *MSc Thesis*. Universidade de Aveiro, Portugal.

Nicholas, D. J. (2008). “Forensic Analysis of Fire Debris Residues”, *Institue of Forensic Science*. Indianapolis. pp. 1-4.

Oommen, C., Jain, S.R. (1999). “Ammonium Nitrate: A Promising Rocket Propellant Oxidizer”, *Journal of Hazardous Materials*. Vol. A67. pp. 253-281.

Otloski, E. L., Sollner, G. H. (1988). “Polyurethane Syntactic Foam Modeling Stock”, *Patent*. US4916173 A.

Pielichowski, K., Njuguna, J. (2005). “Thermal Degradation of Polymeric Materials”, *Rapra Technology Limited*. UK.

Pinto, M. L. (2010). “Formulation, Preparation, and Characterization of Polyurethane Foams”, *Journal of Chemical Education*. Lisbon, Portugal. Vol. 87. pp. 212-215.

Pinto, M. L., Marques, J., Pires, J. (2012). “Porous Clay Heterostructures with Zirconium for the Separation of Hydrocarbon Mixtures”, *Separation and Purification Technology*. Lisbon, Portugal. Vol. 98. pp. 337-343.

Pires, A., Campos, J., (1996). "Incineration of Explosives in a Fluidised Bed", *Proc. of the 27th International Annual Conference of ICT,* Fraunhofer-Institut für Chemische Technologie. Karlsruhe, Germany. pp. 80.1-80.14.

Portugal, P., Campos, J., Portugal, A. (2000). "Combustion Behaviour of Pyrotechnic Mixture based in Ammonium and Sodium Nitrates with Wood Particles", *Proc. of the 31th International Annual Conference of ICT,* Fraunhofer-Institut für Chemische Technologie. Karlsruhe, Germany. pp. 43.1-43.14.

Prager, F. H., Rosteck H. (2006). "Polyurethane and Fire", *WILEY-VCH*. Weinheim, Germany.

Rees, P. (2012). "Portimão Retail Park Burns to the Ground", *algarvedailynews*. http://algarvedailynews.com/news/7601-portimao-retail-park-burns-to-the-ground [March, 2013].

Saetung, A. (2009). "Preparation of Polyurethane Foams from Hydroxytelechelic Oligoisoprenes Obtained by Controlled Degradation of Natural Rubber: Study of Their Physico-mechanical, Thermal, and Acoustic Properties", *PhD Thesis*. Prince of Songkla University, Pattani, Thailand.

Saferstein, R. (2011). "Forensic Science: An Introduction: Forensic Aspects of Fire Investigation", *Pearson Education*. Upper Saddle River. pp. 13.1-13.18.

Singh, H., Jain, A. K. (2009) "Ignition, Combustion, Toxicity, and Fire Retardancy of Polyurethane Foams: A Comprehensive Review", *Journal of Applied Polymer Science*. Vol. 111. pp. 1115-1143.

Steinhaus, T. (1999). "Evaluation of the Thermophysical Properties of Poly(MethylMethacrylate): A Reference Material for the Development of a Flammability Test for Micro-gravity Environments", *MSc Thesis*. University of Maryland, USA.

Tanaka, K., (1983). "Detonation Properties of Condensed Explosives Computed Using the Kihara-Hikita-Tanaka Equation of State", *Report from National Chemical Laboratory for Industry*, Ibaraki, Japan.

Tang, Z., Maroto-Valer, M. M., Andrésen, J. M., Miller, J. W., Listemann, M. L., McDaniel, P. L., Morita, D. K., Furlan, W. R. (2002). "Thermal Degradation Behavior

of Rigid Polyurethane Foams Prepared with Different Fire Retardant Concentrations and Blowing Agents", *Polymer*. Vol. 43. pp. 6471-479.

Tarr, M. (2012). "Differential Scanning Calorimetry (DSC) and Thermogravimetric Analysis (TGA)", *Institut für Technische Chemie*. http://www.itc.tu-bs.de/Abteilungen/Makro/Methods/dsc.pdf [November, 2012].

Théorêt, A., Sandorfy, C. (1964). "Infrared spectra and crystalline phase transitions of ammonium nitrate", *Canadian Journal of Chemistry*. Vol. 42. pp. 57-62.

Torobin, L. (1981). "Hollow Plastic Microspheres", *Patent*. US 4303736 A.

Turchini L., Vallini, G., Gandini, A., Picavez, D. (1995). "Method for the Production of Polyurethanes and of Expanded Polyurethane Foams", *Patent*. EP 0 682 050 A1.

Wang, F. (1998). "Polydimethylsiloxane Modification of Segmented Thermoplastic Polyurethanes and Polyureas", *PhD Thesis*. Faculty of the Virginia Polytechnic Institute and State University. Blacksburg, Virginia.

Wanga H., Hicks, J., Kennedy, E. M., Moghtaderi, B., Delichatsios, M. A., Dlugogorski, B. Z. (2004). "Flame Spread Over PMMA in Narrow Channel", *Nist*. US 1-11.

Wheatley, M. (2003). "Frank-Kamenetskii's Theory of Thermal Ignition", *University of Leeds*. http://www.leeds.ac.uk/fuel/tutorial/frank/Default.htm [February 28, 2013].

Wheatley. M. (2003) "Semenov's Theory of Thermal Ignition", *University of Leeds* http://www.leeds.ac.uk/fuel/tutorial/semenov/Default.htm [February 28, 2013].

APPENDIX A

THOR PREDICTING RESULTS:

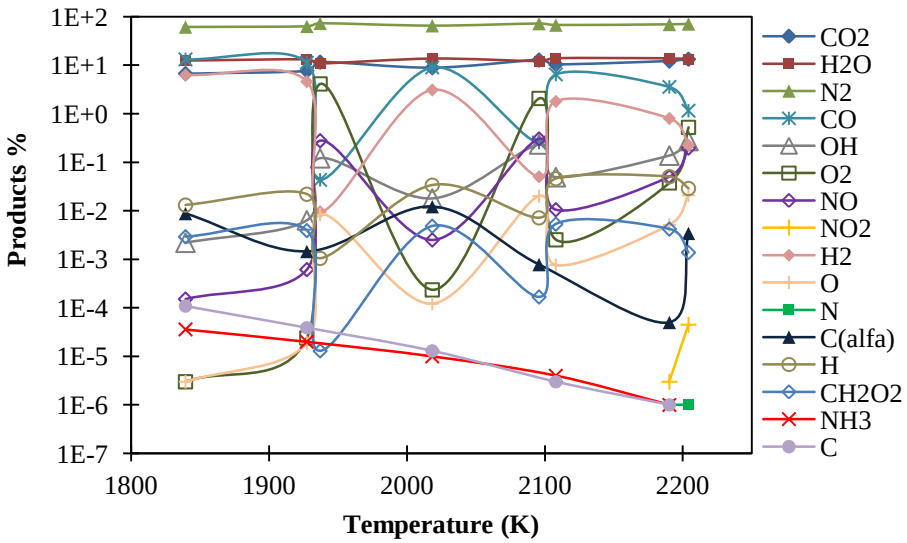

Figure 148 - Products composition as a function of isobare adiabatic combustion temperature, for polyurethane and air mixtures.

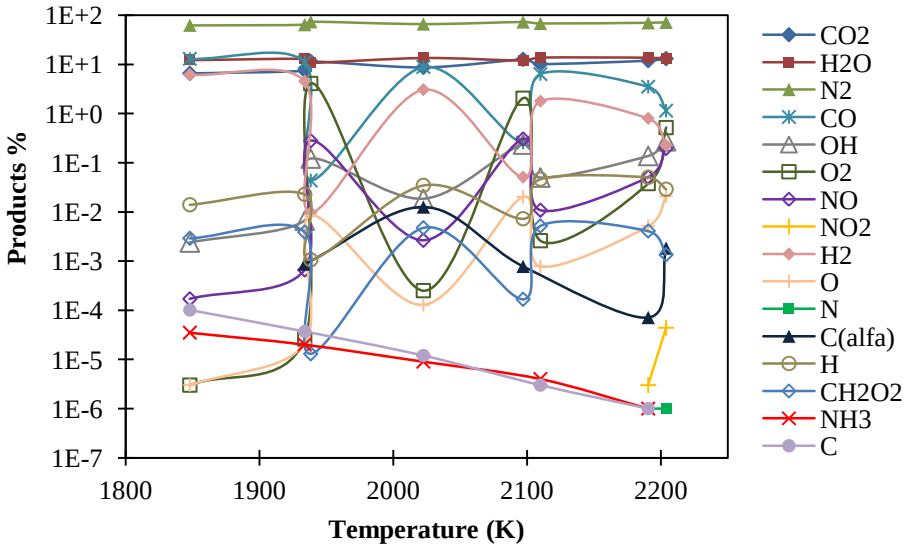

Figure 149 – Products composition as a function of isobare adiabatic combustion temperature, for PU/PE and air mixtures.

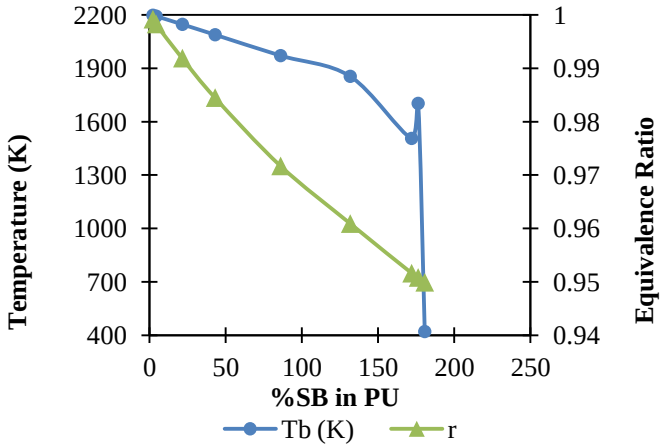

Figure 150 - Calculated values of *Tb* and *r* (equivalence ratio) as a function of % of SB in PU, for PU/SB and air mixtures.

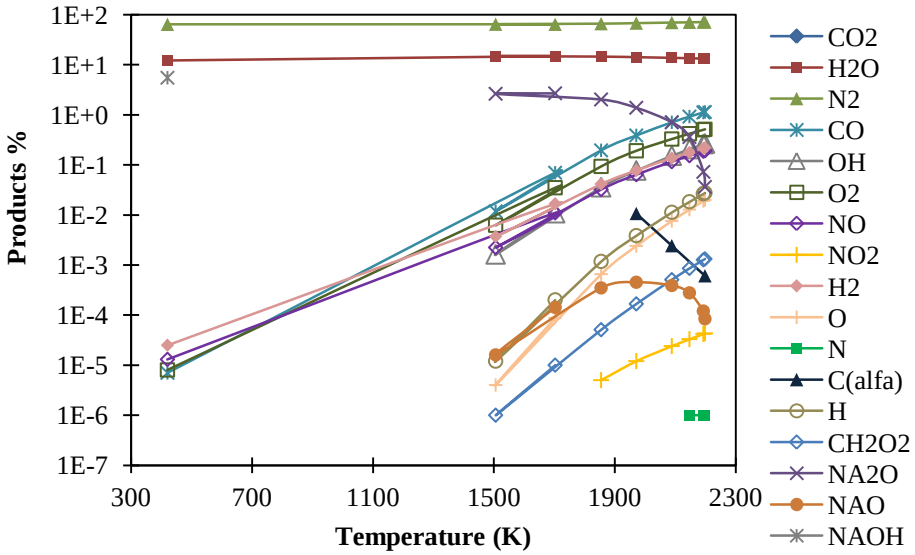

Figure 151 - Products composition as a function of isobare adiabatic combustion temperature, for polyurethane, air and sodium bicarbonate mixtures.

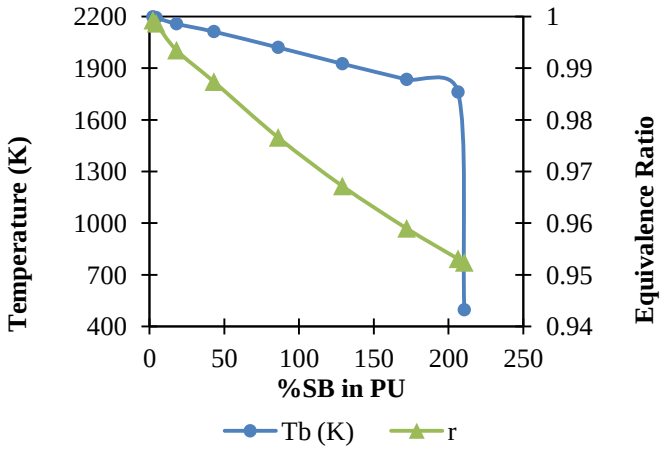

Figure 152 – Calculated values of *Tb* and *r* (equivalence ratio) as a function of % of SB in PU, for PU/PE/SB and air mixtures.

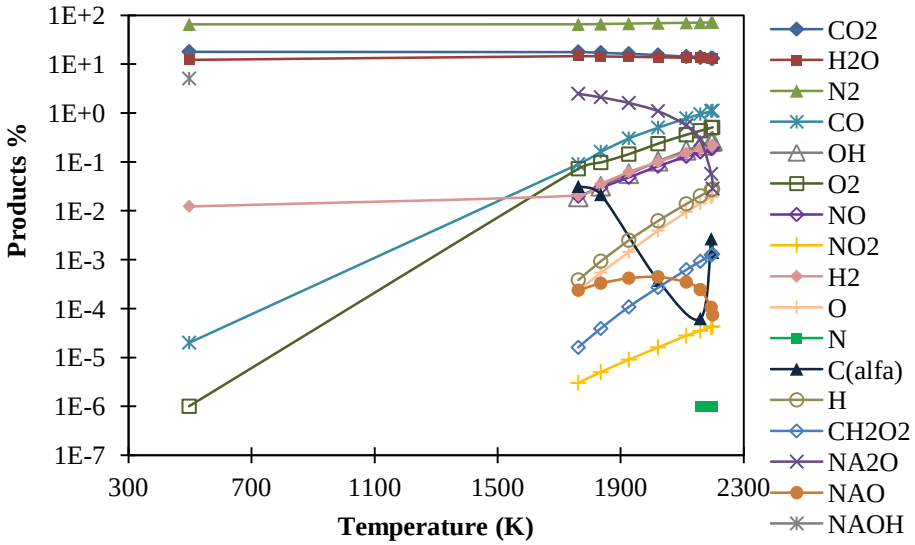

Figure 153 - Products composition as a function of isobare adiabatic combustion temperature for polyurethane, polyethylene, air and sodium bicarbonate mixtures.

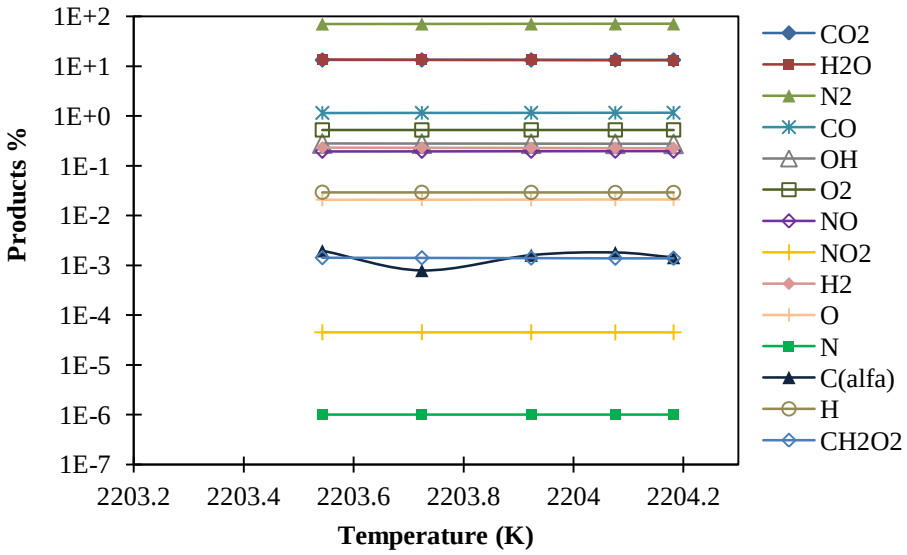

Figure 154 – Products composition as a function of isobare adiabatic combustion temperature for polyurethane, air and ammonium nitrate mixtures.

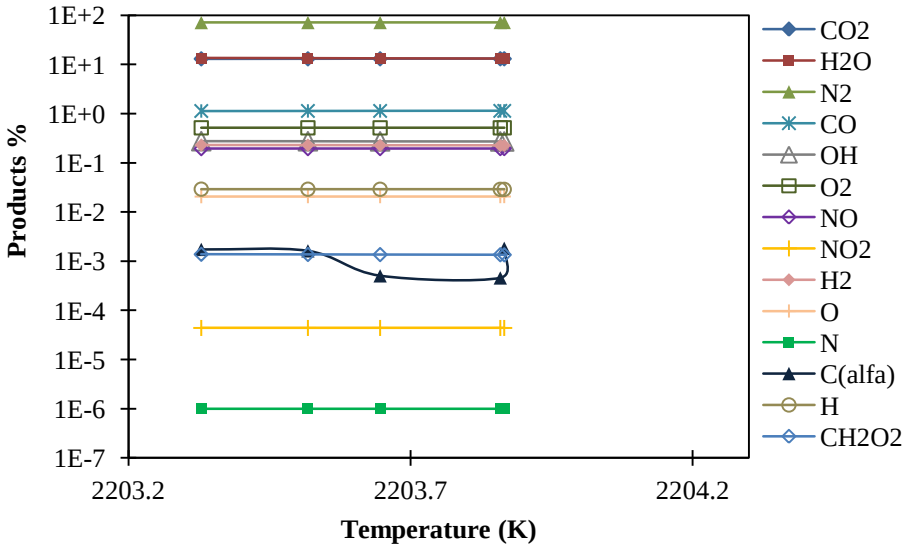

Figure 155 – Products composition as a function of isobare adiabatic combustion temperature for polyurethane, polyethylene, air and ammonium nitrate mixtures.

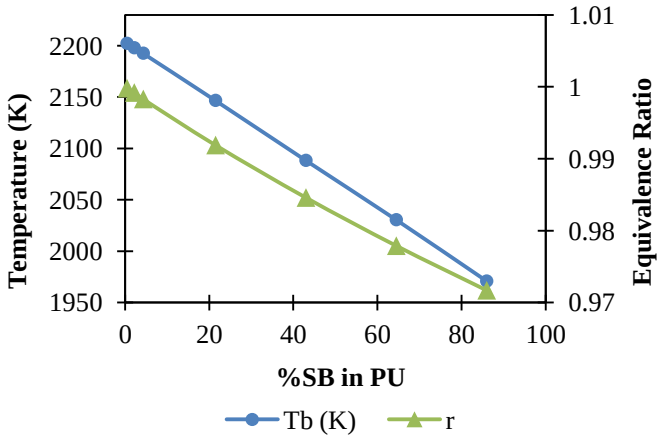

Figure 156 – Obtained values of *Tb* and *r* as a function of % of SB in PU, for PU/0.5 %AN (in PU) and air mixtures.

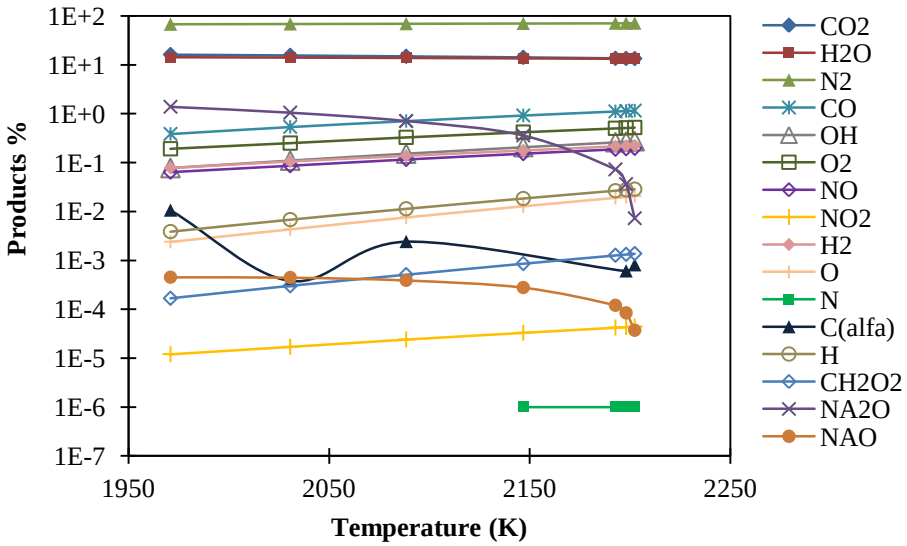

Figure 157 - Products composition as a function of isobare adiabatic combustion temperature, for PU/0.5 %AN (in PU)/air and SB mixtures.

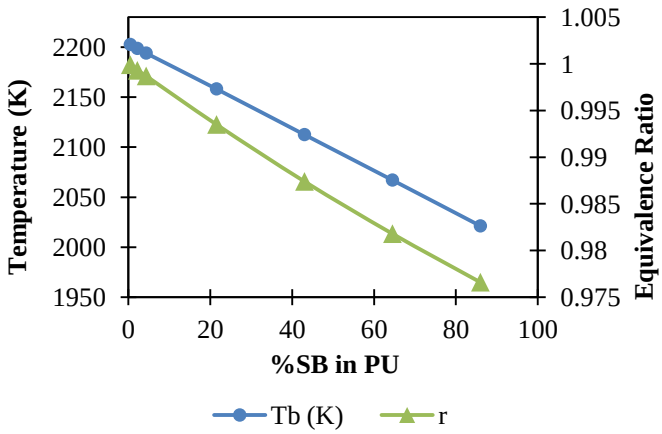

Figure 158 – Obtained values of *Tb* and *r* as a function of % of SB in PU, for PU/PE/0.5 %AN (in PU) and air mixtures.

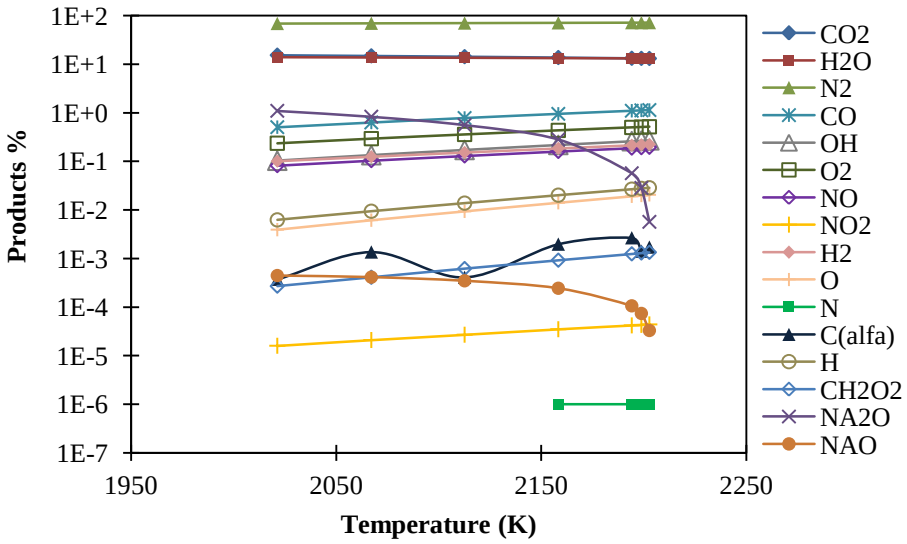

Figure 159 - Products composition as a function of isobare adiabatic combustion temperature, for PU/PE/0.5 %AN (in PU)/air and SB mixtures.

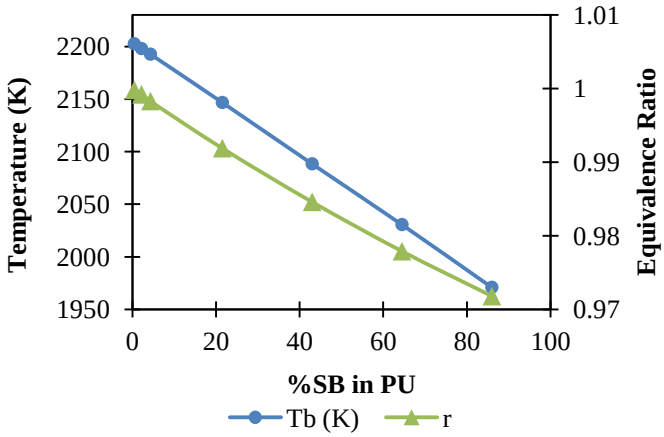

Figure 160 – Obtained values of *Tb* and *r* as a function of % of SB in PU, for PU/1 %AN (in PU) and air mixtures.

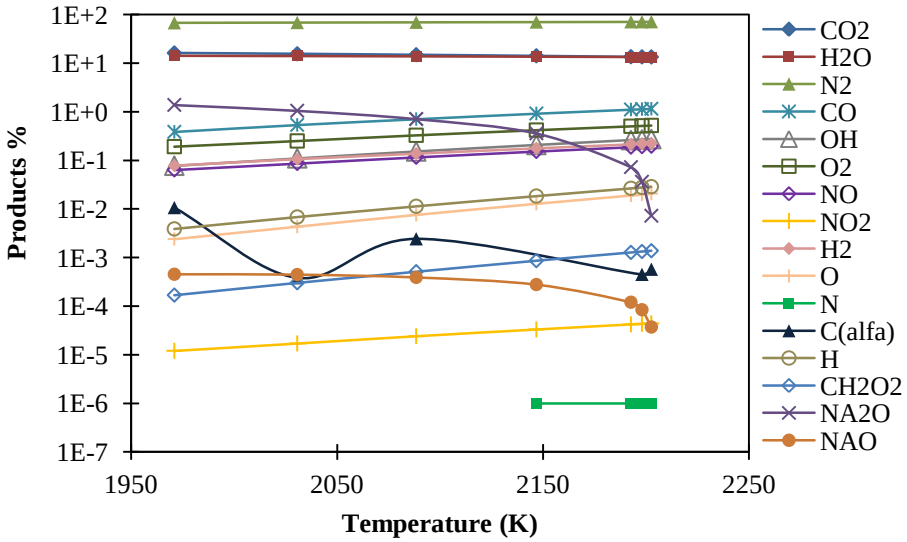

Figure 161 - Products composition as a function of isobare adiabatic combustion temperature, for PU/1 %AN (in PU)/air and SB mixtures.

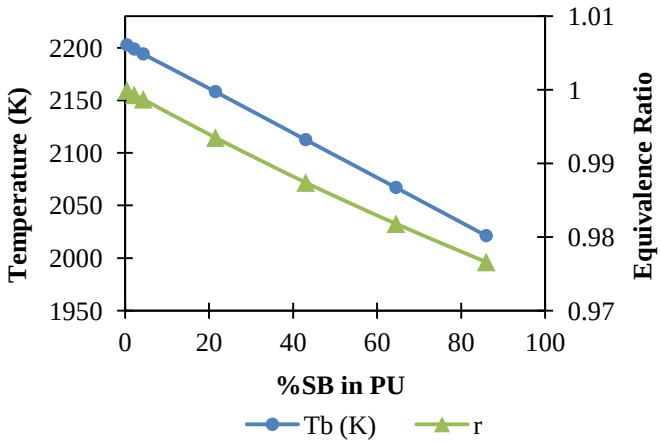

Figure 162 - Obtained values of *Tb* and *r* as a function of % of SB in PU, for PU/PE/1 %AN (in PU) and air mixtures.

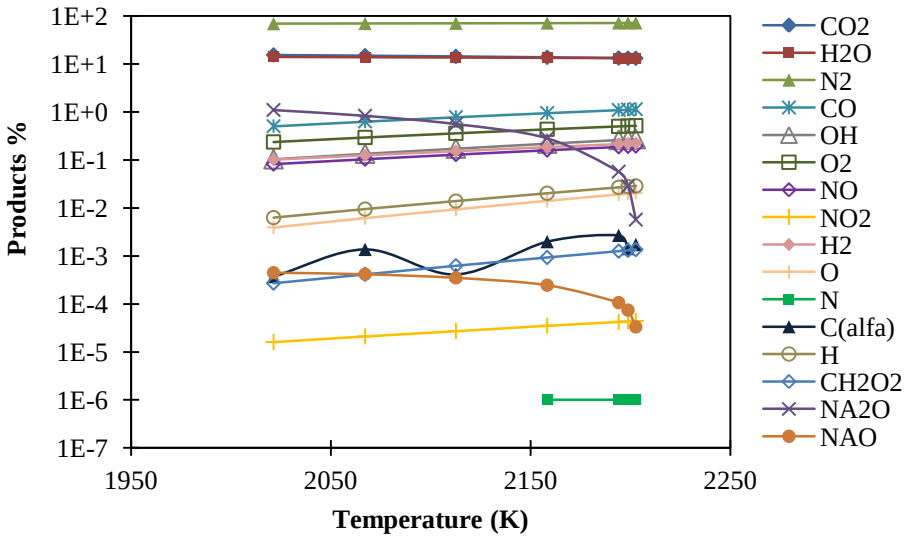

Figure 163 - Products composition as a function of isobare adiabatic combustion temperature, for PU/PE/1 %AN (in PU)/air and SB mixtures.

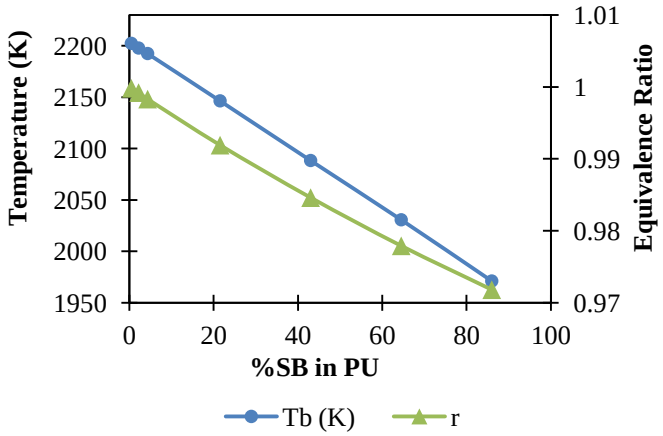

Figure 164 - Obtained values of *Tb* and *r* as a function of % of SB in PU, for PU/3 %AN (in PU) and air mixtures.

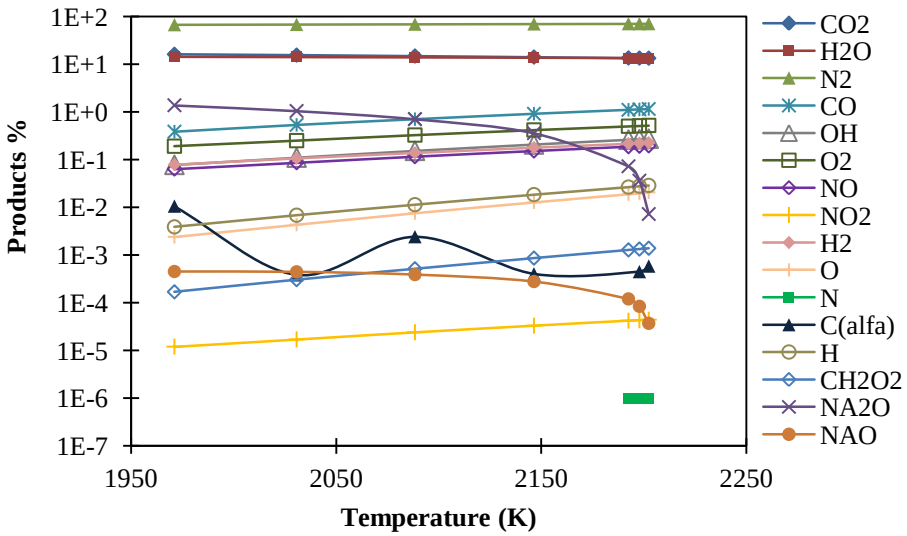

Figure 165 - Products composition as a function of isobare adiabatic combustion temperature, for PU/3 %AN (in PU)/air and SB mixtures.

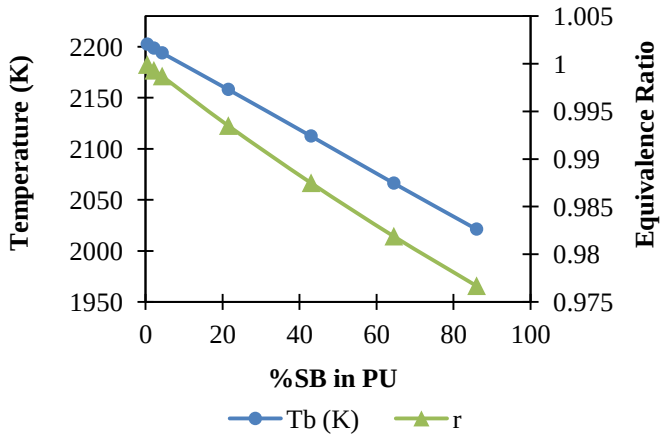

Figure 166 - Obtained values of *Tb* and *r* as a function of % of SB in PU, for PU/PE/3 %AN (in PU) and air mixtures.

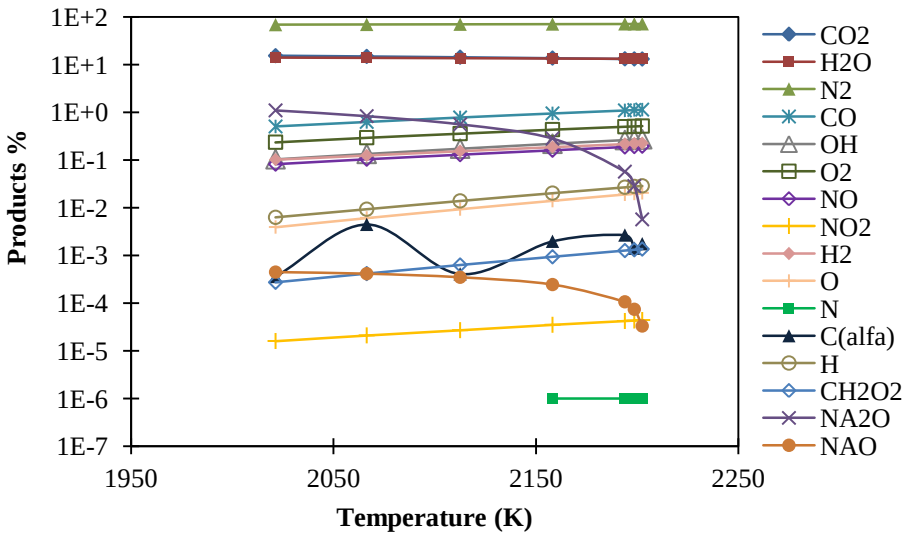

Figure 167 - Products composition as a function of isobare adiabatic combustion temperature, for PU/PE/3 %AN (in PU)/air and SB mixtures.

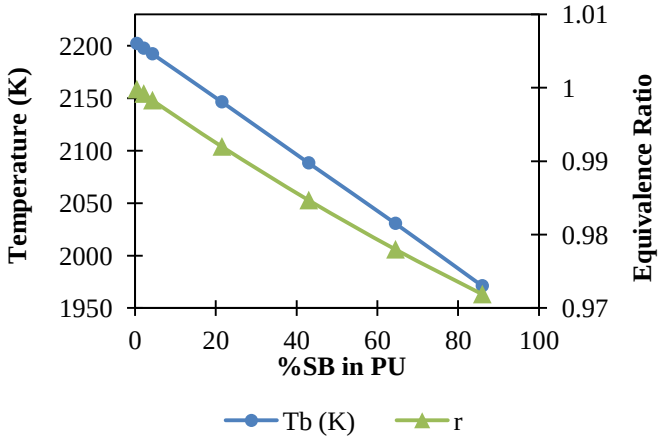

Figure 168 - Obtained values of *Tb* and *r* as a function of % of SB in PU, for PU/5 %AN (in PU) and air mixtures.

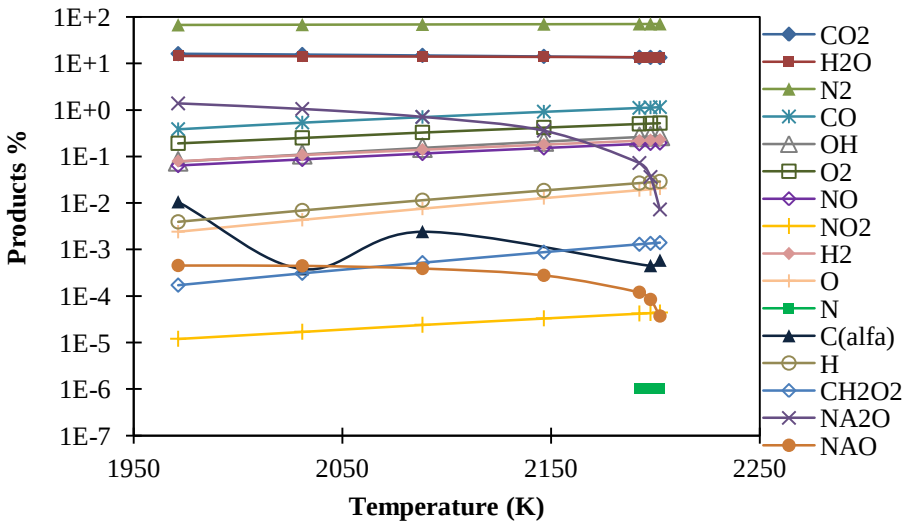

Figure 169 - Products composition as a function of isobare adiabatic combustion temperature, for PU/5 %AN (in PU)/air and SB mixtures.

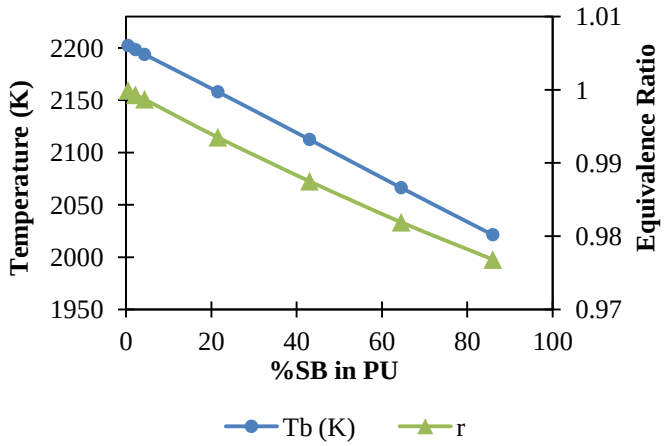

Figure 170 - Obtained values of *Tb* and *r* as a function of % of SB in PU, for PU/PE/5 %AN (in PU) and air mixtures.

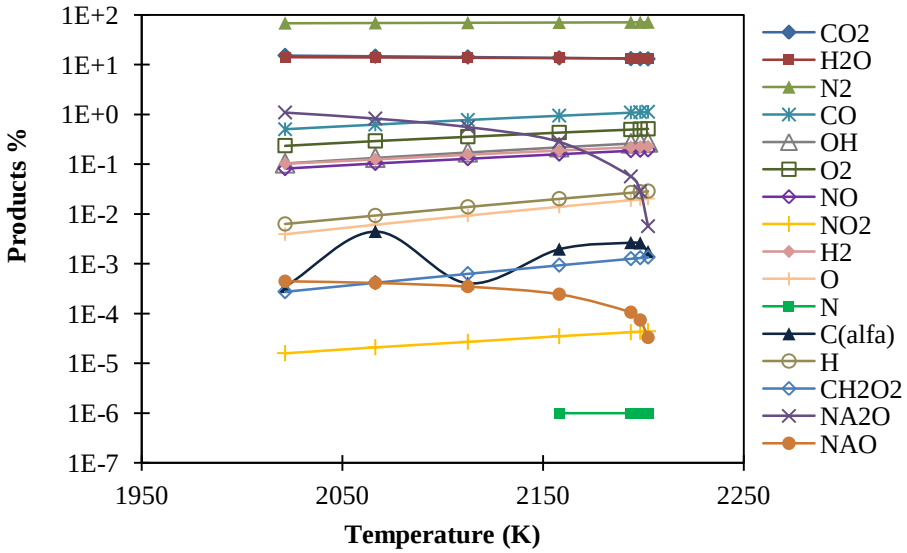

Figure 171 - Products composition as a function of isobare adiabatic combustion temperature, for PU/PE/5 %AN (in PU)/air and SB mixtures.

APPENDIX B

Prediction of temperature and ignition delay:

Table 10 – Numerical values of the constants used in the calculations.

Nu	2
k_f (W.m^{-1}.K^{-1})	$0.000155 \times \left(\frac{T_g}{1000}\right)^{0.609} \times 41867.28072 \times 10^{-2}$
h (W.m^{-2}.K^{-1})	$\frac{Nu \times k_f}{\lambda}$
E_a(J.mol^{-1})	4.35×10^4
A (min^{-1})	1.90×10^4
I_p (J.Kg^{-1})	2.51×10^7
ρ (Kg.m^{-3})	1180
β	0.4689
C_d (J.Kg^{-1}.K^{-1})	$0.43 \times \left(\frac{T_g}{1000}\right)^{0.23} \times 4186.8$
D_0 (m^2.s^{-1})	1.80×10^{-5}
ρ_0 (Kg.m^{-3})	1.429
$[O_2]$ %	21
R (J.K^{-1}.mol^{-1})	8.314
σ_r (W.m^{-2}.K^{-4})	5.67×10^{-8}

APPENDIX C

Burning tests:

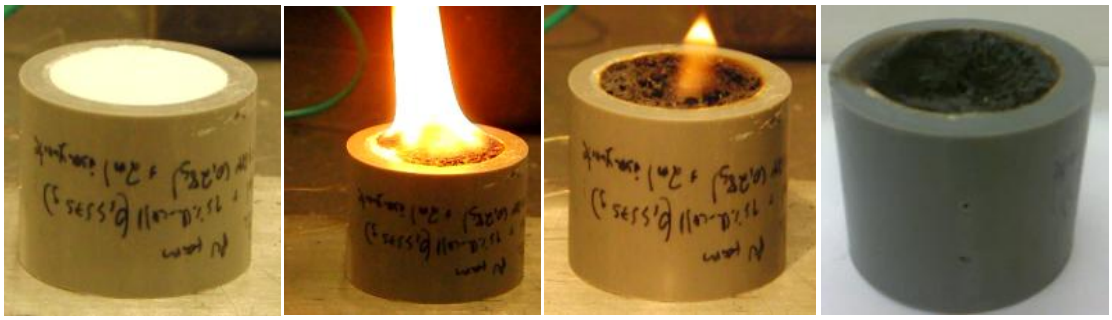

Figure 172 - Syntactic Polyurethane Foam 15% HPM with 7 mass % of AN; ignited from the top, vertical position.

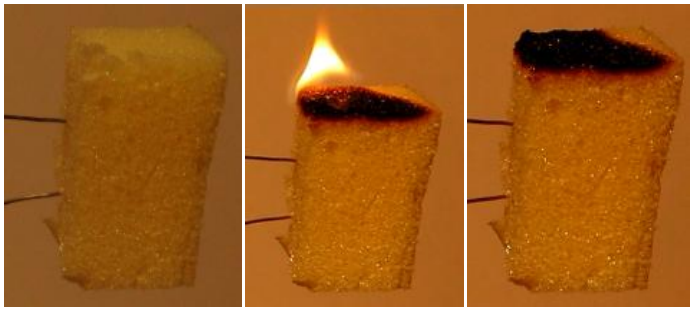

Figure 173 - Expanded Polyurethane Foam with 20 mass % of AN; without test tube; ignited from the top, vertical position.

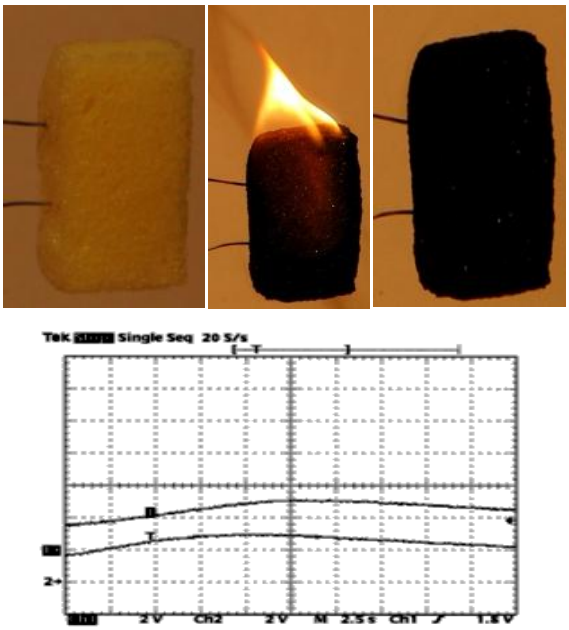

Figure 174 – a) Expanded Polyurethane Foam with 20 mass % of AN without test tube; ignited from the top, vertical position; sample with alcohol (too much); b) Respective temperature records.

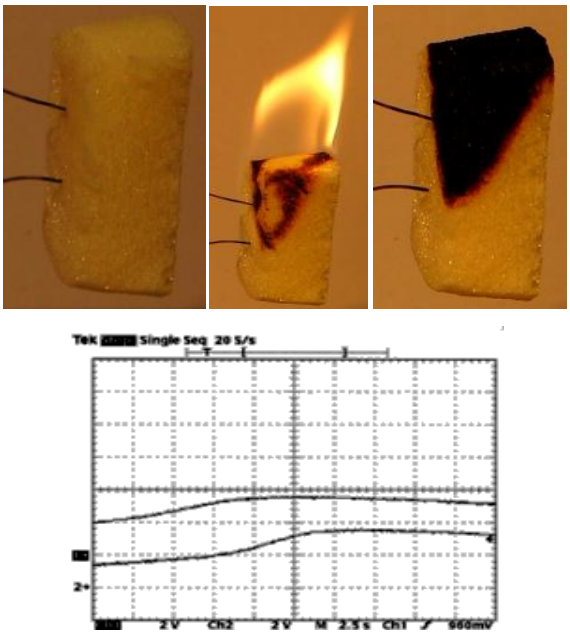

Figure 175 – a) Expanded Polyurethane Foam with, ignited from the top, vertical position; sample with alcohol (low quantity); b) Respective temperature records.

Figure 176 - Expanded Polyurethane Foam with 20 mass % of AN; horizontal position, ignited in the two surfaces.

Figure 177 - Syntactic Polyurethane Foam 15%HPM; ; ignited from the top, vertical position.

Figure 178 - Expanded Polyurethane Foam with 7 mass % of AN; vertical position, ignited in the two surfaces.

Figure 179 - Expanded Polyurethane Foam with 7 mass % of AN cigar_burning_ in a syringe made of pmma.

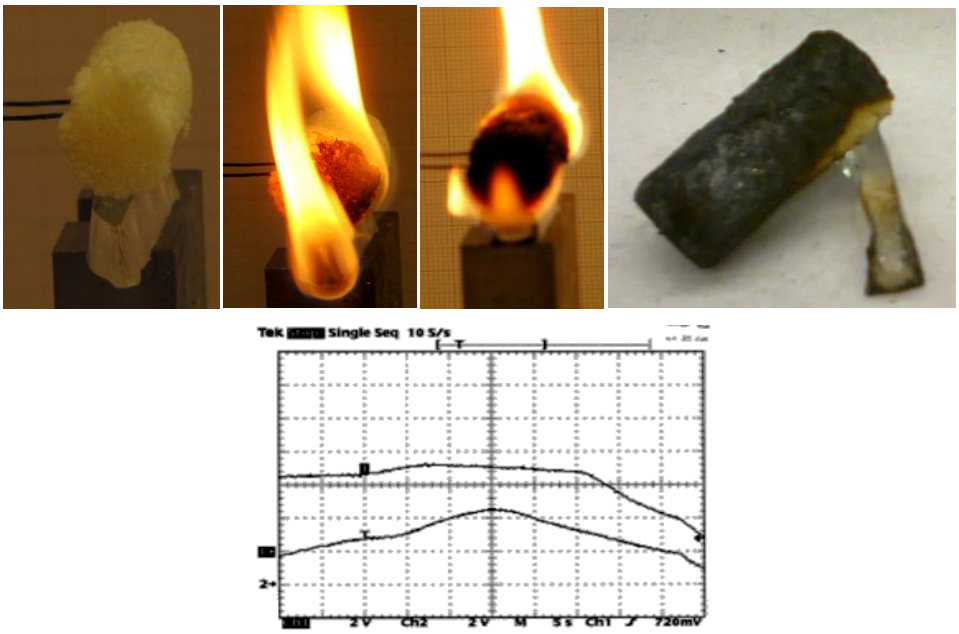

Figure 180 – a) Expanded Polyurethane Foam with 20 mass % of AN without test tube; with PMMA slab; horizontal position; b) Respective temperature records.

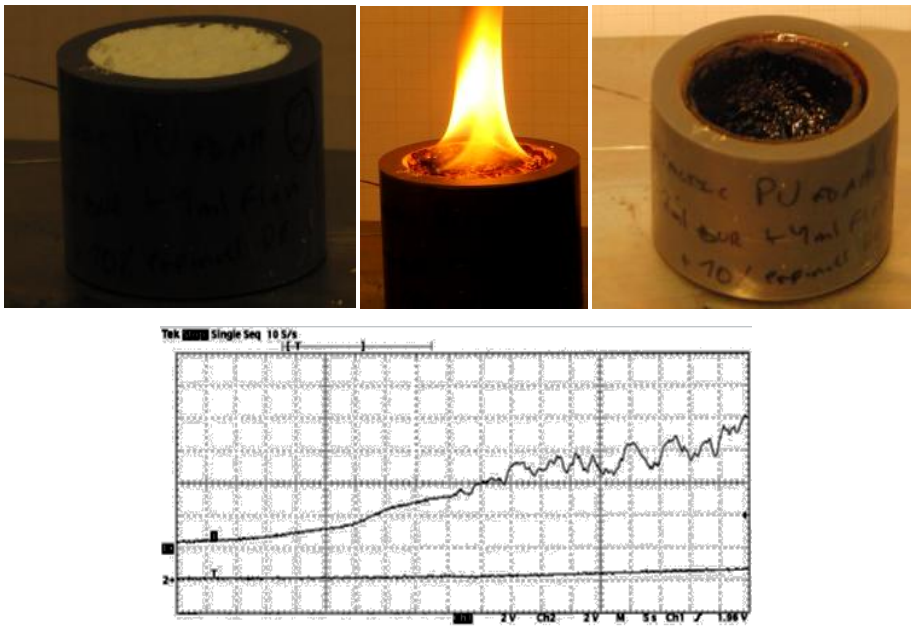

Figure 181 – a) Syntactic Polyurethane Foam 10%HPM; ignited from the top, vertical position; b) Respective temperature records.

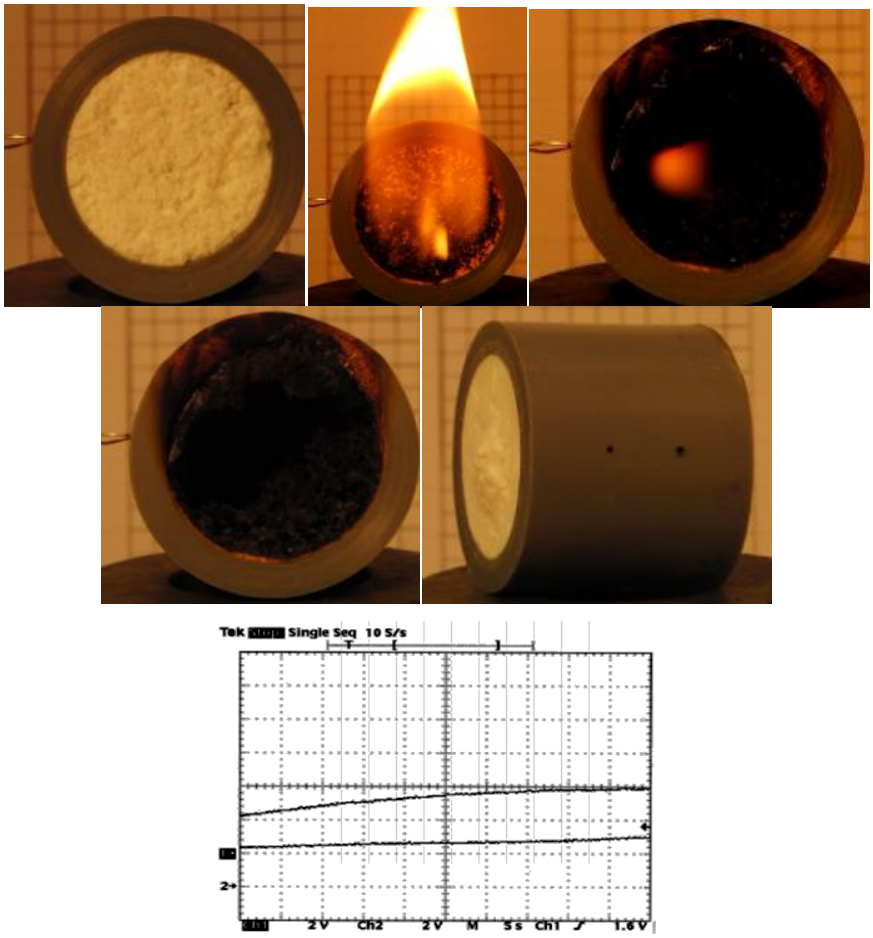

Figure 182 – a) Syntactic Polyurethane Foam 15%HPM with 7 mass % of AN; horizontal position; b) Respective temperature records.

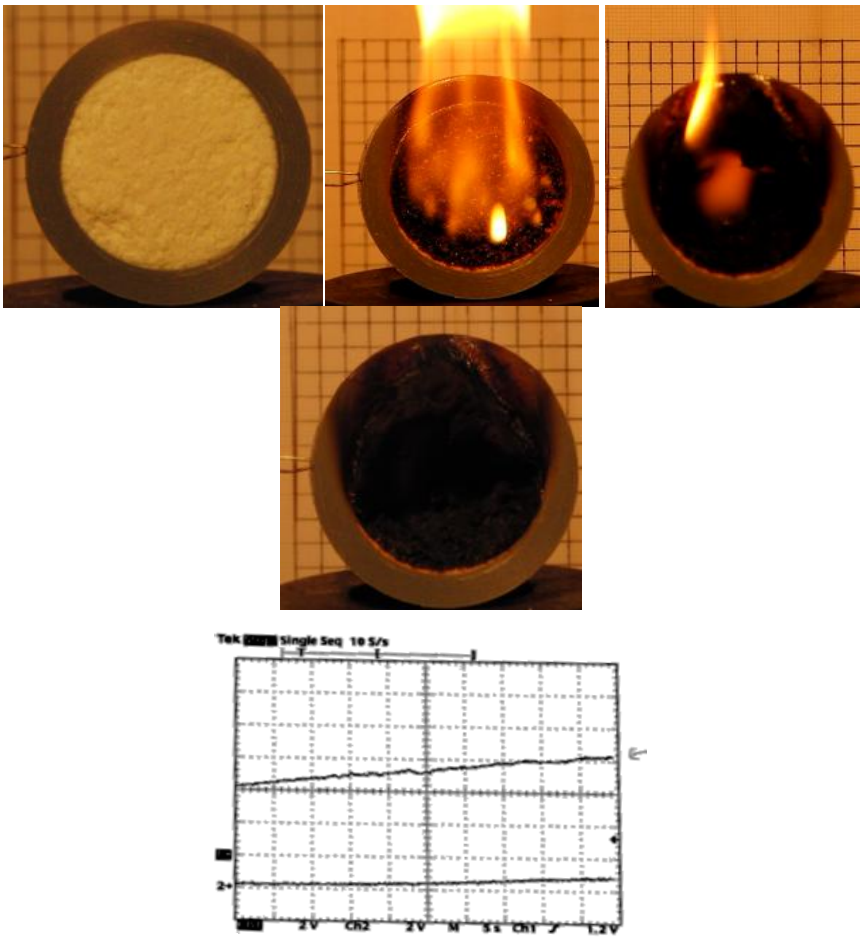

Figure 183 – a) Syntactic Polyurethane Foam 15%HPM with 7 mass % of AN; horizontal position; b) Respective temperature records.

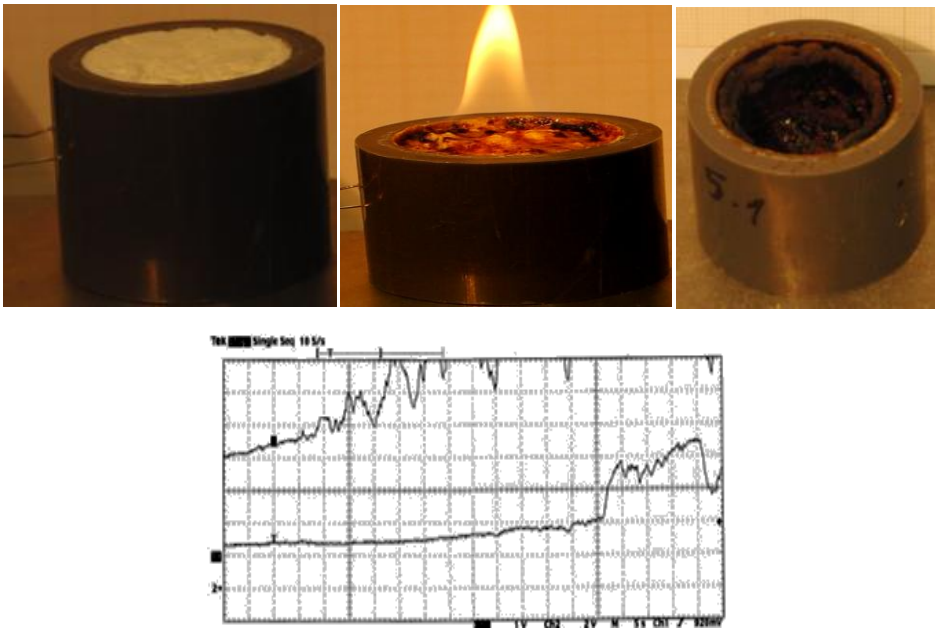

Figure 184 – a) Syntactic Polyurethane Foam 15%HPM; vertical position; b) Respective temperature records.

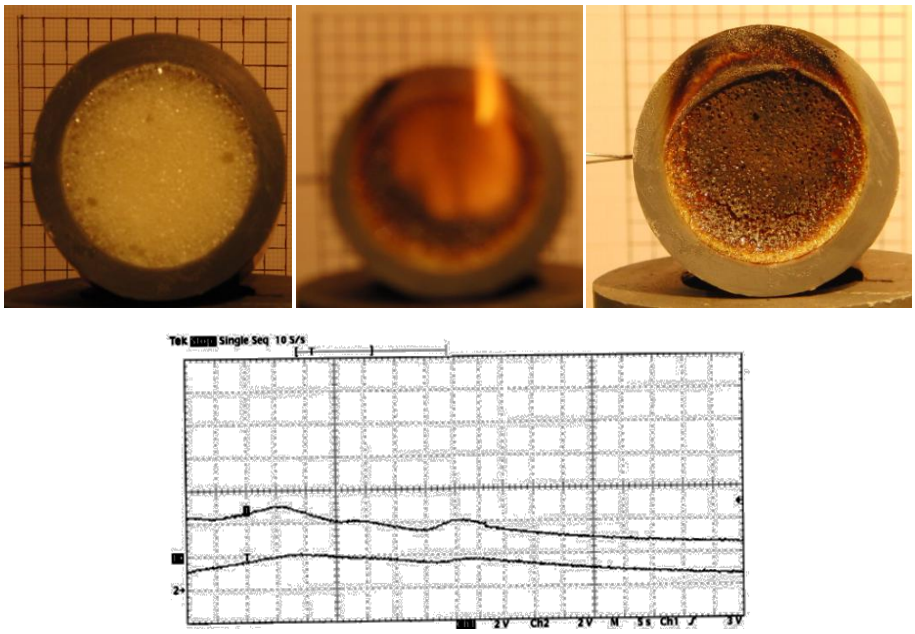

Figure 185 – a) Expanded Polyurethane Foam; horizontal position; b) Respective temperature records.

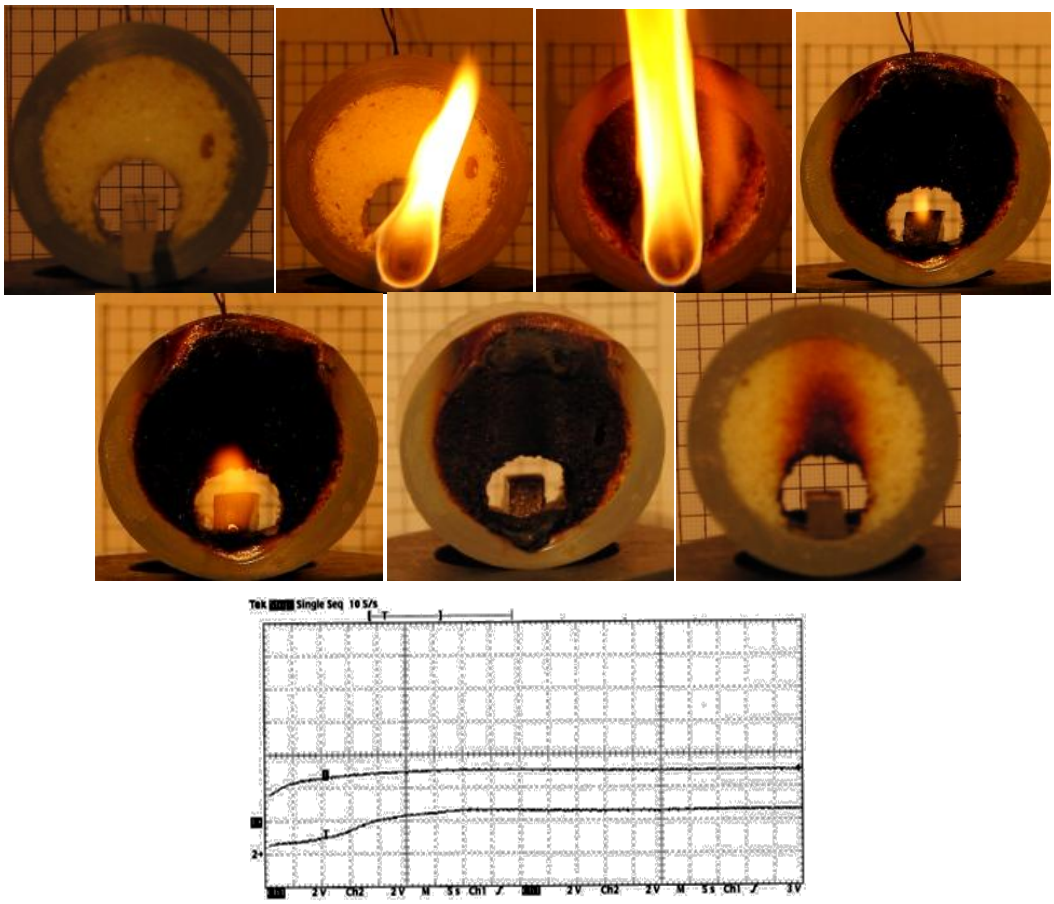

Figure 186 – a) Expanded Polyurethane Foam with 20 mass % of AN; horizontal position; b) Respective temperature records.

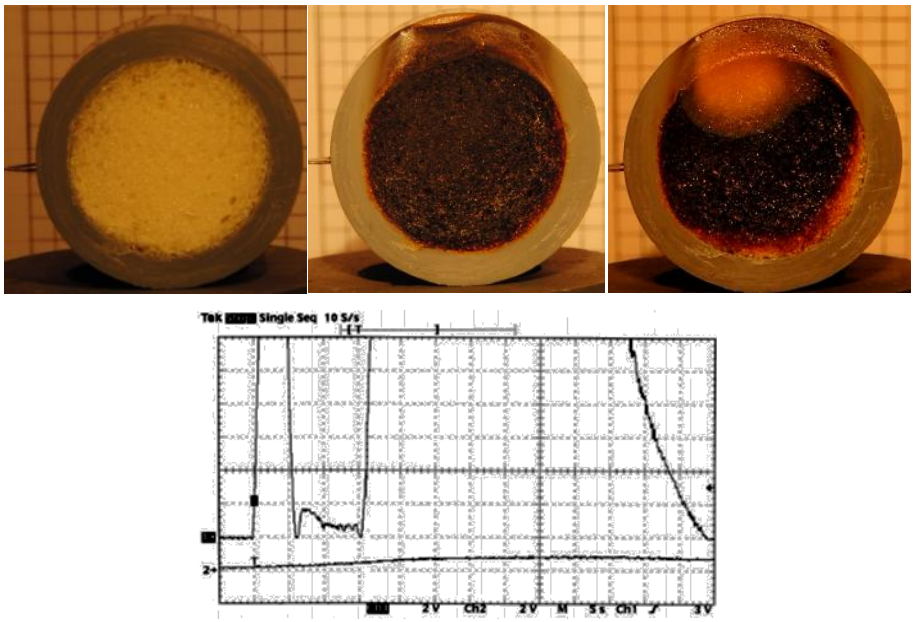

Figure 187 – a) Expanded Polyurethane Foam with 20 mass % of AN; horizontal position; b) Respective temperature records.

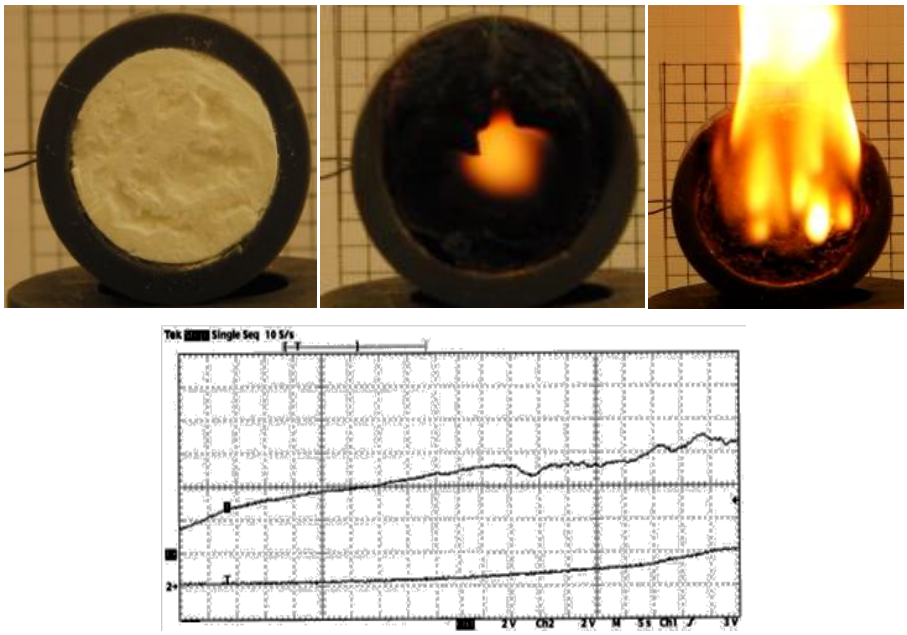

Figure 188 – a) Syntactic Polyurethane Foam 15%HPM with 7 mass % of AN; horizontal position; b) Respective temperature records.

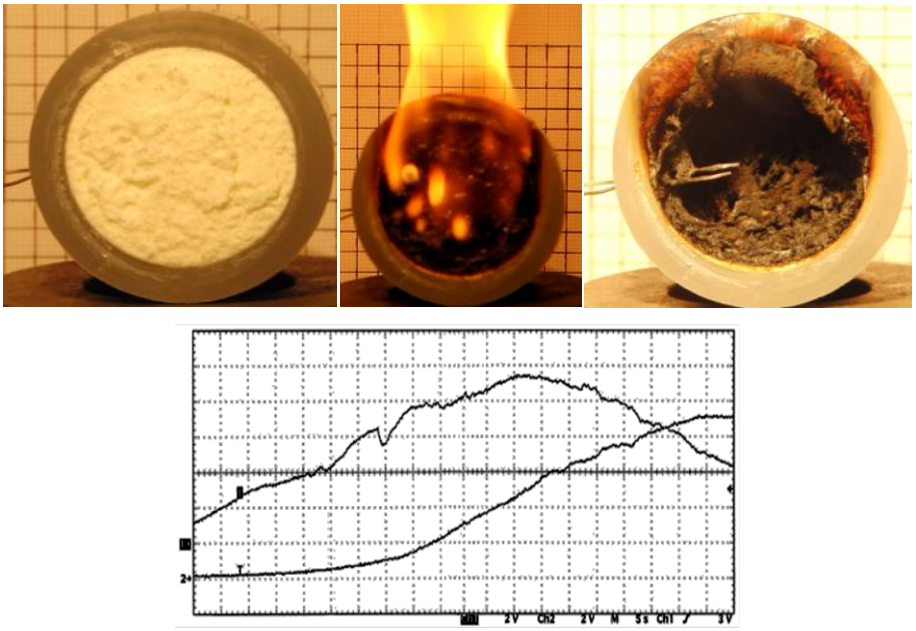

Figure 189 – a) Syntactic Polyurethane Foam 15%HPM with 7 mass % of AN and 5 mass % of SB; horizontal position; b) Respective temperature records.

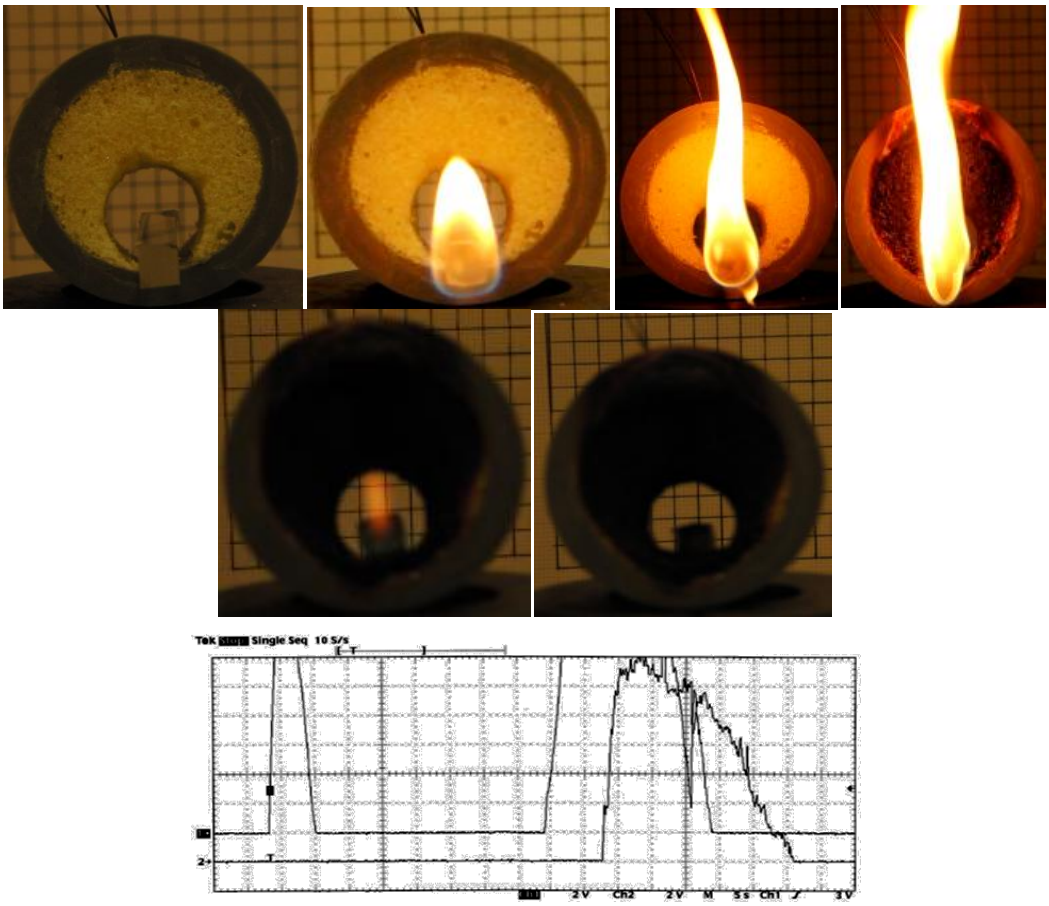

Figure 190 – a) Expanded Polyurethane Foam with 20 mass % of AN; horizontal position; b) Respective temperature records.

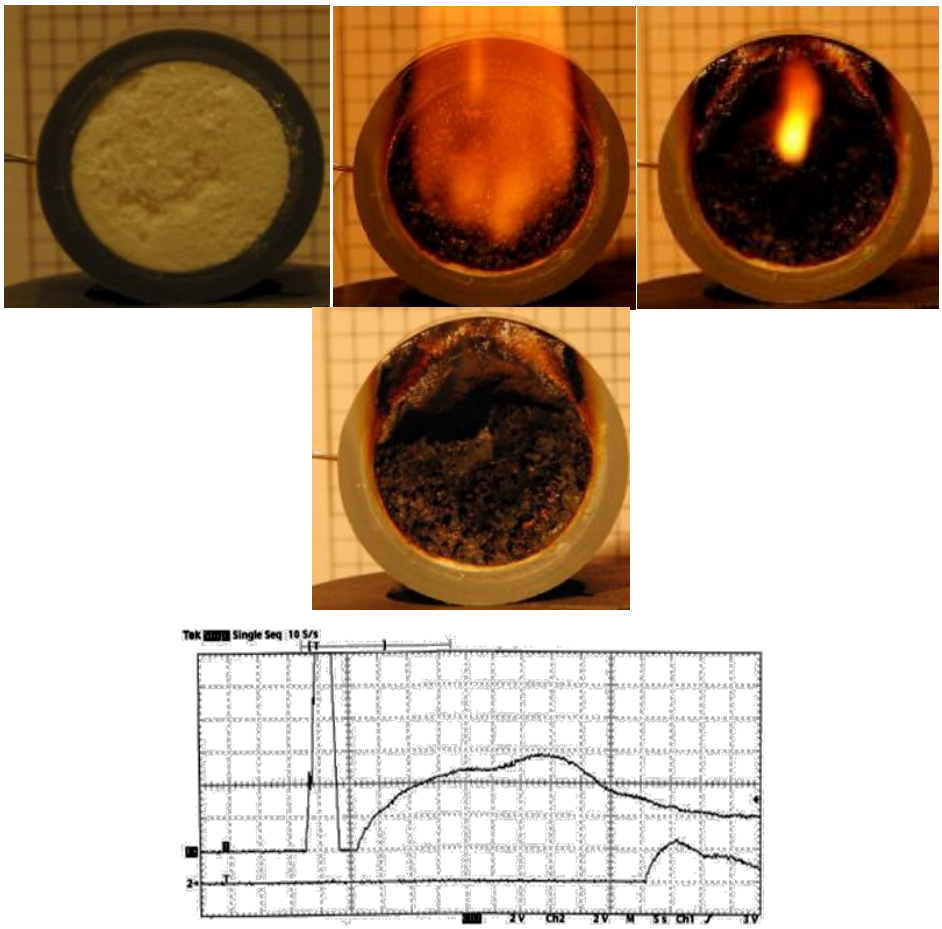

Figure 191 - a) Syntactic Polyurethane Foam 15%HPM with 7 mass % of AN; horizontal position; b) Respective temperature records.

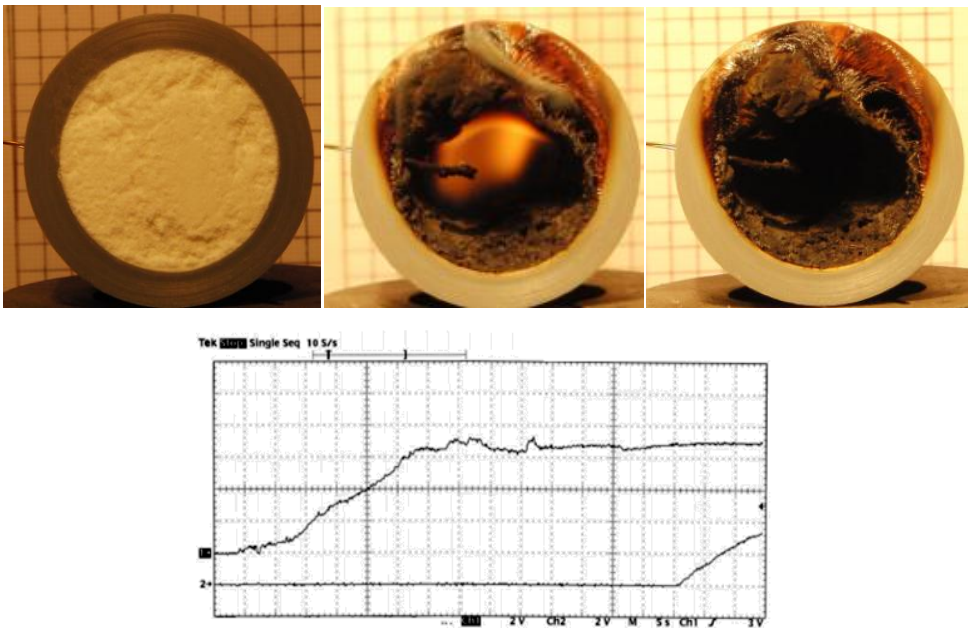

Figure 192 – a) Syntactic Polyurethane Foam 15%HPM with 7 mass % of AN; horizontal position; b) Respective temperature records.

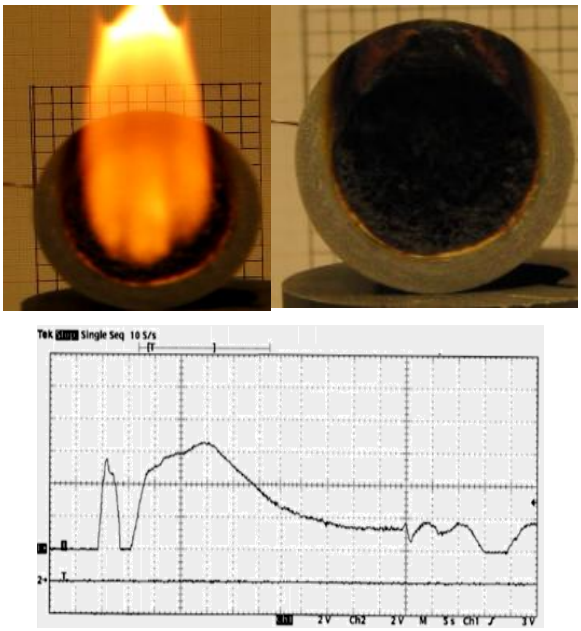

Figure 193 – a) Syntactic Polyurethane Foam 15%HPM with 7 mass % of AN; horizontal position; b) Respective temperature records.

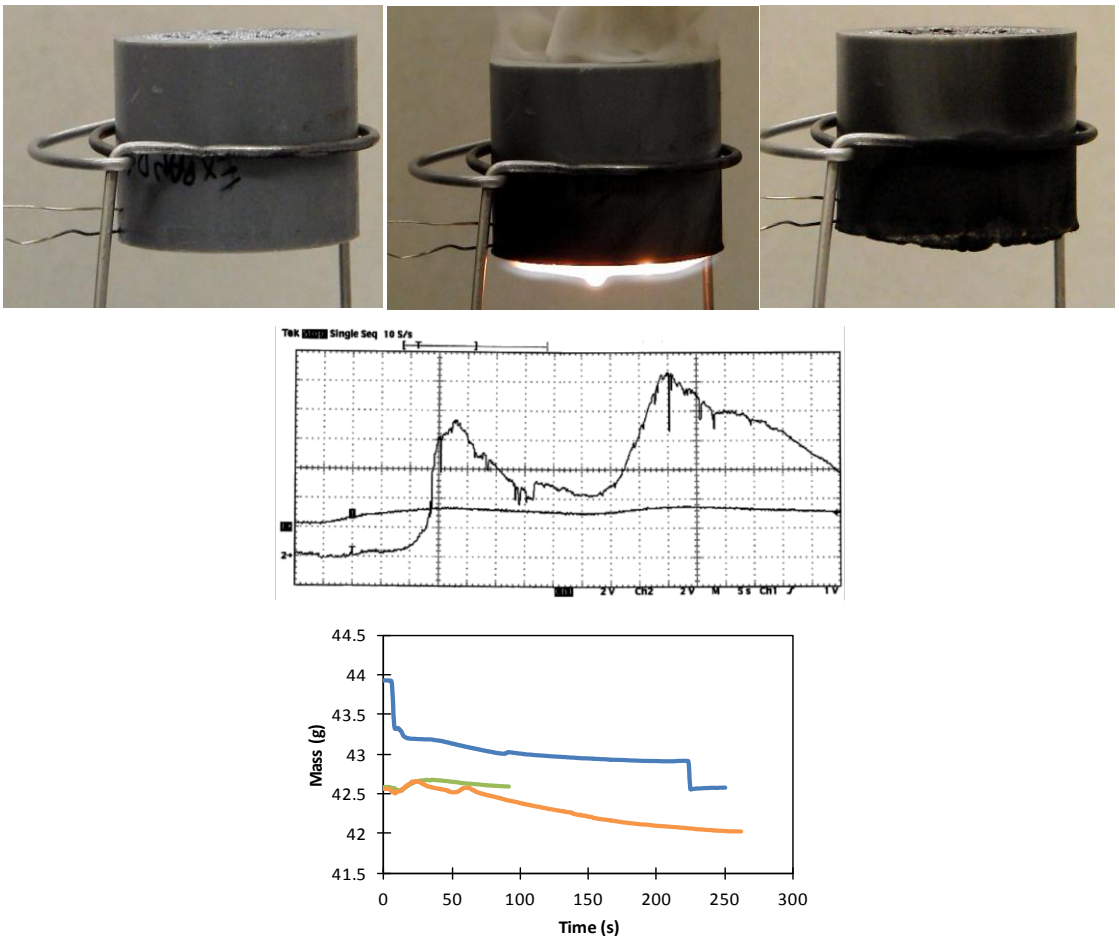

Figure 194 – a) Expanded Polyurethane Foam with paint; vertical position; b) Respective temperature records; c) Mass deplection.

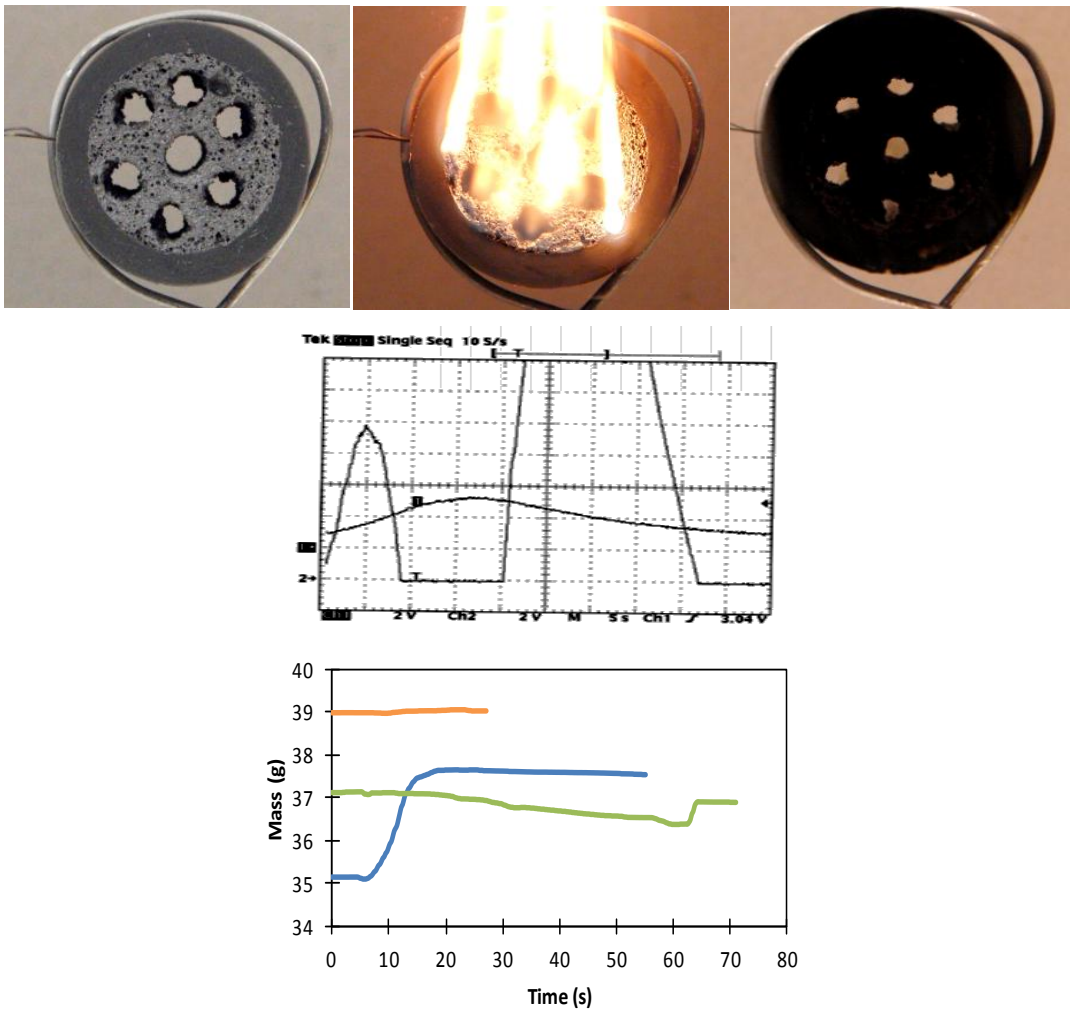

Figure 195 – a) Expanded Polyurethane Foam with 20 mass % of AN + PAINT; horizontal position; b) Respective temperature records; c) Mass deplection.

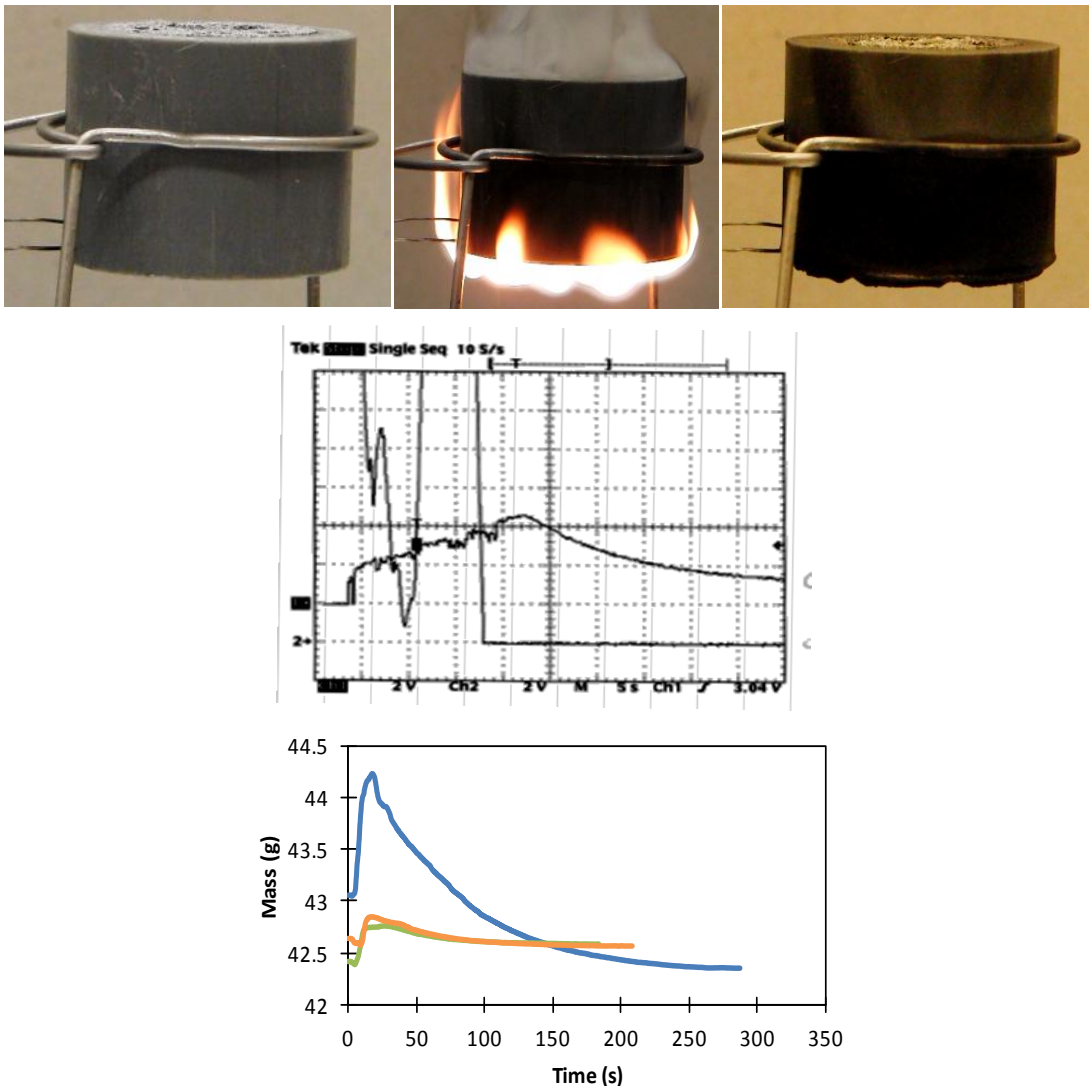

Figure 196 – a) Expanded Polyurethane Foam with 20 mass % of AN; horizontal position; b) Respective temperature records; c) Mass deplection.